# THE ADHESION OF THIN FILMS

Brian Neil Chapman M.A.

A thesis submitted for the
degree of Doctor of Philosophy
in the University of London.

Department of Electrical Engineering
Imperial College
April 1969.

## ABSTRACT

Thin film adhesion is of technological importance in determining the durability of microelectronic devices, and is also of considerable theoretical interest. The adhesion of films has been investigated in several ways:

The expected binding energies due to physisorption of several systems have been calculated from the fundamental dipole-dipole interactions.

Microcalorimetric experiments have been carried out to determine the heat liberated in dissolving a film from its substrate, and hence the adhesion energy.

The kinetics of nucleation and growth have been considered, in order to determine the influence of adhesion on the formation of the film. Experiments have been carried out with evaporated and sputtered beams of gold to determine the significance of the arrival energy of atoms.

The work done in mechanically stripping a film from its substrate has been measured as a function of several parameters. The surrounding gas and the rate of stripping influence the work of removal; an explanation in terms of an electrostatic theory of adhesion has been considered. The mechanical stripping test has also been compared with the scratch test of adhesion.

Although there are severe limitations on the thin film systems that can be studied with the mechanical stripping method, it does appear to offer one means of gaining quantitative adhesion data.

# I N D E X

CHAPTER 111 (contd)

# CHAPTER 1

# INTRODUCTION

## 1.1. THE IMPORTANCE OF ADHESION STUDIES

Adhesion is a familiar but little understood concept. The need for practical adhesives is quite clear; animal glues and epoxy resins usually perform their functions well, but little is known about their bonding mechanisms, and so the preparation of adhesives tends to be an empirical art rather than an ordered science.

But adhesion is of more importance than its obvious practical application, and refers, in general, to the interaction between any two surfaces. For example, the phenomena of friction and wear are closely related to adhesion (Bowden & Tabor, 1950). And adhesion is a very important parameter in thin film technology; because thin films are so thin (usually less than one micron thickness) and so fragile, they must be formed on and supported by a more substantial substrate, and the degree to which the film can share the strength of the substrate depends on the binding between the two. Hence adhesion is important in determining the durability of a thin film device. Furthermore, the growth and hence the structure of the film is also strongly influenced by the adhesion forces. So a study of thin film adhesion has obvious practical and commercial relevance.

Finally, adhesion is important also in many branches of surface physics; it is a fundamental parameter because it depends directly on interatomic and intermolecular forces. Thin films are of special interest in this connection because it is in such systems that conditions of true interfacial contact can most nearly be attained.

So a study of thin film adhesion is of relevance to all practical and academic considerations of adhesion and surface phenomena.

## 1.2. THE NATURE OF ADHESION

Adhesion is qualitatively the phenomenon of materials sticking together, but in order to make quantitative measurements the meaning of the term must be specified more exactly.

Although "adhesion" will continue to be used in its more general sense, in particular adhesion energy will be defined as the work required to reversibly remove unit area of a thin film from its substrate to infinity. This energy is therefore synonymous with the binding energy arising from the intrinsic interactions across the interface.

It is important to distinguish between adhesion and adhesive performance. The latter is the experimentally determined apparent adhesion value; however, such a value is a function of other parameters and properties involved in the determination as well as the adhesion itself. It would appear that a direct experimental measurement of the interfacial interaction only is not possible, so any extraneous work done must be accounted for.

A further important parameter is the adsorption energy; this parameter is applied to single atoms, whereas adhesion energy refers to a continuous interface. The adsorption energy of an adatom, or single atom adsorbed on a substrate, is the work required to reversibly remove the atom to infinity.

## 1.3. PREVIOUS METHODS OF ADHESION MEASUREMENT

The difficulty of determining the adhesion of thin films is apparent from a survey of the methods which have been used. A survey of most of the experimental work to date has been carried out by Campbell (1969), who divides the approaches used into two groups; nucleation methods and mechanical methods.

Nucleation methods are concerned with observations of the way a film grows, particularly with the initial stages of formation. When a film is vacuum deposited, usually by evaporation, material arrives at the substrate in a monomeric form, is adsorbed at a surface site, and then diffuses along the surface from site to site until it coalesces with more deposited material or re-evaporates.

Many theories have been proposed to account for the various stages of nucleation and growth, and used to indirectly measure the energy parameters involved, of which adsorption energy is most relevant to the present study.

The mechanical methods reviewed by Campbell all use some method of removing the film and many attempt to interpret the results quantitatively. Such methods measure the adhesion energy, or, strictly, the adhesive performance.

Some other methods of measuring adhesion not included in Campbell's review are briefly described in Chapter 6.

## 1.4. TYPES OF ADHESION

The adhesion between two materials can be of several types:

The simplest of these is interfacial adhesion, in which the two discrete materials meet at a well-defined planar interface.

A second type is interdiffusion adhesion, which results from a solid state interdiffusion between the two components. A discrete interface is thus replaced by a gradual transition from one material to the other. This mechanism operates in the process of diffusion bonding, which is currently finding considerable industrial application, particularly for the bonding of metals.

A third type is intermediate layer adhesion. The two materials are bonded via one or more layers of compounds of the materials with each other or with environmental gases; oxides are particularly common. Again there is no sharp interface, and there may be clearly defined layers or a gradual transition.

All these different types of adhesion are further complicated in practice because surfaces are never flat and greater or lesser degrees of mechanical interlocking take place.

## 1.5. PRESENT METHODS OF ADHESION MEASUREMENT

The investigation of the adhesion of thin films which is described in this thesis is limited to only the very simplest system, which is weak interfacial adhesion. But of course, an understanding of such an elementary system is a pre-requisite to understanding more complicated systems, and the former is certainly not well understood.

Practical systems which fulfil the requirements of weak interfacial bonding include those of gold and similar metals on glass and rock salt substrates. These materials were chosen for the present study because of their importance in thin film technology and research.

When two microscopic surfaces are pressed together, contact takes place initially at asperities, which may then be considerably

deformed. This does not occur in thin film adhesion since the deposited material arrives in an atomic or molecular species and so is able to adjust to the surface topography. Thus it is when dealing with thin films that one can most nearly attain interfacial contact without deforming the substrate. Furthermore, glass and cleaved rocksalt surfaces can both be made quite physically flat.

The methods of investigation of thin film adhesion which are described herein are as follows:

i. Microcalorimetry. When a film is chemically dissolved from its substrate, the heat liberated is equal to the heat of solution of the film minus the adhesion energy at the interface. This method is described in more detail in Chapter III. Little calorimetric adhesion work has previously been carried out because the heat equivalent of the adhesion energy is so small. Bennett (1959) attempted to measure the temperature change of an alumina substrate 500 Å thick, due to the condensation of material on it, but without significant conclusion.

ii. Nucleation and Growth. The importance of adsorption energy in thin film formation has been stressed above. The kinetics of nucleation and growth are considered in Chapter IV.

iii. Mechanical Stripping. The work done in physically stripping a film from its substrate is related to its adhesion. Using this method, the distinction between adhesion and adhesive performance becomes extremely relevant, as is described in Chapter V.

# CHAPTER II

# ADSORPTION

Thin films are formed by the deposition of material, usually in an atomic or molecular form, on to a substrate surface. The degree of binding between each deposited single atom and the substrate is characterised by the adsorption energy, which has been defined in Chapter 1. Groups, or "islands", of deposited atoms are formed by the collision of single atoms which are able to move across the surface, and the islands subsequently grow so large that coalescence or agglomeration takes place, and the film eventually becomes continuous. It is at this stage that the adhesion may be most usefully discussed, and the adhesion energy may be defined as in the previous chapter.

In this chapter the forces of adsorption will be discussed and theoretical models will be used to estimate the expected binding energies of the systems which have been experimentally investigated in the present work.

## 2.1 ADSORPTION FORCES

As is pointed out in the classic work on adsorption by de Boer (1950), it is important to realise that the intermolecular forces which lead to adsorption are no different from those which exist within bulk material. Even more, the forces are all of the same electronic nature and may be derived from the wave equations describing the atoms. However a categorisation of the forces is expedient, but it must be remembered that the division lines are somewhat arbitrary.

The forces of adsorption may first be classified into those of chemisorption and those of physisorption:

Chemisorption may be defined as that in which electron exchange or sharing takes place and therefore includes inter-ionic bonding and covalent linking. Chemisorption usually leads to high values of binding energy; 1-10 eV per bond would be typical.

Physisorption is usually a much weaker form of bonding, and a bond energy of 0.1 eV would be typical. In physisorption, which is also known as van der Waals' adsorption for historical reasons, the atoms or molecules retain their individual characters and the adsorption is usually reversible.

It has been pointed out in the previous chapter that the aim of the present work is to study weak interfacial bonding since, as will be seen later, the adsorption forces operating in this type of bonding are of a universal nature and are present in any and every atomic and molecular interaction. An understanding of this system is therefore a prerequisite to an understanding of adhesion phenomena in general. Weak interfacial bonding is due to the forces of physisorption and it is because of the reversible nature of this adsorption process that the mechanical stripping method of measuring adhesion, which is described in a later chapter, can be applied. Physisorption only is expected in the thin film systems of gold and similar metals on glass and rocksalt substrates; it is necessary to examine this type of adsorption in more detail to estimate the degree of binding to be expected.

## 2.2 PHYSISORPTION

The forces of physisorption are due to interactions between electric dipoles or higher multipoles ; these dipoles originate from the oscillating charge systems of electrons and protons within atoms and molecules. In general, although there are notable exceptions, the interaction energy increment decreases rapidly with the order of multipole, so that only dipole-dipole interactions are significant. We will therefore be concerned mainly with interactions of this type.

First consider the interaction between two dipoles represented, in Fig. 2.1(a), by positive charges +e at the origin and $\underline{R}$, and negative charges -e at $\underline{r}_1$ and $\underline{r}_2$ respectively relative to their positively charged partners. If $\underline{R}$ lies along the z-axis so that

$$\underline{R} = (0, 0, Z),$$

$$\underline{r}_1 = (x_1, y_1, z_1),$$

$$\text{and } \underline{r}_2 = (x_2, y_2, z_2),$$

then the interaction energy is given by (Appendix 1.1):

$$W = \frac{e^2}{R^3}\,(x_1x_2 + y_1y_2 - 2z_1z_2) \qquad \ldots.(2a)$$

provided $\left|\underline{r}_1\right| + \left|\underline{r}_2\right| \ll \left|\underline{R}\right|$

A polar molecule is one which has a permanent net dipole moment. Along any diameter of an atom which is not externally influenced, the electron probability density is symmetrical with respect to the centre and therefore the atom is non-polar, although it may form a multipole of higher order. Interactions between atoms or molecules depend on whether they are polar or

# FIG. 2.1

## GEOMETRIES FOR CALCULATIONS OF DIPOLE INTERACTIONS

fig 2.1(a)

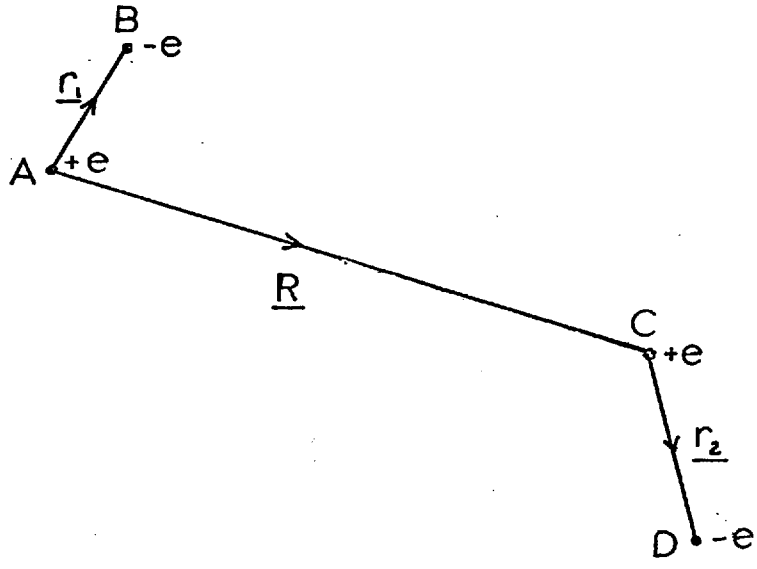


fig 2.1(b)

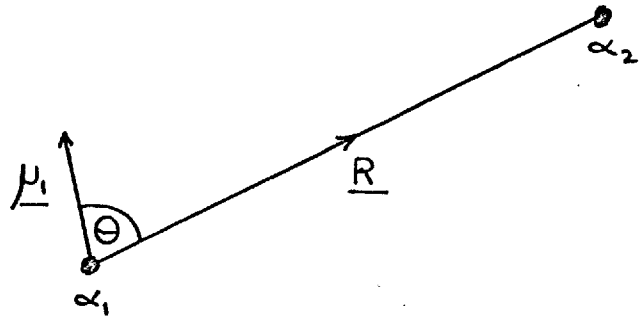

non-polar and may be classified into three types:

i) Polar - polar (Keesom effect)

ii) Polar - non-polar (Debye effect)

iii) Non-polar - Non-polar (London effect)

2.2.1. Keesom effect

This effect is due to interactions between polar molecules. The energy of interaction is given by eqn.(2a); if the dipoles are free to rotate, then they will take up the orientation of least energy, i.e. with $x_1 = y_1 = x_2 = y_2 = 0$ and $z_1$ and $z_2$ with the same sign. Since the dipole moments are $\mu_1 = ez_1$ and $\mu_2 = ez_2$, the interaction energy is then

$$W_K = - \frac{2\mu_1\mu_2}{R^3} \qquad \ldots.(2b)$$

Because the interaction tends to align the dipoles, it is also known as the alignment or orientation effect. The natural thermal rotation of molecular dipoles leads to repulsion as well as attraction, but the attractive orientations which are of lower energy are statistically preferred. According to Boltzmann statistics the net interaction energy is given by:

$$W_K = - \frac{2\mu_1^2\mu_2^2}{3kT\,R^6} \qquad \left[\frac{\mu_1\mu_2}{R^3} \ll kT\right] \qquad \ldots.(2c)$$

At low temperatures, when thermal disordering is insignificant, the net interaction is predictably given by eqn.(2b).

2.2.2. Debye effect

Before discussing the Debye effect it is necessary to introduce the concept of polarisability of an atom. A non-polar atom consists of a nucleus surrounded by a mobile electron

cloud. At any moment, an atom has a net dipole moment which is the vector sum of all the individual moments. But this net dipole moment normally has a time-averaged value of zero, because of the symmetry of the electron configuration. This can be seen by considering the similarity between dipole moment and mechanical moment, and in an undisturbed atom the centre of gravity is at the nucleus.

When an atom is placed in an electric field, the electrons and protons experience forces in opposite directions. The symmetry is then destroyed and a net non-zero dipole moment results. The polarisability of an atom is defined by the value of the resulting dipole $\mu$ and the polarising field E:

$$\mu = \alpha \underline{E}$$

Similarly an already polar molecule will acquire an additional dipole moment by this effect.

The Debye effect takes place between a polar molecule and a non-polar molecule or atom. The former induces a dipole in the latter. Hence the alternative name of the induction effect. Consider a polar molecule of moment $\mu_1$ and polarisability $\alpha_1$ at $\underline{R}$ from a non-polar molecule of polarisability $\alpha_2$ (Fig. 2.1(b)). If $\mu_1$ is at $\theta$ to $\underline{R}$, so that the field due to $\mu_1$ acting on the non-polar molecule is

$$E = \frac{\mu_1}{R^3} ( 1 + 3 \cos^2\theta )^{\frac{1}{2}}$$

then the induced dipole $\mu_2$ is given by:

$$\mu_2 = \frac{\alpha_2 \mu_1}{R^3} ( 1 + 3 \cos^2\theta )^{\frac{1}{2}}$$

The interaction energy $W_D$ is given by a relation of the familiar form ½ stress X strain:

$$W_D = -\tfrac{1}{2}\alpha_2 E^2$$

$$= -\frac{\alpha_2 \mu_1^2}{2R^6}\,(1 + 3\cos^2\theta) \qquad \ldots.(2d)$$

$\theta$ varies as the polar molecule rotates, but because the cosine term is squared the interaction energy is always negative and hence the interaction is always attractive. The mean value of $W_D$ is given by:

$$W_D = -\frac{\alpha_2 \mu_1^2}{R^6} \qquad \ldots.(2e)$$

Between two polar molecules there is a reciprocal Debye effect as well as a Keesom effect.

2.2.3. London effect

This is also known as the dispersion effect since it is closely connected with the phenomenon of optical dispersion.

It has already been pointed out that the instantaneous dipoles present at any time in an atom have a net zero moment when averaged over a finite time because of the symmetry of the atom. But when two such atoms are a finite distance apart, the instantaneous dipoles in each of them interact: the electric field due to one of them will produce both an alignment effect and an induction effect in the other, and vice versa. The orientations which lead to attraction are energetically favourable and therefore predominate, resulting in a net attraction.

The interaction can be understood in terms of a simplified model of linear harmonic oscillators due to London (1937), as is

shown in Appendix 1.2. The interaction energy between identical molecules of polarisability $\alpha$ is given by:

$$W_L = - \frac{3h\nu_o\alpha^2}{4R^6} \qquad \ldots.(2f)$$

where $\nu_o$ is the characteristic frequency of the equivalent oscillators.

A similar treatment for the interaction between two atoms of polarisabilities $\alpha$ and $\alpha'$ and characteristic frequencies $\nu_o$ and $\nu_o'$ respectively predicts an interaction energy of:

$$W_L = - \frac{3h\alpha\alpha'\nu_o\nu_o'}{2R^6(\nu_o + \nu_o')} \qquad \ldots.(2g)$$

2.2.4. Summary of van der Waals' interactions

It can be seen that all the van der Waals' interactions lead to energies which vary as the inverse sixth power of the separation. Because it exists between even non-polar atoms, the London effect is present in every atomic and molecular interaction. When at least one of the molecules participating is polar, then the Debye effect will also contribute. Finally, when both molecules are polar, the above two effects are supplemented by the Keesom effect.

## 2.3. EXPECTED BINDING ENERGIES OF SOME SYSTEMS

We now wish to apply these physisorption formulae to some practical systems. The expected binding energies of silver and aluminium films on glass and alkali halide substrates have been calculated by Benjamin & Weaver (1959). The essential details of their treatment are given in the next section.

2.3.1. Benjamin & Weaver estimation of binding energies

The interaction energy given by eqn.(2g) is for a pair of otherwise isolated atoms. For adsorption on to a surface, there is an interaction between each atom of the adsorbing substrate and the adatom. If the density of atoms in the substrate is N per unit volume, then the total interaction energy is given by the integral of the pair interaction energy over the volume of the substrate:

$$E = -\int_V \frac{C\,N}{R^6}\,dV = -\frac{N\pi C}{6R_o^3} \qquad \ldots.(2h)$$

where $R_o$ is the equilibrium adsorption distance, and C is the dispersion constant given by (from eqn.2g):

$$C = \frac{3h\,\alpha\alpha'\,\nu_o\nu_o'}{2(\nu_o + \nu_o')} \qquad \ldots.(2i)$$

The attraction between a non-polar adatom and an ionic substrate is due to an induction effect as well as to a dispersion effect, but the former is comparatively small (in the cases considered) and may be neglected. Similarly, quadrupole and higher multipole interactions may be neglected.

For the adsorption on to glass, the crystalline silica network described by Zachariasen (1932) was used to deduce the density of adsorbing centres; for this purpose the oxygen ions were assumed to be the adsorbing species since they have a larger polarisability than the silicon ions. A value of $N = 6.05 \times 10^{22}$ $cm^{-3}$ was found. The polarisability of oxygen ions was taken from Van Vleck (1932) and the polarisabilities of

neutral atoms were calculated from:

$$\alpha = \frac{e^2}{4\pi^2 m \nu_o^2} \qquad \ldots\ldots(2j)$$

which is implicit in the simplified London dispersion model of Appendix 1.3. Since the characteristic frequencies of most metals are not known, the usual approximation (London 1937) of employing the frequency equivalent of the first ionisation potential was made. The equilibrium adsorption distance was taken as the mean of the distances of closest approach of atoms in the metal and of ions in the substrate.

The values obtained by Benjamin & Weaver are shown in Table 2.1 together with values for gold on glass and copper on glass obtained by the same method.

The same authors used a similar treatment to estimate the adsorption energies of metals on alkali halide crystal faces. It was assumed, after Orr (1939), that the most favourable position for adsorption on a (100) face is above the centre of a lattice cell; adsorption by each of the crystal ion species must then be considered. The equilibrium adsorption distance was assumed to be governed by the size of the larger ion.

Having stated this as their method, it is not clear how Benjamin & Weaver have obtained their adsorption values, some of which are shown in Table 2.2. They appear to have treated the substrate as composed of NaCl adsorbing centres, each having a polarisability equal to the sum of the polarisabilities of the component ions. The source of the ionisation potential used is less clear. Furthermore, a value of N corresponding to

TABLE 2.1

ADSORPTION ENERGIES OF METALS ON GLASS

(after Benjamin & Weaver)

| | Al | Ag | Au | Cu | $O^{2-}$ |
|---|---|---|---|---|---|
| Polarisability $\alpha$ ($10^{-24}$ $cm^3$) | 3.04 | 1.90 | 1.29 | 1.83 | 3.88 |
| Ionisation potential ($10^{-12}$ erg) | 9.60 | 12.15 | 14.70 | 12.35 | 88.0 |
| Dispersion constant C ($10^{-60}$ erg $cm^6$) | 153 | 117 | 94.4 | 111.5 | |
| Closest approach (Å) | 2.86 | 2.89 | 2.88 | 2.56 | 2.6 |
| Equilibrium adsorption distance (Å) | 2.73 | 2.75 | 2.74 | 2.58 | |
| Adsorption energy (eV $atom^{-1}$) | 0.148 | 0.122 | 0.091 | 0.129 | |

( 1 eV $atom^{-1}$ = $1.6 \times 10^{-12}$ erg $atom^{-1}$ = 23 kcal $mole^{-1}$ )

TABLE 2.2

ADSORPTION ENERGIES OF METALS ON ROCKSALT

(after Benjamin & Weaver)

| | Al | Ag | Au | Cu | NaCl |
|---|---|---|---|---|---|
| Polarisability $\alpha$ ($10^{-24}$ cm$^3$) | 3.04 | 1.90 | 1.29 | 1.83 | 3.27 |
| Ionisation potential ($10^{-12}$ erg) | 9.60 | 12.15 | 14.70 | 12.35 | 16.4 |
| Dispersion constant C ($10^{-60}$ erg cm$^6$) | 90.4 | 65.1 | 49.1 | 63.4 | |
| Equilibrium adsorption distance (Å) | 2.00 | 2.00 | | | |
| Adsorption energy (eV atom$^{-1}$) | 0.165 | 0.117 | 0.087 | 0.148 | |
| Adhesion energy (erg cm$^{-2}$) | 334 | 238 | 176 | 300 | |

individual ions, rather than pairs, has been used. And the equilibrium adsorption distances given are too small, according to the calculations in the next section.

In a later paper (Benjamin & Weaver 1963), the adsorption energies for the same systems have been expressed as energy per unit area of crystal face; these values also are shown in Table 2.2.

2.3.2. Validity of the Benjamin & Weaver treatment

The steps in the Benjamin & Weaver treatment will now be examined.

Integration. The use of the Polanyi-London integral assumes that the substrate appears, to the adsorbed atom, as an adsorbing homogeneous continuum. This is satisfied only if $R_o \gg {}^{1}/_{N}{}^{1}/_{3}$, which is not so for the systems under consideration. A better method is to sum the interaction energies of the adatom with each of the adsorbent atoms within a given radius of the adsorption site, and then to add the integrated contributions from adsorbent atoms beyond this radius. The effect of this procedure is illustrated by an example from de Boer: for argon on smooth graphite, direct application of eqn.(2h) leads to an adsorption value of 0.027 eV, whilst summation over the nearest 24 carbon atoms and integration over the rest gives a value of 0.083 eV, which is in better agreement with the expermental value of 0.096 eV.

Induction. In the cases considered, the neglect of induction effects does not greatly prejudice the treatment. Their influence is little because the inducing electrostatic field

emanating from the surface of an ionic solid is usually very small; the heterogeneous nature of the charge distribution leads to a field which is much smaller than the field due to one surface ion alone. This is well illustrated by the adsorption of argon on to a cubic face of potassium chloride. The induction effect promotes adsorption above one of the surface ions, where the electric field is largest; the dispersion effect promotes adsorption above the centre of a lattice cell where the adatom is closest to the largest number of adsorbent atoms, although in this position the electric field is zero and there is no induction effect. That the latter position is the preferred adsorption site (Orr 1939) demonstrates the lack of influence of the induction effect.

Higher multipoles and repulsion. According to de Boer, the interaction energy of dipole-quadrupole, quadrupole-quadrupole, and even higher multipoles will usually amount to 15-30% of the dipole-dipole energy. However, the energy involved in neglecting these terms is largely offset by a second error in neglecting the repulsion energy of the interaction!

There is an expression, often quoted in ionic crystal theory, which shows that the energy of interaction between an attractive and a repulsive force, which vary as the inverse p th and n th powers respectively of the separation of the atoms or ions concerned, is given by:

$$E = -\frac{a}{R^p}\left(1 - \frac{p}{n}\right)$$ where a is a constant

i.e. the gross attraction energy is reduced by a factor p/n due to repulsion forces. If we use eqn.(2h) for the attraction energy,

then p = 3. For the short range repulsion forces, a typical value of n is 10, hence these forces reduce the total interaction energy by approximately 30%.

The net error involved in neglecting both high multipole interaction energies and repulsion energies is therefore much smaller than the error involved in neglecting either one alone.

Adsorption distance. A further error is introduced by the method used to obtain the equilibrium adsorption distances. The net attraction force between two atoms or ions, and hence their equilibrium separation, can vary appreciably according to their surroundings. For example, the equilibrium separation of the sodium and chlorine ions in an isolated molecule is only 88% of their separation in the ionic crystal, where the net attraction forces are smaller because of the heterogeneous charge distribution.

In the present case, the use of the bulk value for the effective size of a single physisorbed metal atom is not a serious error because the binding is comparatively weak in both cases and thus the effective sizes will be very similar; any change in attraction interaction causes a proportionately much smaller change in separation because of the strong separation dependence of the repulsive interaction.

However, since the surface adsorption energy varies approximately as the inverse third power of the adsorption distance, an x% error in distance results in a 3x% error in adsorption energy.

Adhesion energy. It is not sufficient to multiply the adsorption energy of a single adatom by the density of surface adsorption sites to obatin an adhesion energy per unit area. London has demonstrated the additivity of dispersion interactions, i.e. that

the interaction between two molecules is virtually unaffected by the influence of a third molecule. But in the case of gold, silver, and copper adatoms, the interaction between adjacent adatoms is not only a dispersion effect; Ackerman et al. (1964) have shown that each of these materials form strong covalent bonds between pairs, considerably modifying their wave functions, although the interatomic bonding becomes weaker as the pair is joined by more atoms and the island progresses towards the bulk metal.

Furthermore, the density of adatoms is not well known. The interface structure results from a compromise between the "natural" structure of the condensate and the influence of the adsorbing surface. However, since we have no better method of calculating adhesion energies, we can use only this approach but values so obtained must be treated as very approximate.

Characteristic frequency and polarisability. There is a tacit assumption in the application of the simple London dispersion equation (eqn.2g) to real systems. The equation was derived for a system of a single electron orbing a nucleus. Real atoms consist of many such electrons and can be considered as an assembly of many different harmonic oscillators, each having a corresponding characteristic frequency (London).

The connection between the London effect and optical dispersion phenomena has already been noted, and in the latter case one similarly encounters, in theoretical treatments, an assembly of oscillators. However, the dispersion curves of many simple gases can be represented empirically, in a large frequency interval, by a dispersion formula with one frequency only. This is the basis of the application of eqn.(2g) to real systems.

Values of characteristic frequency $\nu_o$ and polarisability $\alpha$ are required to evaluate the interaction energy. London found that the frequency equivalent of the first ionisation potential of many simple gases is very close to the characteristic frequency determined from optical measurements, as is shown in Table 2.3. Furthermore, it can be seen from eqn.(2i) that the resulting error in the dispersion constant C is always less than the error in $\nu_o$. But the approximation is clearly untenable for doubly ionised atoms such as $O^{2-}$ which have a negative ionisation energy. What is needed in these cases is an effective ionisation energy in the lattice. The problem is similar, though less obvious, for singly charged ions.

Benjamin & Weaver used the simple oscillator model to predict the polarisabilities of neutral atoms. Again the characteristic frequency is involved, so if the ionisation energy is substituted for this parameter, the above comments apply. When it is possible to compare the predicted polarisability with experimentally determined values, the agreement is only moderate and deteriorates with increasing atomic number, as can be seen in Table 2.3. The poor agreement results from a misapplication of the oscillator model: as we have already pointed out, a real atom consists of many electrons and there is a contribution to the polarisability from each of these. It is not sufficient to multiply the one-electron polarisability (eqn.2j) by the atomic number because the inner shell electrons are very tightly bound to the nuclear core and are little affected by polarising electric fields; hence their contribution to the atomic polarisability is small. An inspection of the gas polarisabilities in Table 2.3 shows that a better

TABLE 2.3

CHARACTERISTIC FREQUENCIES & POLARISABILITIES

| Atom | Atomic number | $h\nu_I$ eV | $h\nu_o$ eV | $\alpha$ exper. | $\frac{e^2}{4\pi^2 m\nu_I^2}$ | $\frac{Z^{\frac{1}{2}} e^2}{2^{\frac{1}{2}} 4\pi^2 m\nu_I^2}$ |
|---|---|---|---|---|---|---|
| He | 2 | 24.5 | 25.5 | 0.20 | 0.18 | 0.18 |
| Ne | 10 | 21.5 | 25.7 | 0.39 | 0.25 | 0.56 |
| Ar | 18 | 15.4 | 17.5 | 1.63 | 0.47 | 1.41 |
| Kr | 36 | 13.3 | 14.7 | 2.46 | 0.62 | 2.63 |
| Xe | 54 | 11.5 | 12.2 | 4.00 | 0.83 | 4.32 |
| Al | 13 | 5.99 | | | 3.04 | 7.74 |
| Cu | 29 | 7.72 | | | 1.85 | 7.04 |
| Ag | 47 | 7.58 | | | 1.92 | 9.40 |
| Au | 79 | 9.2 | | | 1.3 | 8.16 |
| $Na^+$ | "10" | 47.3 | | 0.22 | 0.05 | 0.11 |
| $Cl^-$ | "18" | 4.00 | | 3.00 | 6.87 | 20.6 |

$\alpha$ of gases : Pauling (1927)

$h\nu_I$, $h\nu_o$ of gases : London (1937)

$h\nu_I$ of metals : Leighton (1959)

$\alpha$ of ions : Böttcher (1943)

$h\nu_I$ of $Na^+$ : Richtmeyer et al. (1955)

$h\nu_I$ of $Cl^-$ : Dekker (1963)

approximation is given by:

$$\alpha = \left(\frac{Z}{2}\right)^{\frac{1}{2}} \frac{e^2}{4\pi^2 m \nu_I^2} \qquad \ldots.(2k)$$

This empirical multiplying factor has little justification other than that it produces results in reasonable agreement with experiment.

Not surprisingly, in view of our previous remarks about the characteristic frequencies of ions, the polarisabilities of ions obtained with either eqn.(2j) or eqn.(2k) using ionisation potential data are not in good agreement with experimentally determined values.

So we still require reliable values of the characteristic frequencies of ions, to determine the relevant adsorption energies.

There is yet a further difficulty in dealing with ions: Mayer (1933) has shown that, for the rare-gas-like ions, one is not justified in using a single frequency for the dispersion relation. By using a treatment which is beyond the scope of the present discussion to deal with the assembly of oscillators, Mayer has obtained values for the dispersion constants of $Na^+$-$Na^+$, $Cl^-$-$Cl^-$, and $Na^+$-$Cl^-$ interactions. These values are shown in Table 2.4 together with corresponding values obtained using a single frequency derived from the ionisation potentials; it can be seen that the agreement is not very good.

There are other expressions for the dispersion energy. One of these is the Kirkwood-Muller equation (Muller 1936):

$$E = \frac{6mc^2}{R^6} \frac{\alpha\alpha'}{\left(\alpha/\chi + \alpha'/\chi'\right)}$$

TABLE 2.4

DISPERSION CONSTANTS OF ION INTERACTIONS

(in units of erg $cm^6$ x $10^{-60}$)

| | $Na^+$-$Na^+$ | $Cl^-$-$Cl^-$ | $Na^+$-$Cl^-$ |
|---|---|---|---|
| Mayer | 4.28 | 176-206 | 28.5 |
| Kirkwood-Muller | 5.50 | 298 | 33.8 |
| Single frequency model (using ionisation frequencies) | 1.72 | 27.0 | 5.84 |

where $\chi$ and $\chi'$ are the atomic diamagnetic susceptibilities. This expression, which is semi-empirical and relies on the similarity between the mechanisms of electric and magnetic polarisation, has been found to give very good agreement between calculated and experimental values of rare gas interaction energies and adsorption energies on alkali halides (Orr). However, the expression is rejected by de Boer; he considers that the interaction of electrons with a magnetic field is too different from the interaction producing dispersion forces.

If we apply the Kirkwood-Muller expression to calculate ion interaction energies, the agreement with Mayer's values is quite reasonable (Table 2.4).

We have seen that dispersion energies of ion interactions, calculated from the single frequency model, are subject to serious errors. However, we can make a better approximation by using values derived from Mayer's values of the dispersion constants (Table 2.4) as effective characteristic frequencies for the ions. The sodium-sodium and chlorine-chlorine dispersion constants yield effective characteristic energies of 73.8 eV and 28.3 eV respectively. These values are consistent with the $Na^+$-$Cl^-$ data, for they yield a dispersion constant value of $32.8 \times 10^{-60}$ erg $cm^6$, compared with Mayer's value of $28.5 \times 10^{-60}$.

It appears from the above considerations that the error involved in neglecting induction effects, repulsion effects, and high multipole interactions is not very great, but that there are larger errors involved in not considering the discrete nature of the adsorbent and in using too simple a model to calculate polarisabilities and characteristic frequencies, particularly when ions

are concerned. We are now in a position to reevaluate the adsorption energies of current interest, with the aid of both the London and Kirkwood-Muller equations, taking these problems into account.

2.3.3. Metals on glass.

In considering the adsorption of metals on to such amorphous adsorbents as glass, it is not possible to carry out a $\sum(1/r^6)$ calculation; Benjamin & Weaver were therefore justified in using the Polanyi-London integral. Furthermore, their neglect of the contribution of the silicon ions to the total adsorption interaction introduces virtually no error because the polarisability of silicon ions is about one hundred times smaller than that of oxygen ions.

We could calculate the adsorption energy using the modified atomic polarisability values suggested in the last section but we are unable to suggest a more reliable value for the characteristic frequency of the oxygen ions, and there is thus little to be gained.

However, we have all the information required to apply the Kirkwood-Muller equation. The values thus obtained are shown in Table 2.5 (no values for the diamagnetic susceptibility of paramagnetic aluminium were found in the literature), and it can be seen that these are all somewhat larger than the values obtained by Benjamin & Weaver.

The adhesion energies per unit area of interface have been obtained by multiplying the single adatom adsorption energy by the density of adatoms, assuming close packing. These values are very

TABLE 2.5

ADSORPTION ENERGIES OF METALS ON GLASS

| | Ag | Cu | Au | $O^{2-}$ |
|---|---|---|---|---|
| Polarisability $\alpha$ ($10^{-24}$ $cm^3$) | 9.40 | 7.04 | 8.16 | 3.88 |
| Diamagnetic susceptibility $\chi$ ($-10^{-29} cm^3$) | 3.24 | 0.98 | 4.66 | 2.3 |
| Dispersion constant C ($10^{-60}$ erg $cm^6$) | 393 | 142 | 455 | |
| Adsorption distance (Å) | 2.75 | 2.58 | 2.74 | |
| Adsorption energy (eV $atom^{-1}$) | 0.37 | 0.16 | 0.44 | |
| Adhesion energy (ergs$cm^{-2}$) | 783 | 384 | 938 | |

Polarisabilities of atoms: Table 2.3, column 7; of ions: Pauling(1927)

Susceptibility of $O^{2-}$: Bozorth (1951)

approximate, as was explained in the last section.

2.3.4. Metals on rocksalt.

When we are considering adsorption on a (100) rocksalt face, we are able to consider the discrete nature of the adsorbent. If the adatom is adsorbed above the centre of a lattice cell, and if $\sum(1/r^6)$ is the sum of the inverse sixth powers of the distances of the adsorbed atom from each ion of the adsorbent, then the total interaction energy is given by:

$$E = \tfrac{1}{2} C_+ \sum \frac{1}{r^6} + \tfrac{1}{2} C_- \sum \frac{1}{r^6}$$

where $C_+$ and $C_-$ are the dispersion constants of the adatom-anion and adatom-cation interactions respectively.

The quantity $\sum(1/r^6)$ has been evaluated by Orr, summing over at least the nearest 250 points and integrating over the rest. The dispersion constants have been evaluated by both the London and the Kirkwood-Muller equations. The amended (atomic number weighted) polarisabilities given in Table 2.3 and calculated from eqn.(2k), have been used for the neutral atoms, and the ion characteristic frequencies have been derived from Mayer's data, as explained above.

The equilibrium adsorption distance is governed by the size of the larger chlorine ion. The separation of chlorine ions in the surface is 3.98 Å, so that if the adatom radius is r, then the adsorption distance $R_o$ is given by:

$$R_o^2 = (1.81 + r)^2 - 1.99^2$$

The adhesion energies per unit area of interface were obtained by multiplying the single atom adsorption energy by the density of adsorption sites; all of the comments made above about this

procedure apply.

The adsorption values obtained are given in Table 2.6, and it can be seen that the two derivations give values in very good agreement for copper, and agree within a factor of about two for gold and silver.

2.3.5. Further considerations

There are some further difficulties in the calculation of adsorption energies which we have so far ignored, but most of these are 'second generation' problems and beyond the scope of the present treatment.

The London dispersion model breaks down at both long and short distances. At large atom separations, the finite velocity of electromagnetic waves introduces phase problems in the oscillating charge systems, reducing their mutual attraction. But this phenomenon, known as electromagnetic retardation, is not important in the present case. But the model also breaks down at short distances, when the atom separation becomes comparable with the dipole length- in the London derivation (Appendix 1.3), it is assumed that the former is very much greater than the latter. The argument of the derivation breaks down because it is then no longer true that the polarising field due to one atom is homogeneous throughout the other. This obviously affects induction in a similar way. For example, argon is preferentially adsorbed on a cubic face of potassium chloride above the centre of a lattice cell. At this point there is no electric field and thus, according to our simple model, no induction effect. But the adsorbed argon atom has a finite size, and not all of it can be exactly above the lattice cell centre. As a result, there is an induction effect

TABLE 2.6

ADSORPTION ENERGIES OF METALS ON ROCKSALT

| | Al | Ag | Au | Cu | $Na^+$ | $Cl^-$ |
|---|---|---|---|---|---|---|
| $\alpha$ ($10^{-24}cm^3$) | 7.74 | 9.40 | 8.16 | 7.04 | 0.22 | 3.00 |
| Adsorption distance (Å) | 2.56 | 2.58 | 2.57 | 2.36 | | |
| $\sum(1/r^6)$ ($10^{45}$ $cm^{-6}$) | 4.48 | 4.38 | 4.42 | 5.21 | | |
| London: | | | | | | |
| Characteristic energy ($10^{12}$erg) | 9.60 | 12.15 | 14.70 | 12.35 | 118.2 | 45.3 |
| Dispersion const. ($10^{-60}$erg $cm^6$): | | | | | | |
| $C_+$ | 21.8 | 31.9 | 33.0 | 24.2 | | |
| $C_-$ | 134 | 173 | 163 | 132 | | |
| Adsorption energy (eV) | 0.22 | 0.28 | 0.27 | 0.25 | | |
| Adhesion energy (erg $cm^{-2}$) | 445 | 572 | 551 | 517 | | |
| Kirkwood-Muller: | | | | | | |
| $\chi$ ($-10^{-29}cm^3$) | | 3.24 | 4.66 | 0.91 | 1.01 | 4.03 |
| $C_+$ | | 32.6 | 45.0 | 9.58 | | |
| $C_-$ | | 381 | 478 | 122.5 | | |
| Adsorption energy (eV) | | 0.57 | 0.72 | 0.22 | | |
| Adhesion energy (erg $cm^{-2}$) | | 1150 | 1470 | 437 | | |

Ion susceptibilities: Dekker (1963) Ion polarisabilities: Pauling

although it is quite small. Lenel (1932) has calculated an induction energy for this case of 0.016 eV compared with the dispersion energy of 0.065 eV. Lenel's experimentally determined value of the total adsorption energy was 0.090 eV.

We have ignored the true nature of the adsorbing surface, which was assumed to be flat and regular in all of the above calculations. This is never so, and defects such as charged or uncharged vacancies, interstitials, and steps, are formed. These defects can drastically alter the adsorption energy at those sites; preferential decoration of steps on alkali halide surfaces in thin film deposition is a frequently observed phenomenon (e.g. Stirland 1966). Such defects will be important when considering the adhesion of a continuous film only if there is a sufficient number of them. They are discussed further and illustrated in Chapter 4, section 4.2.6.3.

A further change in the adsorbing surface has been described by Verwey (1946); According to his calculations for sodium chloride, the surface chlorine ions are displaced 0.05 Å away from the sodium ions beneath them, whilst the sodium ions in the outer layer are similarly displaced 0.15 Å inwards. However, the effect of the electric double layer consequently formed is nearly compensated by the effect of the dipoles set up in the outer plane of negative chlorine ions.

Throughout this chapter, we have assumed that, in thin film evaporation deposition, the incident metal atoms are adsorbed as neutral atoms. But a gold ion on an ionic substrate would form a much stronger Coulombic bond and would be energetically preferred. This does not normally occur because the ionisation energy is too great compared with the thermal energy of the beam. But when the

deposit grows and becomes metallic there is then the possibility of free electron transfer to the substrate; this is discussed in more detail in Chapter V.

## 2.4. CONCLUSIONS.

The various mechanisms which produce the phenomena of physisorption have been discussed, and in view of the simplicity of the models used and the approximations made, it is surprising how good agreement is in those cases where theoretical and experimental data can be compared.

The adsorption energies of metals on glass and rocksalt substrates have been calculated by several methods. But it must be remembered that these are to be considered as approximate values; this is particularly so of the adhesion values obtained.

# CHAPTER III

# MICROCALORIMETRY

When a film is chemically dissolved from its substrate, the energy liberated is equal to the heat of solution of the film minus the energy of adhesion between film and substrate. An instrument which is potentially capable of measuring the very small heat changes involved is the microcalorimeter.

## 3.1. THE MICROCALORIMETER

Calorimeters using thermoelectric effects to measure small heat changes have been in existence for nearly half a century, but have been developed only comparatively recently. There are two main types of calorimeter:

a) In the first type the absolute temperature change in an enclosure due to a reaction is measured; this is, of course, the classic calorimeter method. The temperature change may be measured by a resistance thermometer (Westrum & Eyring, 1952), or a thermistor (Argue et al., 1961). A single temperature-sensing element is normally used, and so the temperature of the enclosure must be uniform; this is usually achieved by stirring the contents, and therefore this type of calorimeter is most suitable for liquids.

The inner enclosure is isolated as far as possible from its environment, which is usually a further enclosure controlled to $\pm 10^{-3}$ degC, and the calorimeter is therefore quasi-adiabatic. Corrections are made for the heat of stirring, for the heat generated in

the temperature-sensing element, and for the heat exchange between the enclosures. The heat capacity of the reaction enclosure is typically 10 cal $degC^{-1}$, and the temperature sensitivity $10^{-5}$ degC.

b) The second type of microcalorimeter relies on the heat flow between the inner and outer enclosures. This is achieved by using a symmetrical array of thermocouples between the enclosures; the thermocouples are thermally in parallel but electrically in series so that their individually small e.m.f.s. combine to form a measurable signal. The e.m.f. generated by a thermocouple and the heat flow along it are both proportional to the temperature difference between the junctions and hence to each other. Thus the e.m.f. is a measure of the heat flow from the inner enclosure at any time and the integral of the e.m.f. with respect to time is a measure of the total heat change.

Because of the symmetry of the thermocouple array and because of the additivity of the generated e.m.f.s. the individual heat outputs along each thermocouple are integrated; therefore this type of calorimeter can measure the total heat output from an enclosure which is not necessarily at a uniform temperature, and so is much more suitable for the sort of reaction that we wish to study. The calorimeter can also be used to study reactions with varying heat outputs over long periods. An instrument of this type was first produced by Tian (1923) and has been considerably developed by Calvet & Prat (1956, 1963). Several modified versions have since been built, including those of Attree et al. (1958), Benzinger & Kitzinger (1962), Benjamin & Benson (1962), Chavet (1963), and Hodges & Acherjee (1965).

One of Calvet's most important developments was the use of a differential arrangement. The accuracy of a thermocouple measuring device is limited by the temperature stability of the reference junction; but if the temperature difference between two points is measured by using two thermocouples electrically connected in opposition and measuring the net e.m.f. output, the accuracy of measurement is limited by the temperature difference of the reference junctions, which can be as small as $10^{-6}$ degC if the reference junctions are symmetrically arranged in an enclosure with a point variation of $\pm 10^{-3}$ degC. Using this arrangement, Calvet was able to develop a calorimeter which could measure heat outputs as small as 1μW (= 10 erg $sec^{-1}$), and was sufficiently stable to be used to study reactions occuring over periods of several months.

The construction of a calorimeter of this type was commenced, but before this had proceeded far, a commercial calorimeter of Calvet's design, made by the D.A.M. Co. of Lyons, France, and installed at Keele University, became available. The calorimeter is described in some detail in Appendix 2, where it is also shown that there is an error in Calvet's method of calculation for the optimum sensitivity of the instrument.

## 3.2. EXPERIMENTAL DETAILS

For comparison with the other methods of adhesion measurement described in this thesis, the gold-rocksalt system was used in the calorimeter. This system is convenient because the rocksalt can be dissolved in water without the evolution of gas, which would cause a pressure change in the reaction cell and hence an energy change which would have to be accounted for, adding an unnecessary

complication.

The D.A.M. calorimeter utilises glass reaction cells (Fig. 3.1.) of 1.0 cm internal diameter and 3.8 cm length, of which about 2.5 cm is useable. One of the reactants is contained in a glass phial which can be cracked by a central plunger, thus bringing the two reactants into contact and initiating the reaction; the plunger is operated mechanically through a long ($\simeq$ 1 m) teflon rod to ensure good thermal insulation. The two reaction cells used in the differential arrangement are known as the laboratory and reference cells.

By using a composite gold-rocksalt film consisting of alternate layers of the constituents, the interfacial area could be considerably increased, similarly increasing the total heat output. By measuring the heat of solution of n layers of gold and n layers of rocksalt in the laboratory cell differentially against the heat of solution of n layers of rocksalt and one layer of gold in the reference cell, it can be seen from Fig. 3.2 that the net output is given by:

$$\Delta E = A(n-1)\ (2E^{Au}_{NaCl} - E^{NaCl}_{NaCl} - 2\ E^{Au}_{H_2O}) \qquad \ldots\ldots(3a)$$

where A is the substrate area, and $E^{Au}_{NaCl}$, $E^{NaCl}_{NaCl}$, and $E^{Au}_{H_2O}$ are the adhesion energies per unit area at interfaces of gold-rocksalt, rocksalt-rocksalt, and gold-water respectively. Of the energy parameters, the first is the largest and is the parameter that we wish to measure; the other two can be measured in subsidiary experiments. Strictly, the solution after the reaction is a weak sodium chloride solution.

FIG. 3.1

MICROCALORIMETER REACTION CELL

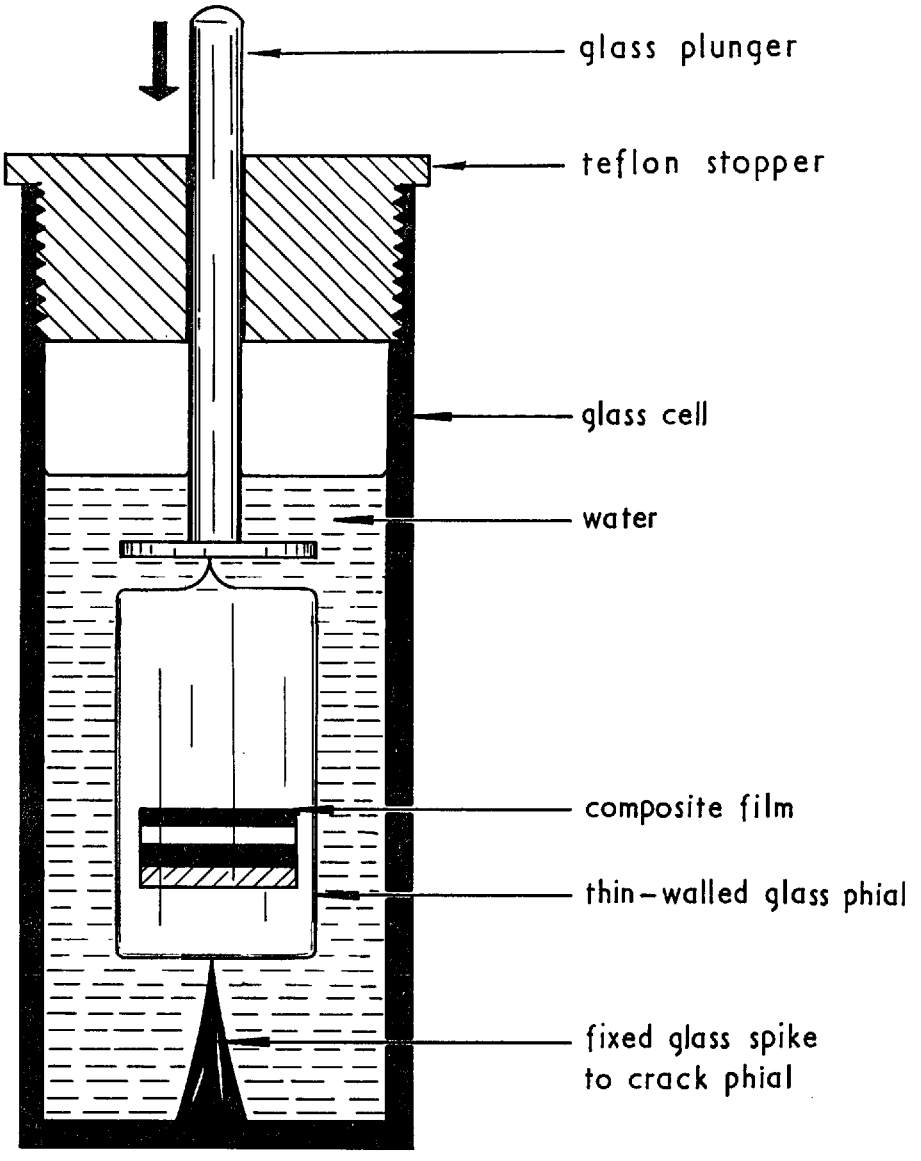

## FIG 3.2

## USE OF Na Cl - Au MULTILAYER FILMS FOR THE MEASUREMENT OF ADHESION ENERGY

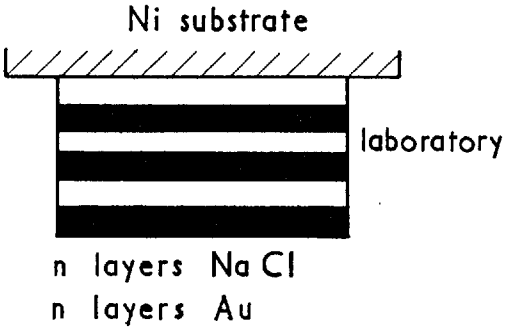


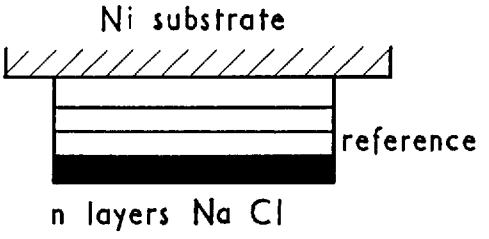


$$E_{lab.} = nE^{NaCl}_{cohesive} + E^{Ni}_{H_2O} + 2nE^{Au}_{H_2O} - E^{Ni}_{NaCl} - (2n-1)E^{Au}_{NaCl}$$

$$E_{ref.} = nE^{NaCl}_{cohesive} + E^{Ni}_{H_2O} + 2E^{Au}_{H_2O} - E^{Ni}_{NaCl} - (n-1)E^{NaCl}_{NaCl} - E^{Au}_{NaCl}$$

$$E = (n-1)\left( 2E^{Au}_{NaCl} - E^{NaCl}_{NaCl} - 2E^{Au}_{H_2O} \right)$$

3.2.1. Preparation of the composite films

Nickel substrates, of 0.65 cm diameter punched from sheet, were used for the preparation of the composite films since these could be handled magnetically without interfering with the films. The substrates were thoroughly washed in isopropyl alcohol and in distilled water before deposition. The rocksalt films were required to be as thin as possible to reduce the gross heat of solution, but continuous; the gold films were required to be continuous only. A thickness of 220Å for each film layer was chosen.

The experimental arrangement for the deposition of the composite films is shown in Fig. 3.3. Deposition was carried out at a pressure $\simeq 5 \times 10^{-5}$ torr in an oil diffusion pumped system with a liquid nitrogen trap. The nickel substrates were arranged in two groups of five on a magnetic substrate holder (it was recognised that the magnetic field could have influenced the growth of the film) so that the rotatable mask could cover one group of substrates when the mask was brought into the line of evaporation and the magnet was stationary in a given position.

The amount of material arriving at the substrates was measured with a quartz crystal film thickness monitor (Edwards High Vacuum Ltd.). Rocksalt was first evaporated to the required thickness on to all the substrates with the mask out of line and the substrate holder rotating to ensure a uniform deposit on all the substrates. The magnet was then stopped in the pre-determined position, the mask was rotated into position to cover one group of substrates, and gold was evaporated onto the second group; it was not necessary that the thickness of gold was identical on each substrate provided that it

FIG. 3.3

EXPERIMENTAL ARRANGEMENT FOR THE PREPARATION OF COMPOSITE GOLD-ROCKSALT FILMS ON NICKEL FOR USE IN THE MICROCALORIMETER

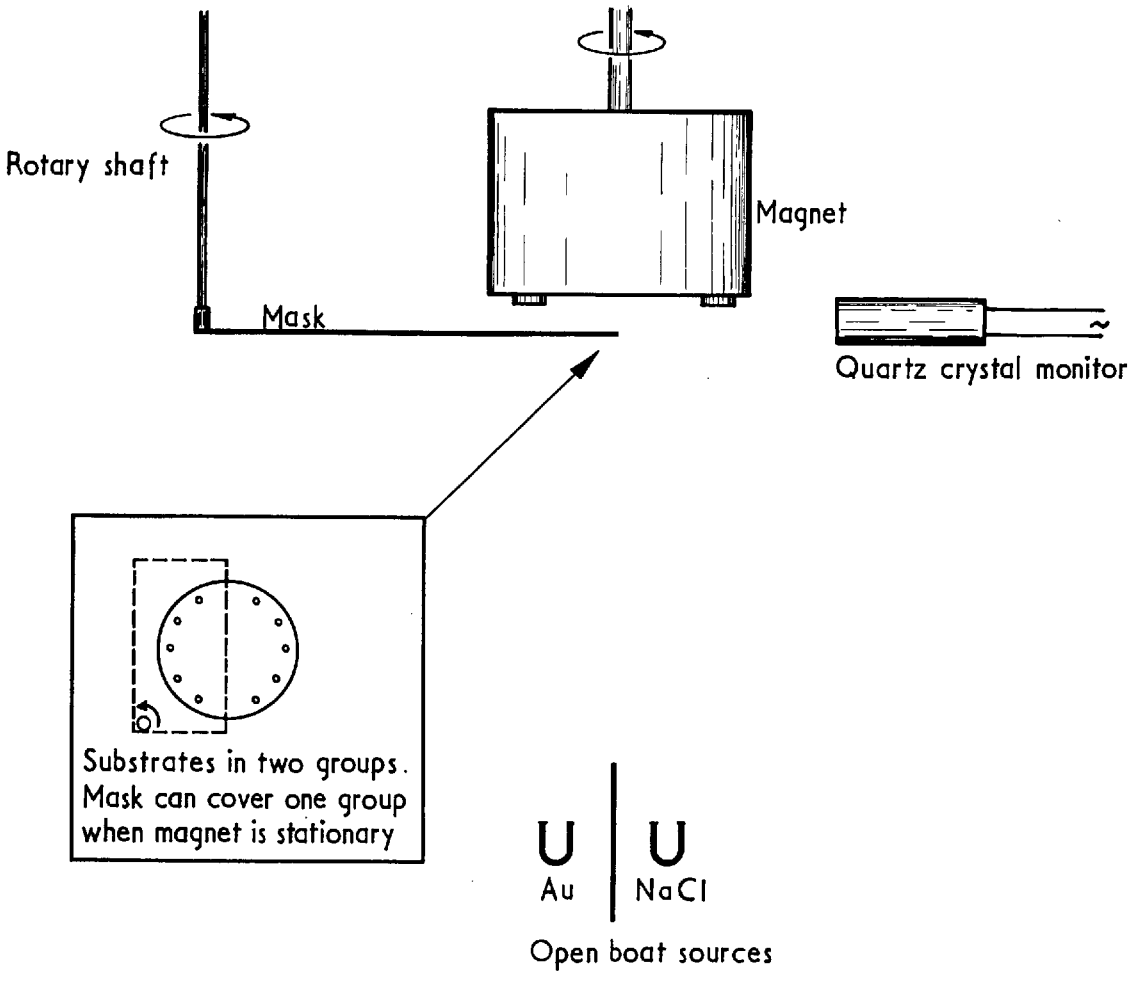

was continuous, since the gold was not dissolved.

This procedure was repeated until the required number of film layers had been deposited. The final layer of gold was deposited onto both groups of substrates to act as a protective layer for the rocksalt.

3.2.2. Encapsulation of samples

In the calorimeter, the composite films and solvent were separated, until the reaction was initiated, by encapsulating the films in glass phials of internal diameter 0.7 cm, wall thickness 0.1 cm, and overall length 1.5 cm (Fig. 3.4), made from a length of 'Kodial' glass tubing (Plowden & Thompson Ltd.). One end of each phial was drawn out to a fragile spike. The tubes were cleaned, to eliminate reactions between the water and any wall contaminants, by heating to 400°C for 4 hours.

Several substrates and films were placed in each phial, and the phials were then sealed by a thin glass membrane (blown from the same Kodial tubing) cemented to the phial with 'Araldite' (Ciba Ltd.). The joints were cured at room temperature for one day, and then at 100°C overnight, to render the cement inert to water.

3.2.3. Calibration of the microcalorimeter

The net e.m.f. from the calorimeter was fed to a sensitive suspension galvanometer, the deflection of which was recorded by a light-spot follower and pen recorder. The rate of heat flow from the calorimeter cells was proportional to the deflection of the galvanometer, and thus the total heat flow was proportional to the area under the recorded curve.

FIG. 3.4

GLASS PHIAL CONTAINING SPECIMENS FOR MICROCALORIMETRY

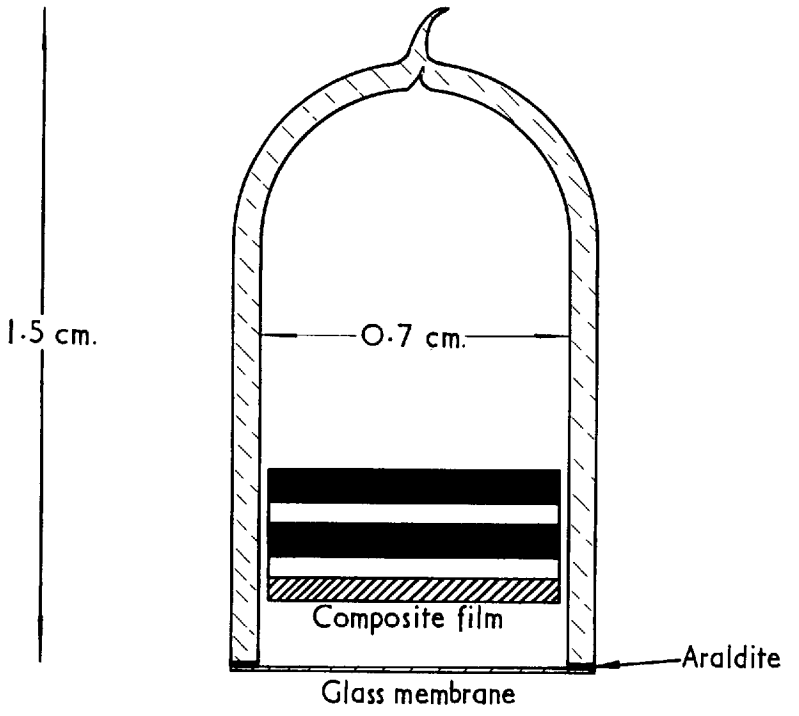

The calorimeter was calibrated by using the Joule heating effect in a wire-wound resistor in the laboratory cell; this gave values of 79.6 erg $sec^{-1}$ per mm galvanometer deflection and $2.90 \times 10^4$ erg per $mm^2$ under the recorded curve. The fluctuations of the experimental baseline were less than 0.1 mm over the observed periods of several hours, so the claimed sensitivity of 1 μW appeared to be justified.

## 3.3. RESULTS

The first experiment was carried out with 5 substrates in each phial, so that the total substrate area was 1.65 $cm^2$. The encapsulated samples were placed in their respective reaction cells together with 1 ml distilled water. The cells were then placed in their respective sockets in the calorimeter block; the small annular gaps around the cell were filled with dibutyl pthalate to ensure good thermal conductivity.

The calorimeter was left for several hours to come to equilibrium and establish a steady experimental baseline. The reaction was then initiated by depressing the plungers simultaneously and cracking the membranes and spikes of the phials.

In the first experiment, n = 12, and the total heat liberated was $1.79 \times 10^6$ erg. Substituting in equation (3a):

$$(2E^{Au}_{NaCl} - E^{NaCl}_{NaCl} - 2E^{Au}_{H_2O}) = 9.9 \times 10^4 \text{ ergs cm}^{-2}$$

If this is correct, then the minimum value of $E^{Au}_{NaCl}$ is $5 \times 10^4$ erg $cm^{-2}$ which is more than a hundred times greater than the value expected. Three further experiments were carried out with composite

films of 6 to 24 layers; all produced large outputs, and it was found that the glass phials were breaking rather irregularly.

Experiments were then carried out with empty glass phials to see if an identical pair produced a net zero output when broken in the calorimeter. The phials were prepared, cleaned, and sealed as before.

Carrying out the experiments as before, it was found that a net non-zero output was recorded in each case and that this value varied greatly, depending for example on how hard the plungers were depressed. This may not appear surprising, but experiment initiation by this method is referred to as a standard method by Calvet & Prat; they claim that thermal spikes due to the breaking of the phials are constant and measurable, and cancel out when used in the differential arrangement.

## 3.4. DISCUSSION

Clearly, there were parasitic phenomena occuring in the reaction cells, producing heat effects many times larger than those we wished to measure. It seems (Lafitte 1968) that there are three priv. comm.
likely sources of parasitic e.m.f:

The first is due to the friction of the glass plunger used to initiate the reaction, against the walls of the teflon stopper (Fig. 3.1). This perturbation can be reduced considerably by drilling out the stopper so that the plunger can pass through, touching the walls only very gently. The seal of the lid is then imperfect and as a result there is a slow but very regular evaporation of the liquid in the cell; this does cause the baseline of the galvanometer

deflection record to be continuously displaced, but only in a very regular and stable manner and therefore introducing no error.

The second is due to be breaking of the glass phial. If the phial is redesigned so that only the fragile spike breaks (i.e. with the thin glass membrane replaced by a stronger lid), then this thermal energy can be reduced to $\simeq 10^4$ erg; the difference between the breaking energies of the phials in the laboratory and reference cells would of course be much smaller.

The third of these parasitic phenomena is due to the evaporation of a quantity of the solvent sufficient to maintain the equilibrium partial pressure of the vapour above the liquid. The initial volume $\gamma$ of the vapour is expanded to $\gamma+\delta$ by the experimental process, where $\delta$ is the dead volume of the phial. The magnitude of this phenomenon is proportional to $\delta$ and is $\simeq 10^6$ erg $ml^{-1}$ when the solvent is water. The error so introduced can be eliminated by making a standardising curve with an empty phial, measuring the thermal effect as a function of the dead volume of the phial, or by measuring the effect on a standard empty phial and then carrying out all further experiments with phials of the same dead volume, which is equivalent to using pairs of laboratory and reference phials with equal dead volumes in the differential arrangement.

A further source of spurious output may be due to inaccurate compensation by the reference sample for the heat of solution of the rocksalt due to different amounts of rocksalt in the two cells; The first layer of rocksalt was deposited onto gold in the laboratory sample, but onto rocksalt in the reference sample; any difference in condensation coefficient would result in different film thicknesses

for the same amount of incident material. This could be eliminated by substantially cooling the substrates during deposition so that the condensation coefficient is uniformly unity.

## 3.5. CONCLUSION

The calorimetry approach to the determination of adhesion energies was beset with difficulties; theoretically the difficulties might have been overcome, but they were numerous and required tedious or technically difficult solutions. Most of the problems arose because we were trying to use the microcalorimeter beyond its limit. This particular approach to the measurement of thin film adhesion is attractive because of its versatibity, but is seems that the microcalorimeter must first be further developed. There is, of course, considerable scope for improvement; a more suitable experiment initiation method would be a great improvement.

# CHAPTER IV

# NUCLEATION & GROWTH

## 4.1. THEORIES OF NUCLEATION

The condensation of a vapour beam on to a substrate depends on the formation and growth of nuclei (groups of atoms) of the condensate. For a given incident vapour flux, the formation rate of nuclei of a given size exceeds their decay rate only if the nuclei are above a certain critical size; this is because the stability of a nucleus increases rapidly as its size increases from a single atom to a large cluster. The term "nucleation" refers to the establishment of stable nuclei, i.e. those with a greater chance of growing than of decaying.

There are two distinct ways of theoretically considering the kinetics of nucleation and growth: the capillarity model and the atomistic model.

According to the capillarity model, the nuclei are treated as homogeneous and are ascribed macroscopic thermodynamic properties in order to estimate their free energies of formation. This model obviously has serious limitations for small nucleus sizes.

The atomistic model is presented in terms of energy parameters relating to individual atoms rather than to groups, and is therefore particularly applicable to nuclei containing only a few atoms.

These two approaches to nucleation theory have been manipulated into forms which may be directly compared (Lewis 1967), and it was concluded that the atomistic model is usually more

suitable, particularly since critical nuclei are seldom larger than two atoms. This model has therefore been used exclusively throughout this chapter.

## 4.2 THE DEVELOPMENT OF THE ATOMISTIC MODEL

The formation processes, i.e. nucleation and growth, of a thin film are governed by several energy parameters (Fig.4.1a):

i. The adsorption energy $E_a$ of a single atom to the substrate

ii. The surface diffusion energy $E_d$; this is the energy required for an adatom to move between adjacent adsorption sites.

iii. The binding energy per atom $E_i$ of adatoms in a nucleus of i atoms.

The adsorption and diffusion energies can also be described in terms of an energy diagram of the substrate (Fig.4.1b): the adsorption sites of depth $-E_a$ relative to the vacuum level are periodically separated by an energy barrier of amplitude $E_d$.

The foundation of the atomistic model is the classic work of Frenkel (1924), in which a condition for condensation was derived. The development of the theory has subsequently received considerable attention, notably that of Walton (1962). Two features which have been of particular interest are nucleation rate and the time-dependence of island density.

In the formation of a thin film deposit, the island density $n_s$, i.e. the number of discrete nuclei or groups of atoms per unit substrate area, increases from its initial zero value to a density at which agglomeration occurs, and then decreases to unity as the film becomes continuous.

The nucleation rate J is the rate at which stable groups of atoms are formed. It was suggested by Walton, Rhodin, and

FIG. 4.1

THE ENERGY PARAMETERS OF NUCLEATION THEORY

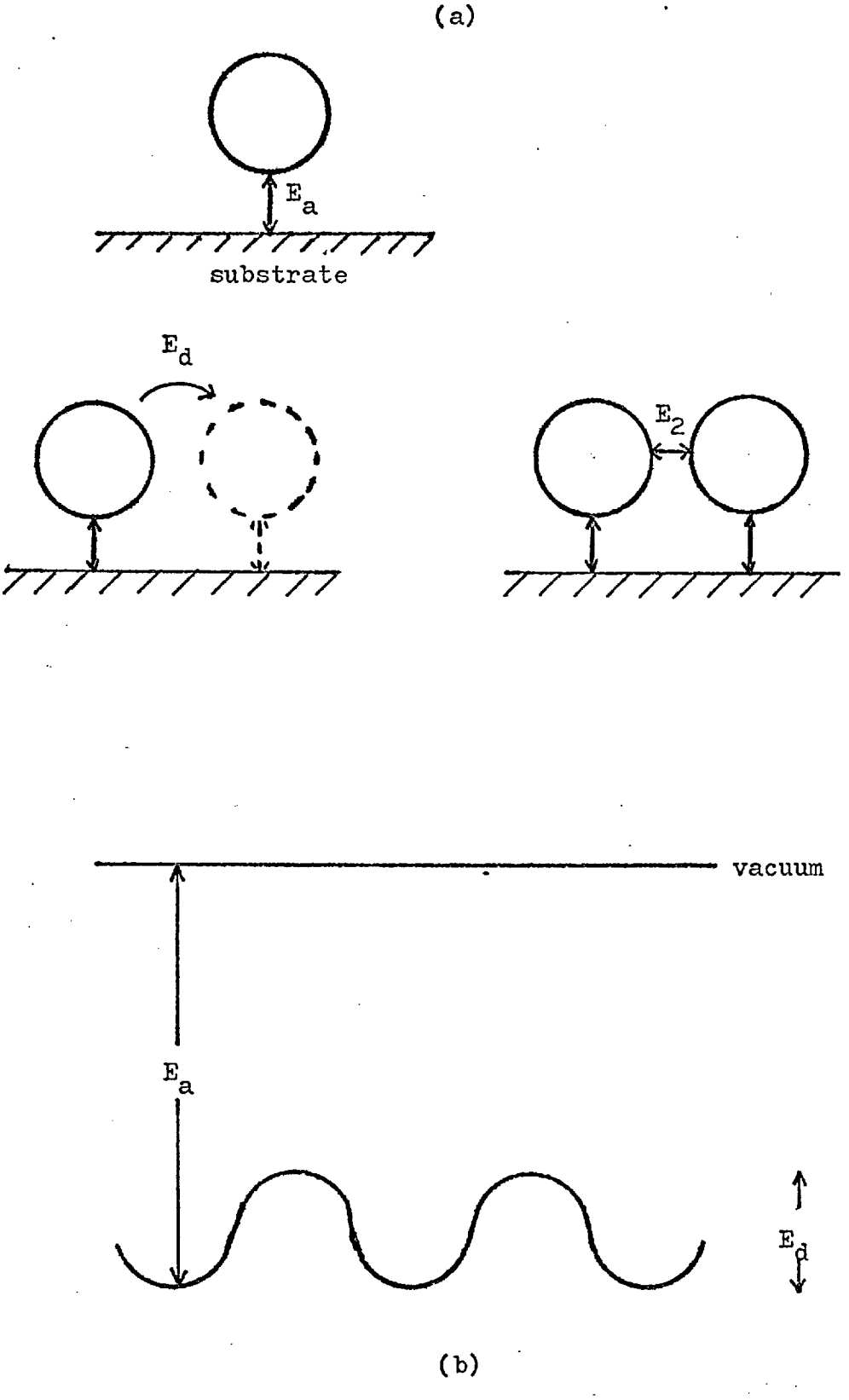

Rollins (1963) that the nucleation rate decreases from its initial value until nucleation stops, the island density then remaining constant until agglomeration occurs, further incident material producing an increase in island size rather than in island numbers. This suggestion was developed by Lewis & Campbell (1967); using average values of nucleation processes, they showed that a saturation island density $N_s$ is established, and that this density is a function of the energy parameters controlling the nucleation and growth of the deposit, and of the incidence rate and substrate temperature. Their treatment is reviewed briefly below. We will then show that, by considering the random nature of single atom desorption and the competition between various modes of removal of single atoms from the system, a more precise theory can be produced which predicts that saturation does not occur, but which can still be used to evaluate the energy parameters.

4.2.1. The Lewis-Campbell saturation model

The number $m_a$ of adsorption sites which a diffusing single adatom visits before it evaporates is given by the product of the surface diffusion rate v sites per unit time and the lifetime before evaporation, $\tau_a$:

$$m_a = v\tau_a = \exp\left(\frac{E_a - E_d}{kT}\right) \qquad \ldots.(4a)$$

where $E_a$ is the adsorption energy of a single atom, $E_d$ the surface diffusion energy, T the absolute temperature of the substrate, and k the Boltzmann constant. The area which an adatom can cover in its lifetime is $m_a / N_o$, where $N_o$ is the

surface density of adsorption sites; if there is a capture site (i.e. another single or group of atoms) within that area, the atom will be captured. If the capture site is considered to be mobile and the single atoms to be fixed, then it can be seen that a capture site absorbs as many atoms as are incident within the catchment area $m_a / N_o$ around it. Hence the capture rate $\omega$ of single atoms, assuming no competition between capture sites, is given by:

$$\omega = \frac{R\, m_a}{N_o} \qquad \ldots.(4b)$$

where R atoms per unit time per unit substrate area is the incidence rate.

When there are $n_s$ stable nuclei, a number of sites $m_c$ can be associated with each nucleus such that all the surface sites are equally distributed amongst the $n_s$ nuclei, i.e. $m_c = N_o/n_s$. Two cases must then be considered:

i. $m_c > m_a$

Of the R atoms which arrive on the substrate in each unit time interval, only $n_s\omega$, which equals $Rn_s m_a / N_o$, are captured by $n_s$ nuclei. The remaining $Rn_s(m_c - m_a) / N_o$ atoms either form new nuclei or evaporate. This is a condition of initially incomplete condensation and arises when the incidence rate and substrate temperature are such that the initial density of stable nuclei is less than $N_o / m_a$; this occurs when $R\tau_a m_a < N_o$. As fresh nucleation takes place, more stable nuclei are produced and $m_c = N_o/n_s$ decreases until the catchment areas of adjacent areas meet, i.e. $m_c = m_a$. Nucleation then stops and a saturation

density $N_s$ is established:

$$N_s = \frac{N_o}{m_a} = N_o \exp \frac{-(E_a - E_d)}{kT} \qquad \ldots.(4c)$$

$N_s$ is rate independent and increases as T increases. It can be shown that the island density increases exponentially to its saturation value.

ii. $m_c < m_a$

In this case the density of stable nuclei is initially greater than $N_o/m_a$ and condensation is complete. When pairs of atoms are stable, the condition for nucleation to cease is that only one atom at a time is present within the area $m_c$ around each stable pair. Then, if $N_1$ is the density of single atoms,

$$N_s = N_1 = \frac{R\, m_c}{v} = \frac{R\, N_o}{v\, N_s}$$

$$\therefore \quad N_s = \left(\frac{R\, N_o}{\nu_o}\right)^{\frac{1}{2}} \exp\left(\frac{E_d}{2kT}\right) \qquad \ldots.(4d)$$

where $\nu_o$ is a vibrational frequency. In this case, $N_s$ is rate dependent and decreases as T increases. Furthermore, $N_s$ is established almost immediately deposition commences and then remains constant until agglomeration occurs.

Since the temperature dependence is different in the two cases, a graph of log $N_s$ against 1/T produces two straight lines with gradients of opposite sign.

The theory has been further developed by Lewis (reported by Joyce, Bradley, & Booker 1967) to include initially complete condensation with critical nuclei containing more than one atom.

The saturation density for complete condensation with a critical nucleus of $i^*$ atoms is given by:

$$N_s = \left(\frac{N_o R^{i^*}}{\nu_o i^*}\right)^{1/(i^*+1)} \exp\left(\frac{E_i^* + i^* E_d}{(i^*+1)kT}\right)$$

where $E_i^*$ is the gain in potential energy on forming a critical nucleus from $i^*$ single adatoms. Thus, under conditions of initially complete condensation, the gradient of the log $N_s$ v. 1/T graph becomes increasingly positive as the critical nucleus size increases.

Fig. 4.2. shows the variation of $N_s$ with 1/T for a constant incidence rate as the temperature increases and conditions change from initially complete condensation with $i^* = 1$, then $i^* = 2$, and then to initially incomplete condensation. Several combin- of $E_a$, $E_d$, and $E_2$ (pair binding energy) are considered.

4.2.2. Some experimental results and apparent discrepancies

The Lewis-Campbell model predicts that under conditions of complete condensation (low temperature and/or high incidence rate):

(a) the saturation density is established almost immediately at the commencement of deposition and then remains constant until the onset of agglomeration;

(b) the condensation coefficient is always very close to unity;

(c) d (log $N_s$)/ d(1/T) is positive and constant.

Experimental results with gold on rocksalt at low temperature obtained by Lewis & Campbell and by Jordan & Stirland (to be published ) show a time-dependent $n_s$, in contradiction to (a), and a condensation coefficient of 0.3 in contradiction to (b).

FIG. 4.2

THEORETICAL VARIATION OF $N_s$ WITH TEMPERATURE

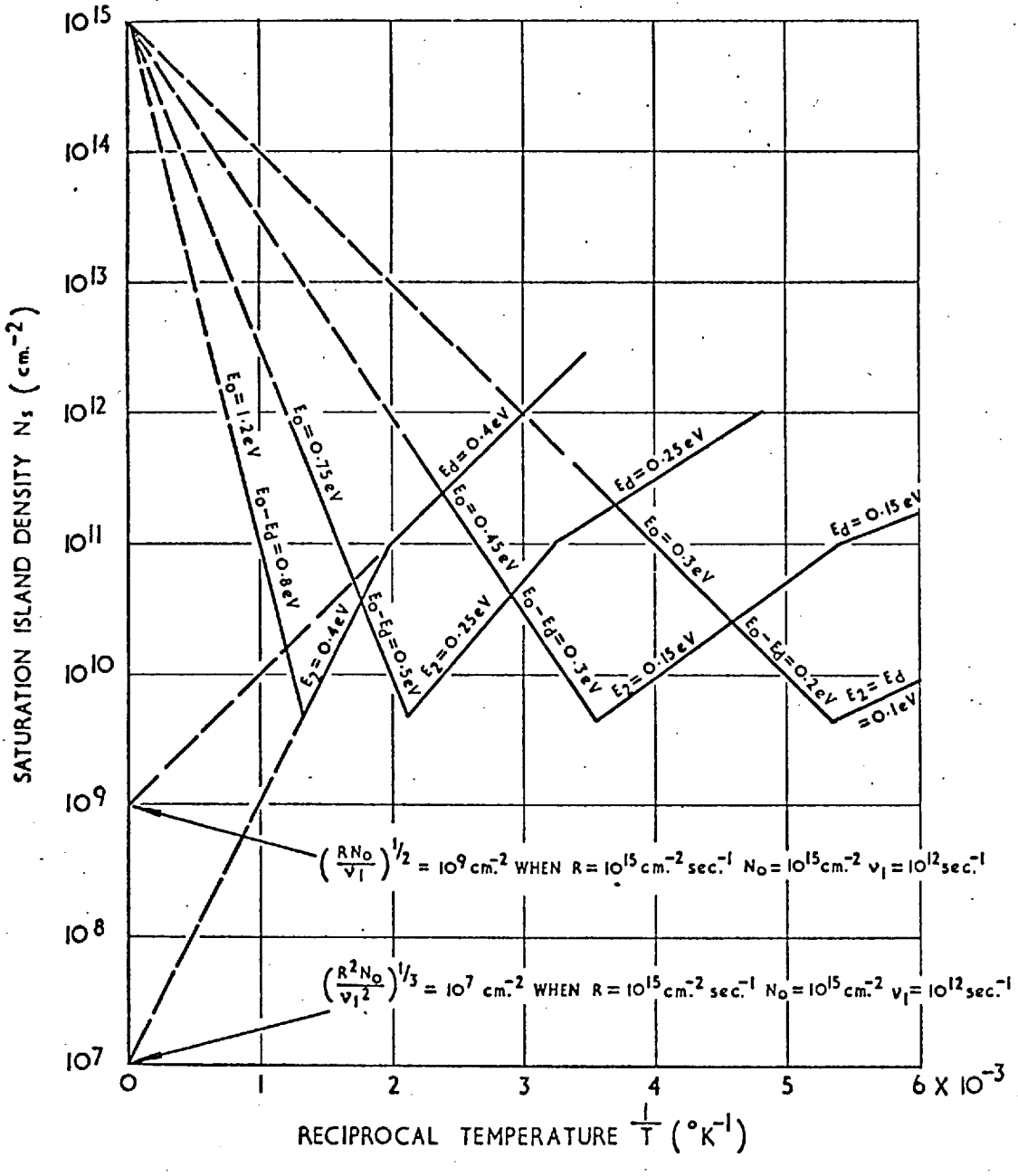

Assuming that the $n_s$ v. time curve did flatten asymptotically, Jordan & Stirland estimated values of $N_s$ and constructed a log $N_s$ v. 1/T curve; this was linear and positive in slope as predicted in (c). Lewis & Campbell attributed the time dependence of $n_s$ to fresh nucleation due to statistical fluctuations which their model neglects; the low condensation coefficient was not discussed.

Venables & Ball (to be published) have made island density observations of the deposition of rare gases on carbon at temperatures below 50°K. Plotting their results as log $N_s$ v. 1/T they observed transitions between regions of different positive slopes, corresponding to changes in the critical nucleus size. We do not know their method of determining the value of $N_s$.

Poppa (1965, 1967) has made in situ observations of the initial growth of silver on carbon and bismuth on carbon. His results show a time-dependent $n_s$. If Jordan & Stirland's method of determining $N_s$ is applied to Poppa's results, it is found that $N_s$ is rate dependent and that $d(\log N_s)/d(1/T) > 0$.

Under conditions of incomplete condensation (high temperature and/or low rate) the Lewis-Campbell model predicts that:
(d) the island density increases exponentially with time to a saturation value $N_s$;
(e) the instantaneous condensation coefficient increases with time to unity when $N_s$ is attained;
(f) $d(\log N_s)/d(1/T)$ is constant and negative.
Lewis & Campbell conducted experiments using gold on rocksalt at high temperatures and found a time dependent density which

could be fitted to an exponential curve as predicted, and that the values of $N_s$ so obtained showed the predicted temperature dependence. However, there appear to be no other reported results which show a region where $d(\log N_s)/d(1/T) < 0$.

Thus there appear to be certain discrepancies between the theoretical model and experiment, concerning the time dependence of $n_s$ and the condensation coefficient at low temperatures, and the transition from positive to negative slope of the $\log N_s$ v. $1/T$ graph as the temperature is increased.

As we have pointed out previously, Lewis & Campbell assumed that all atoms had the same lifetime and also considered, at any given time, only the dominant of several processes consuming single atoms. We will now show that, by taking into account the random nature of single atom desorption which results in a distribution of lifetimes, and by considering the competition between various modes of removal of single atoms from the system, a theory in better agreement with experiment can be derived.

4.2.3. The parameters of nucleation and growth

Adatom lifetime. An adatom diffusing across a regular substrate has the same chance of evaporating at each and every site, independent of how long it has already been on the substrate. The probability of evaporating in any time interval $\delta t$ is given by:

$$q.\delta t = \nu_o \cdot \exp\left(\frac{-E_a}{kT}\right) . \delta t$$

with the usual terminology. ($\nu_o$ is treated as a temperature independent term; a more exact treatment suggests that this is

not true. However the exponential term varies with temperature much more rapidly than $\nu_o$; this is confirmed by linear Arrhenius plots obtained, for example, from bulk diffusion data).

Let the probability of an adatom remaining adsorbed for a time t be P(t). Then

$$P(t + \delta t) = P(t)\ (1 - q.\delta t)$$

Assuming that P(t) is a continuous well-behaved function of t,

$$P(t + \delta t) = P(t) + \frac{d\,P(t)}{dt} . \delta t$$

and hence

$$P(t) = \exp(-qt)$$

The constant is eliminated by considering the mean lifetime $\tau$ given by:

$$\tau \int_o^\infty P(t).dt = \int_o^\infty t\ P(t).dt$$

Hence $$\tau = \frac{1}{\nu_o} \exp\left(\frac{E_a}{kT}\right)$$

which is the mean lifetime of eqn.(4a), and thus:

$$P(t) = \exp\left(\frac{-t}{\tau}\right) \qquad \ldots.(4e)$$

Adatom diffusion rate. In the same way, the probability of an adatom jumping between adjacent adsorption sites in time $\delta t$ is:

$$\nu_1 \exp\left(\frac{-E_d}{kT}\right). \delta t$$

where $E_d$ is the surface diffusion energy and $\nu_1$ is another vibrational frequency constant. The number of diffusion hops made in the lifetime of an adatom will usually be very large, and we are therefore justified in using the mean diffusion rate $\bar{v}$, even for a single atom.

$\bar{\nu}$ is given by:

$$\bar{\nu} = \nu_1 \exp\left(\frac{-E_d}{kT}\right) \qquad \ldots.(4f)$$

which is the same value used in eqn.(4a).

Capture rate of single atoms. This parameter is one which we consider has yet to be satisfactorily dealt with. The basic problem is:- if an atom lands a certain distance away from a nucleus of known size, what is the probability of the atom being captured by the nucleus? It is possible to calculate the probability of the atoms being at any given point in a given number of steps by a random walk process. This yields a Gaussian distribution, but does not take account of the past history of the diffusing atom, i.e. whether it has already visited a capture position. But a more valid treatment is extremely complex and we are not yet able to offer a solution.

The size of the capturing nucleus is not of paramount importance. It has been theoretically shown by Lewis & Campbell and experimentally confirmed by Poppa (1967) that the capture nucleus size is only a correction term to its capture rate, provided that the number of sites covered by the nucleus is small compared with the average number of sites covered by an adatom before capture.

We will now derive the capture rate of single atoms, taking into account the randon re-evaporation of incident material; the method adopted is not very satisfactory.

Consider those atoms landing from the vapour phase into the annulus (r, r + dr) from a capturing nucleus. For a random walk, the probability of an adatom being captured by a nucleus

distance r away is the probability of that atom covering $\pi r^2 N_o$ sites;(the factor of $\pi$ may not be quite correct, but an error in this factor would produce only a small numerical error in the result we derive). From eqn.(4e), this probability is equal to $\exp(-\pi r^2 N_o/m)$, where m is the number of sites covered by an adatom in a mean lifetime:

$$m = \bar{v}\tau = \frac{\nu_1}{\nu_o} \exp\left(\frac{E_a - E_d}{kT}\right) \qquad \ldots.(4g)$$

The area of the annulus is $2\pi r.dr$ and if we assume that there are $2\pi rR.dr$ atoms incident within it per unit time (which is a reasonable assumption provided that it is understood that the capture rate so derived is an average over a period which is long compared with the interval between the arrival of consecutive atoms, then the capture rate at the nucleus is:

$$\omega = \int R\, 2\pi r \exp\left(\frac{-N_o \pi r^2}{m}\right) . dr$$

If the nucleus captures only that material incident within an area A around the nucleus, then the integration limits are 0 and $(A/\pi)^{\frac{1}{2}}$ and hence:

$$\omega = \frac{R\,m}{N_o}\left[1 - \exp\left(\frac{-A\,N_o}{m}\right)\right] \qquad \ldots.(4h)$$

Note that as A tends to $\infty$, $\omega$ tends to $Rm/N_o$ which is the expression derived by Lewis & Campbell for capture by a nucleus from the catchment area of m sites around it under conditions of complete condensation. But taking the random desorption of atoms into account, when $A = m/N_o$ then:

$$\omega = \frac{R\,m}{N_o}\left(1 - \frac{1}{e}\right)$$

so that even under these conditions, condensation is incomplete.

Single atom population. A single atom which is adsorbed on the substrate surface will eventually combine with another single atom or group of atoms, or re-evaporate. The number of single atoms on the substrate at any moment is determined by the incidence rate R and the rates of consumption by each of the loss processes. It has been shown by Halpern (1967) that it is unnecessary to consider capture of single atoms by sub-critical nuclei since the numbers of these remain quasi-constant. If there are $n_1$ single atoms, $n_i^*$ critical nuclei and $n_s$ stable nuclei, then the rate of increase of the single atom population is equal to the incidence rate minus the evaporation rate and the capture rate by critical and stable nuclei:

$$\frac{dn_1}{dt} = R - \frac{n_1}{\tau} - (n_i^* + n_s)\,\omega \qquad \ldots.(4i)$$

In this equation we have made the assumption that critical and stable nuclei are equal competitors in the capture of single atoms; this is equivalent to neglecting the capture size dependence of $\omega$, which should be valid provided that the capturing nuclei are not too large. Under these conditions, each critical and stable nucleus has a chance of capturing R/n single atoms from an area 1/n, where $n = n_i^* + n_s$. Therefore, from eqn.(4h) with A = 1/n, the capture rate is given by:

$$\omega = \frac{R\,m}{N_o}\left[1 - \exp\left(\frac{-N_o}{n\,m}\right)\right] \qquad \ldots.(4j)$$

Therefore $\omega \rightarrow \dfrac{R\,m}{N_o}$ as $\dfrac{n\,m}{N_o} \longrightarrow 0$

and $\omega \longrightarrow \frac{R}{n}$ as $\frac{n\,m}{N_o} \longrightarrow \infty$

Eqn.(4i) is not generally soluble. We will therefore make the usual approximation, $dn_1/dt = 0$, i.e. that equilibrium conditions obtain at any given time. The population of single atoms is then given by:

$$n_1 = R\tau - \frac{R\,m\,n\,\tau}{N_o}\left[1 - \exp\left(\frac{-N_o}{n\,m}\right)\right]$$

$$= R\tau\,F(x)$$

where $F(x) = 1 - x + x\exp\left(\frac{-1}{x}\right)$ and $x = \frac{n\,m}{N_o}$

The function F(x) is shown in Fig.4.3. It can be seen that F(x) can be replaced by simpler functions, to a very good approximation, in three distinct regions:

$$\left.\begin{array}{lll} \text{(i)} & 0 < x < 0.1 : & F(x) \simeq 1 \\ \text{(ii)} & x > 1 : & F(x) \simeq 1/2x \\ \text{(iii)} & 0.1 < x < 1 : & F(x) \simeq 1 - x + x^2/e \end{array}\right\} \quad \ldots.(4k)$$

Region (i) corresponds to the condition that the numbers of critical and stable nuclei are so low that the capture rate of any nucleus is very much like that of an isolated nucleus. Region (ii) corresponds to the condition that the numbers of critical and stable nuclei are so high that re-evaporation is very unlikely and nearly all incident atoms are captured. Region (iii) corresponds to the continuous transition from (i) to (ii); it should be noted that this transition covers a very limited range of x. The condition x = 1 is very similar to the Lewis-Campbell criterion for the catchment areas to just cover the substrate surface.

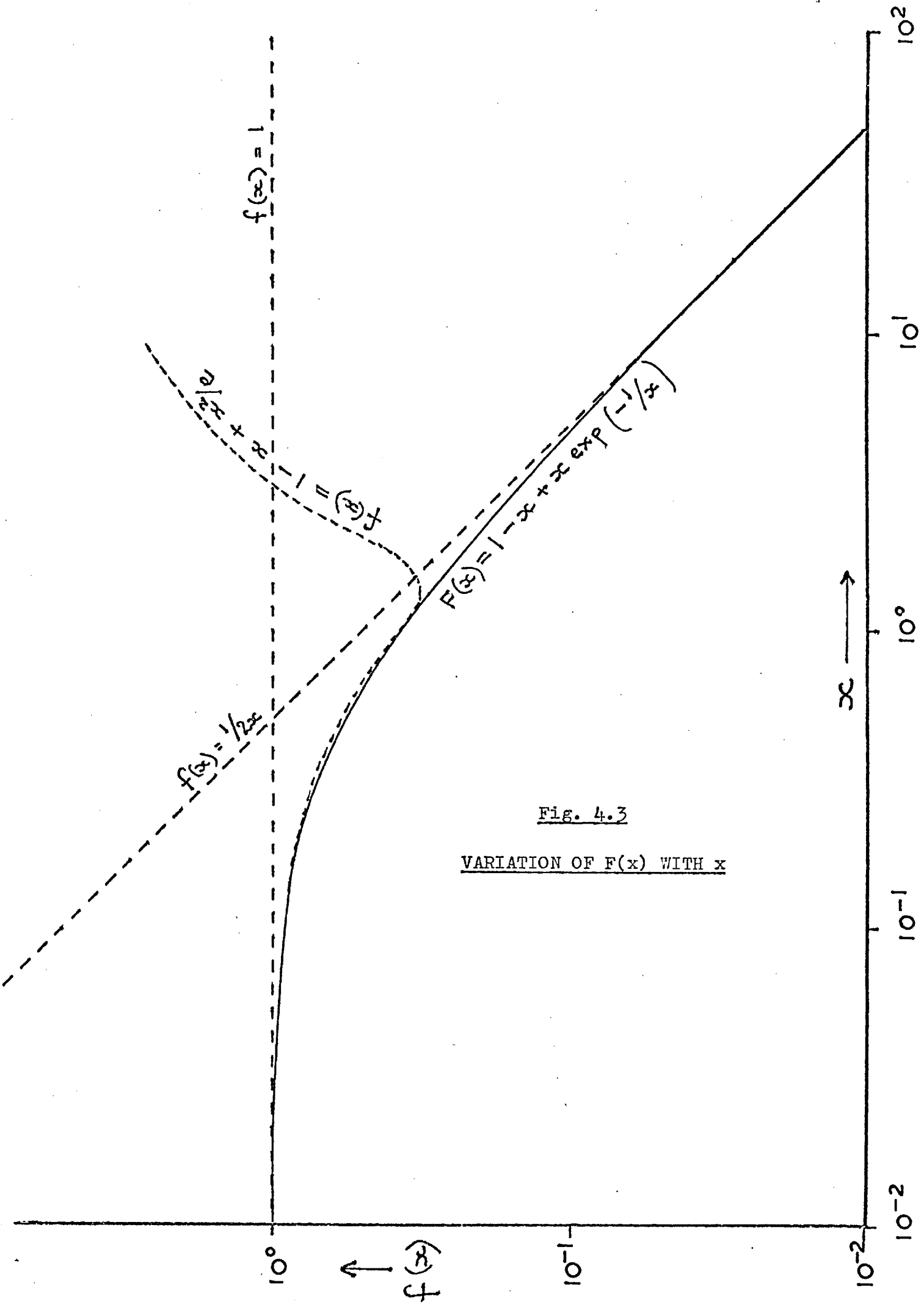


Fig. 4.3

VARIATION OF F(x) WITH x

A further observation from Fig.4.3 is that $F(x) \neq 0$ for all finite x, hence $n_1 \neq 0$ and $\omega \neq 0$.

Nucleation rate. The nucleation rate J is the formation rate of stable clusters and so is the product of the critical nuclei density $n_i^*$ and the capture rate of single atoms:

$$J = n_i^* \omega$$

Furthermore, $$n_i^* = N_o \left(\frac{n_1}{N_o}\right)^{i^*} \exp\left(\frac{E_i^*}{kT}\right)$$

which is the statistical distribution of clusters according to Walton (1962) and Halpern(1967). It was shown in the last section that neither $n_1$ nor $\omega$ is ever zero for finite positive values of x ($= nm/N_o$), hence the nucleation rate is never zero and saturation is never reached.

Since $J \propto n_1^{i^*} \omega$ , we can express J in terms of n. By differentiation, it can then be shown that $dJ/dn < 0$ for all finite positive n. But $J = dn/dt$, therefore the curve relating n to time t is of constantly decreasing gradient. That proportion of n large enough to be observed experimentally always shows this dependence.

4.2.4. Experimentally observable parameters.

Since we have shown that a true saturation density is never attained, we require an experimentally observable parameter to replace the hitherto apparently useful saturation island density.

4.2.4.1 The fractional nucleation rate

It was shown in the last section that the nucleation rate decreases as the density of stable nuclei increases. We will call the ratio of these two parameters the fractional nucleation rate

y, i.e. $$y = \frac{J}{n_s} = \frac{dn_s/dt}{n_s} = \frac{d(\log n_s)}{dt}$$

Whereas the value of $n_s$ at which "saturation" occurred was not well defined, the fractional nucleation rate y has a precise value at any time. The general relation between y and the island density $n_s$ can be derived from the above equations:

$$y = \frac{\omega N_o}{n_s} \left(\frac{R \tau F(x)}{N_o}\right)^{i^*} \exp\left(\frac{E_i^*}{kT}\right) \quad \ldots.(41)$$

The solution of this equation is now considered separately for each of the regions specified by eqns.(4k).

(i) $x < 0.1$

Under these conditions, $F(x) \to 1$ and $\omega = Rm/N_o$ (eqn.4j). Eqn. (41) can then be simplified to:

$$n_s = \frac{N_o \nu_1}{y} \left(\frac{R}{N_o \nu_o}\right)^{i^*+1} \exp\left(\frac{E_i^* + (i^*+1)E_a - E_d}{kT}\right) \quad \ldots.(4m)$$

For given y, $i^*$, and R, it can be seen that $d(\log n_s)/d(1/T) > 0$ and constant, since $E_a \gg E_d$. The theoretical intercept at $(1/T) = 0$ is given by the pre-exponential term. The relation can be solved simply for particular values of $i^*$:

$$n_s = \frac{R^2 \nu_1}{y N_o \nu_o^2} \exp\left(\frac{2E_a - E_d}{kT}\right) \quad \text{when } i^* = 1$$

$$n_s = \frac{R^3 \nu_1}{y N_o^2 \nu_o^3} \exp\left(\frac{E_2 + 3E_a - E_d}{kT}\right) \quad \text{when } i^* = 2$$

and similarly for larger values of $i^*$.

The condition $x < 0.1$ corresponds to the early stages of formation when the density of critical and stable nuclei is so low that

the single atom population is determined essentially by re-evaporation, i.e. $n_1 = R\tau$. Under these conditions the nucleation rate is quasi-constant, and $y \propto 1/n_s$.

(ii) $x > 1$

In this case, $F(x) \simeq 1/2x$ and $\omega \simeq R/n$ (eqn.4j). We can then write eqn.(4l) as:

$$y = \frac{2N_o\nu_1}{n_s}\left(\frac{R}{2n\nu_1}\right)^{i^*+1} \exp\left(\frac{E_i^* + i^*E_d}{kT}\right)$$

This can be simplified further if $y$ ($= n_i^*\omega/n_s$) is chosen to be small enough that $n_i^* \ll n_s$; then $n \simeq n_s$ and

$$n_s = \left[\frac{2N_o\nu_1}{y}\left(\frac{R}{2\nu_1}\right)^{i^*+1}\right]^{1/(i^*+2)} \exp\left(\frac{E_i^* + i^*E_d}{(i^*+2)kT}\right) \quad \ldots\ldots(4n)$$

$d(\log n_s)/d(1/T)$ is again positive and constant for given R, $i^*$ and $y$ (cf. eqn.4m), and the theoretical intercept at $1/T = 0$ is given by the pre-exponential term. Furthermore,

$$n_s = \left(\frac{R^2N_o}{2y\nu_1}\right)^{1/3} \exp\left(\frac{E_d}{3kT}\right) \qquad \text{when } i^* = 1,$$

$$n_s = \left(\frac{R^3N_o}{4y\nu_1^2}\right)^{1/4} \exp\left(\frac{E_2 + 2E_d}{4kT}\right) \qquad \text{when } i^* = 2,$$

and similarly for larger values of $i^*$.

Values of $x > 1$ are obtained at the stage when most of the single atoms are being captured rather than re-evaporating.

Since $J = n_i^*\omega$

then, when $x > 1$ $J \propto \dfrac{(n_1)^{i^*}}{n}$ from eqn.(4j)

and therefore $J \propto \left(\dfrac{1}{n}\right)^{i^*+1}$ from eqn.(4k)

When the fractional nucleation rate is so low that $n \simeq n_s$, then the absolute nucleation rate decreases as $(1/n_s)^{i^*+1}$. This leads to the quasi-plateau of the $n_s$ v. t curve which has been mistaken for the approach to saturation. In fact, the nucleation rate is never zero.

(iii) $0.1 < x < 1$

Under these conditions $F(x) \simeq 1 - x + (x^2/e)$ and the capture rate $\simeq Rm(e - x)/eN_o$. Eqn.(41) then becomes:

$$y = \frac{N_o \nu_1}{n_s} \left(\frac{R}{N_o \nu_o}\right)^{i^*+1} \exp\left(\frac{E_i^* + i^* E_a - E_d}{kT}\right)\left(1 - \frac{x}{e}\right)\left(1 - x + \frac{x^2}{e}\right)^{i^*}$$

If log $n_s$ is plotted against 1/T for constant y in this region, a continuous curve is obtained, representing the transition between the two corresponding straight line regions of $x \gg 1$ and $x \ll 1$. In any growth experiment, these intermediate values of x are obtained when the population $n_1$ of single atoms is determined by both re-evaporation and capture.

4.2.4.2 The temperature dependence of $n_s(y)$

We will define $n_s(y)$ as the value of the island density $n_s$ corresponding to a particular fractional nucleation rate y. In any deposition experiment, $x = nm/N_o = 0$ at commencement. It then increases, rapidly at first, and passes through the three regions described above, provided that agglomeration does not first occur.

By experimentally finding values of $n_s(y)$ over a range of substrate temperatures, all other parameters remaining constant, and plotting $n_s(y)$ v. 1/T, a curve of the form shown in Fig.4.4 would be obtained. Both n(y) and m decrease with increased substrate temperature; therefore, for constant y, x decreases as the substrate temperature increases. Thus eqn.(4n) applies at low

temperatures, whilst eqn.(4m) applies at high temperatures; the temperature range of the transition region depends on the value chosen for y. The curves shown have been drawn for a constant value of $i^*$. Any increases in the critical nucleus size would produce further transitions to regions of greater positive gradients.

For a given constant critical nucleus size, $n_s(y)$ increases as y decreases Therefore a whole family of curves is obtained as the fractional nucleation rate is varied. Curves are shown in Fig.4.4 for two values of y, with $y_2 < y_1$. The extrapolated intercepts at $1/T = 0$ are given by the pre-exponential terms of eqns. (4m) and (4n).

4.2.4.3. Application of the fractional nucleation rate

The density of stable nuclei large enough to be seen in the electron microscope is a parameter which can be easily measured. But this is not the density of stable nuclei $n_s$. However, for small nuclei, the capture rate of single atoms is independent of nucleus size, and therefore the rates of growth of all stable nuclei too small to be seen are equal; this is assumed in the derivation of our model and has been confirmed experimentally by Poppa (1967). Hence the number of stable nuclei at a given time is equal to the number of observable nuclei at some time later, the interval being determined by prevailing conditions.There have been several reports of such "induction" periods.

The variation of $n_s$ with time, and hence $n_s(y)$, can therefore be obtained by measuring the density of observable nuclei at various stages of deposition either in situ (e.g. Poppa) or by depositing for different time periods on to sections of the same

FIG. 4.4

THEORETICAL VARIATION OF Log $n_s(y)$ WITH 1/T

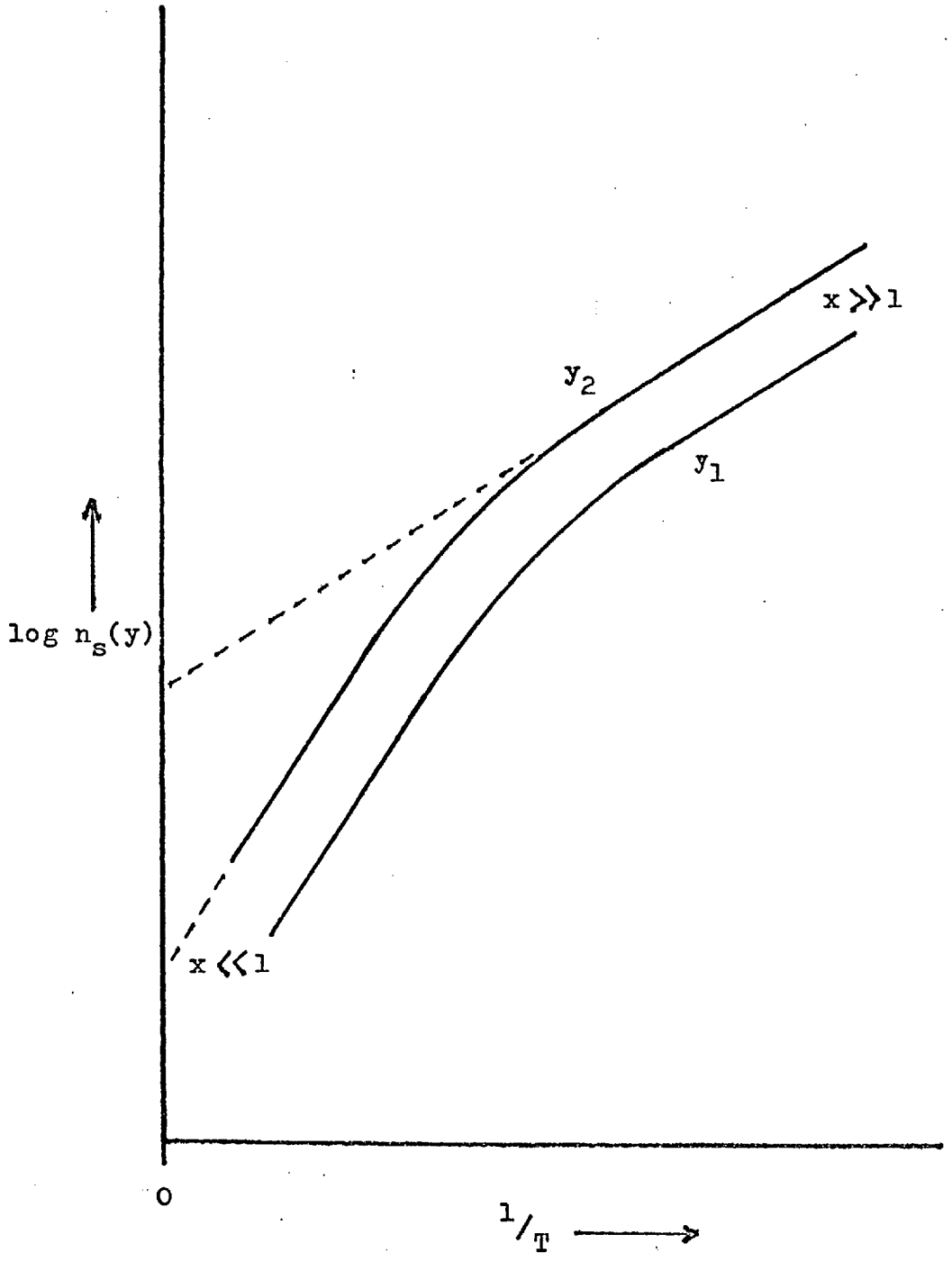

substrate by masking techniques (e.g. Chapman & Campbell 1968); the fractional nucleation rate at any given island density is simply the slope of a log $n_s$ v. t curve at that density. Note that $n_s(y)$ is time-independent and thus unaffected by the time lag between establishment and observation.

We have pointed out above that the increase in island density is finally terminated by the onset of agglomeration, which then causes the density to decrease until complete coverage of the substrate is obtained. It has been shown by Lewis (1968, private communication) that the island density at which agglomeration becomes significant decreases as the substrate temperature increases. But the island densities at constant fractional nucleation rate decrease in the same way and therefore observations can be made without the complications of agglomeration by suitable choice of the fractional nucleation rate used; this sets an upper limit to the densities which can be usefully interpreted.

It has been shown by Jordan & Stirland that, at low densities, random nucleation can be completely masked by the decoration of surface defects. Great care must therefore be exercised to ensure that only the island density due to random nucleation is counted. This can lead to a lower limit of meaningful densities.

The theory can be confirmed only by experiments which explicitly use the concept of fractional nucleation rate. But, in previous saturation experiments, the judgement of the approach of apparent saturation unconciously involved a mental appraisal of this parameter. Apparent saturation is acheived only when $x > 1$; the saturation experiments already carried out may thus be

re-interpreted in terms of the present theory, and would confirm the theory for $x > 1$.

4.2.5. Explanation of Lewis & Campbell's results

Lewis & Campbell observed, at low temperatures, an island density which increased only very slowly. They interpreted this as saturation (accompanied by secondary nucleation) and so obtained their saturation island density $N_s$ which increased with decreasing temperature in agreement with their predictions.

The fractional nucleation rate model predicts that $n_s(y)$ increases with decreasing temperature. In the later stages of nucleation, when y is very small and eqn.(4n) applies, $n_s(y)$ is not very sensitive to changes in y. Therefore one would still expect reasonable linearity on a log $n_s(y)$ v. 1/T graph, in spite of large temperature-to-temperature variations in y. Lewis & Campbell's low temperature results from the quasi-plateau region of their $n_s$ v. t curve are therefore quite consistent with the predictions of our model.

The saturation island densities derived by Lewis & Campbell from their experiments at higher temperatures under conditions which they describe as initially incomplete condensation, show a temperature dependence which is completely contrary to that expected from constant fractional nucleation rate measurements. The densities were derived by fitting experimental results of island density against time to an exponential curve, which the saturation model predicts, and taking the asymptotic value as the saturation density. At each temperature the deposition was continued long enough to obtain a similar island density v. time curve, i.e. to a roughly constant value of the ratio of initial and final

slopes. According to our model, this means that they reached a similar constant value of x at each temperature. Fitting an exponential curve to such results yields a value of $N_s$ which is some constant factor larger than than the value of $n_s$ corresponding to the particular value of x used. Since $x = nm/N_o$, it can be seen from eqn.(4g) that the temperature variation of n for constant x is given by:

$$n = x \frac{N_o \nu_o}{\nu_1} \exp \frac{-(E_a - E_d)}{kT}$$

which has the temperature dependence predicted by Lewis & Campbell, and bears a striking resemblance to their equation for the saturation density under these conditions (eqn.4c), remembering that they assumed that $\nu_o = \nu_1$.

4.2.6. Experimental details: evaporated gold on rocksalt

Condensation experiments with gold on rocksalt were carried out to confirm the predictions of our nucleation model, and to compare the energy parameter values thus obtained with the theoretical predictions of Chapter II.

Lewis & Campbell's application of their saturation density model to the gold/rocksalt system yielded values of $E_a - E_d = 0.4$eV and $E_d \simeq 0.2$eV, compared with our theoretical values for $E_a$ of 0.27eV or 0.72eV, according to the method of calculation.

4.2.6.1. Experimental arrangement

The apparatus used is shown in Fig.4.5. The molybdenum evaporation source was resistively heated, and the evaporation rate was measured with a suspended disc ratemeter (Beavitt 1966). The rocksalt substrate was heated by a thermostatically controlled

# FIG. 4.5

EVAPORATION SYSTEM FOR CONDENSATION EXPERIMENTS

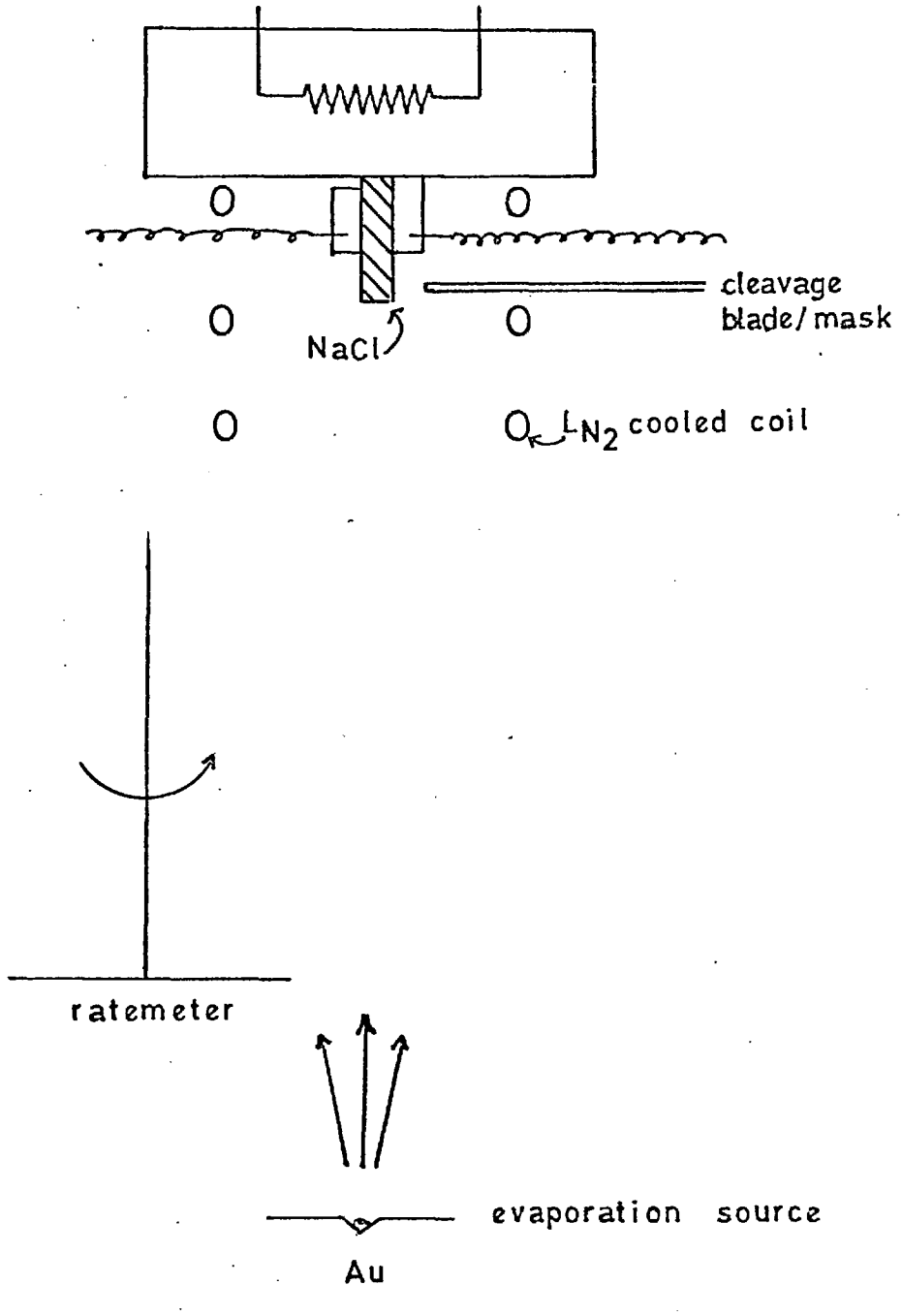

resistive coil embedded in the comparatively massive supporting block, and its temperature was measured with thermocouples. The substrate region was surrounded by a liquid nitrogen cooled coil to eliminate problems of vapour phase accumulation (Lewis 1968).

Experiments took place at pressures $\sim 10^{-6}$ torr in an oil diffusion pumped system with a liquid nitrogen trap. Having adjusted the substrate temperature and the evaporation rate to the required values, the experiment was commenced by cleaving the substrate with a blade which also acted as a mask to provide three thicknesses of deposit on the substrate. After deposition, the substrate was allowed to cool below $50^{\circ}C$ before coating with carbon for examination in an electron microscope.

4.2.6.2. Results

In almost every case the decoration patterns of the islands on the substrate were highly irregular, even on areas remote from steps, where these could be recognised. This irregularity was distinct from the non-uniformity of decoration that results from the randomness of nucleation, and is reflected in the results of island density against deposition time; a typical sample of results is shown in Fig.4.6. The figures given on each curve refer to the substrate temperature in $^{\circ}C$ followed by the incidence rate in $\mathring{A}\ min^{-1}$. Even allowing for the variation in rates, there appears to be no systematic variation of the density-time dependence as expected from our model of nucleation on ideal substrates.

4.2.6.3. Conclusions

It was concluded that the substrate surface was highly irregular and therefore the results cannot be fitted to a theory

FIG. 4.6

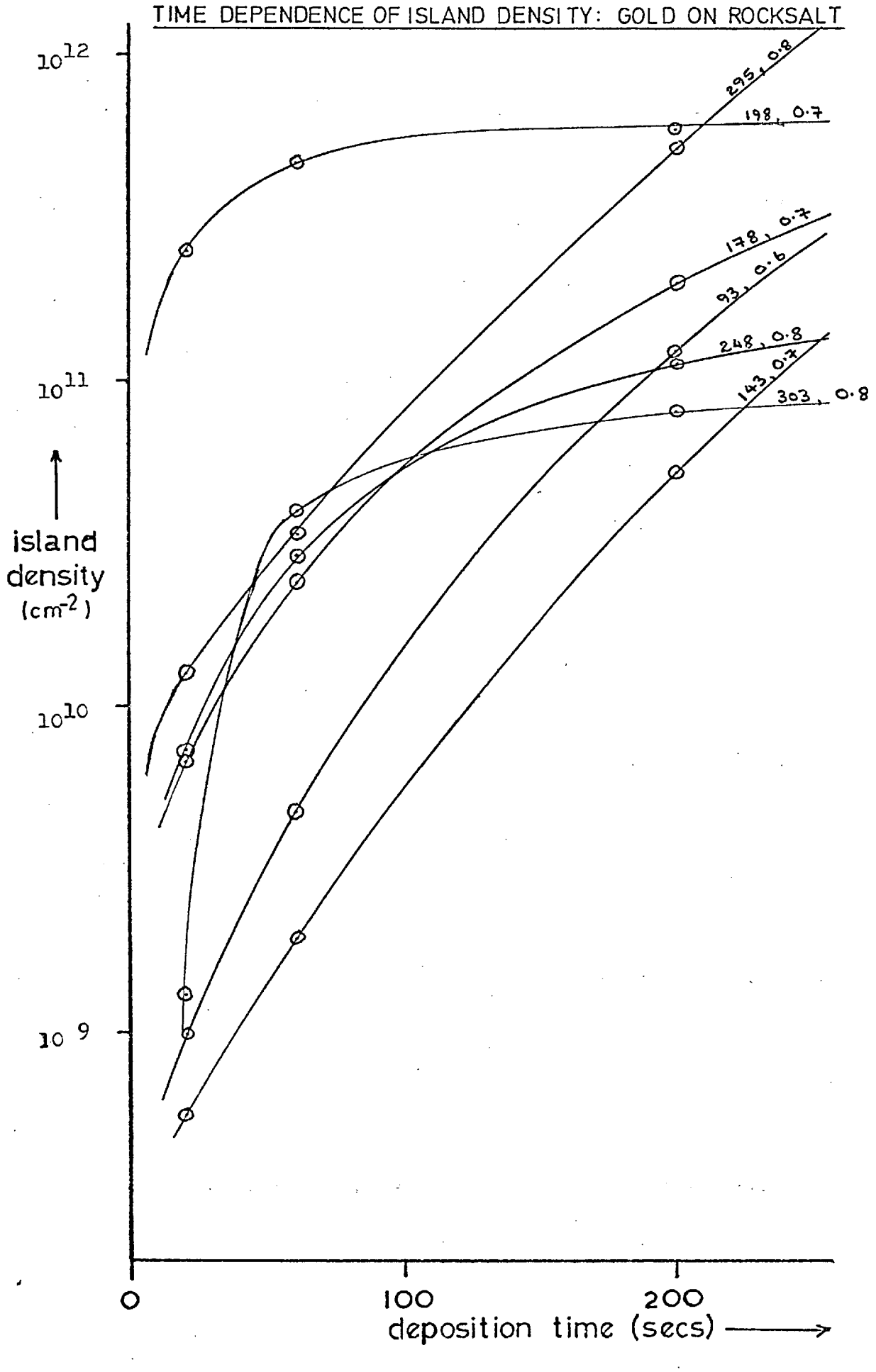
TIME DEPENDENCE OF ISLAND DENSITY: GOLD ON ROCKSALT
$10^{12}$
$10^{11}$
$10^{10}$
$10^{9}$
island density ($cm^{-2}$)
295, 0·8
198, 0·7
178, 0·7
93, 0·6
248, 0·8
143, 0·7
303, 0·8
0
100
200
deposition time (secs)

of uniform heterogeneous nucleation.

The surface irregularity may have been due to variations in surface topography, producing preferred nucleation sites of the types shown in Fig.4.7 for a crystal. A grossly damaged surface can be produced by poor cleavage, but the same substrate holder and cleavage mechanism had been successfully used earlier for the epitaxial deposition of lead telluride on rocksalt (Lewis & Stirland 1968).

The irregular decoration may instead have been due to an irregular electrical charging of the surface. Such charging has been observed on rocksalt surfaces (Ryan & Grossman 1968). It is interesting to note that variations of topography of an ionic surface can produce strong surface electrical fields, which may play a major role in adsorption and hence nucleation.

Jordan & Stirland encountered similar anomalous decoration problems with gold on rocksalt. After rigorous electron microscope examination of the substrate, they found very small areas of lower island density than the rest; they concluded that only these small areas resembled the idealised surface. A similar examination of the present deposits was unsuccessful.

4.2.7. Other results: silver and bismuth on carbon

Poppa (1967) has observed the growth of silver on carbon and of bismuth on carbon using in situ electron microscopy techniques. His results for the time dependence of island density are shown in Figs.4.8 & 4.9. These curves have been analysed in terms of the fractional nucleation rate model, and are quite consistent with its predictions, as can be seen from Figs.4.10 & 4.11 where $n_s(y)$ has been plotted against reciprocal substrate

FIG. 4.7

POSSIBLE NUCLEATION SITES ON A CRYSTAL SURFACE.

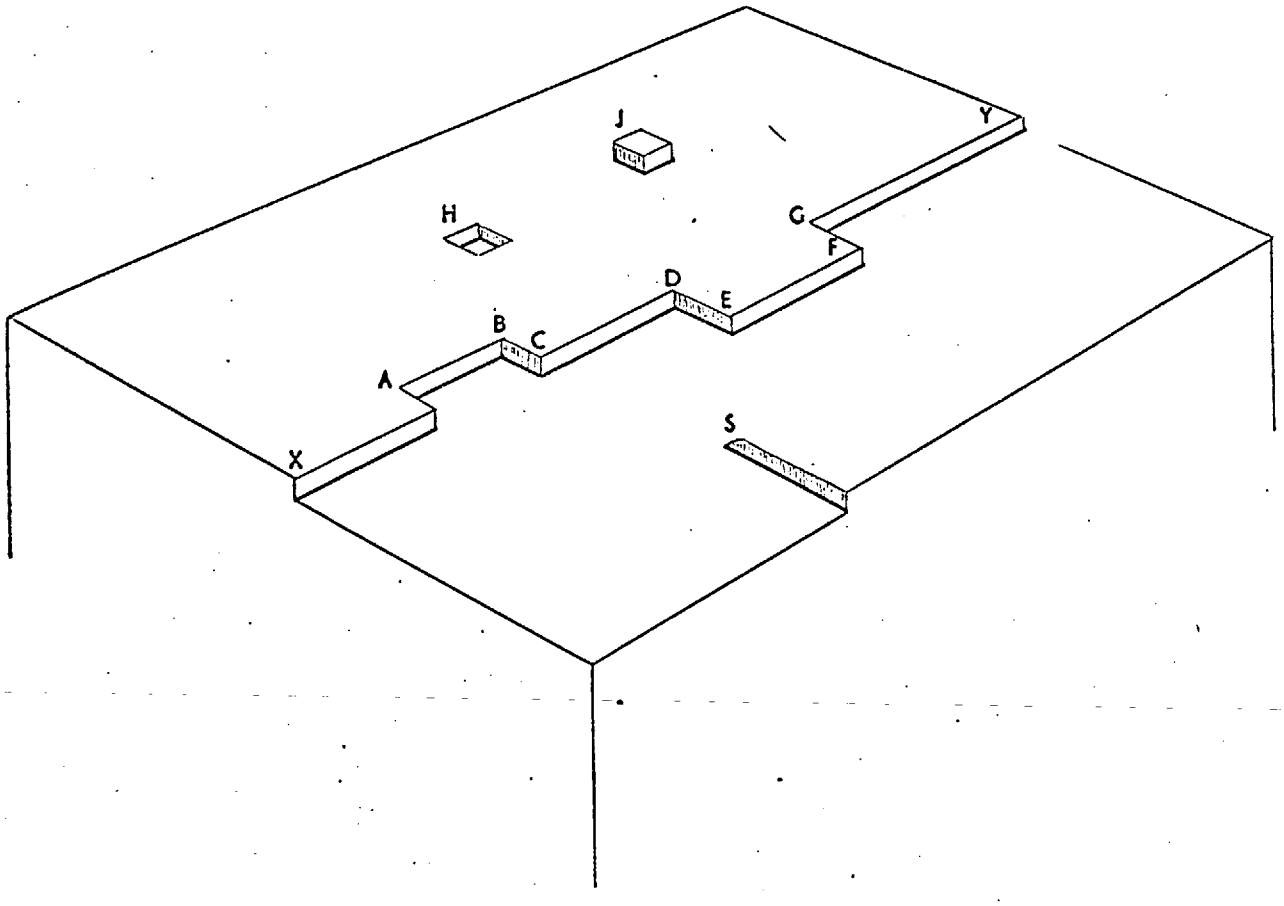

# FIG. 4.8

TIME DEPENDENCE OF ISLAND DENSITY: SILVER ON CARBON

(POPPA 1967)

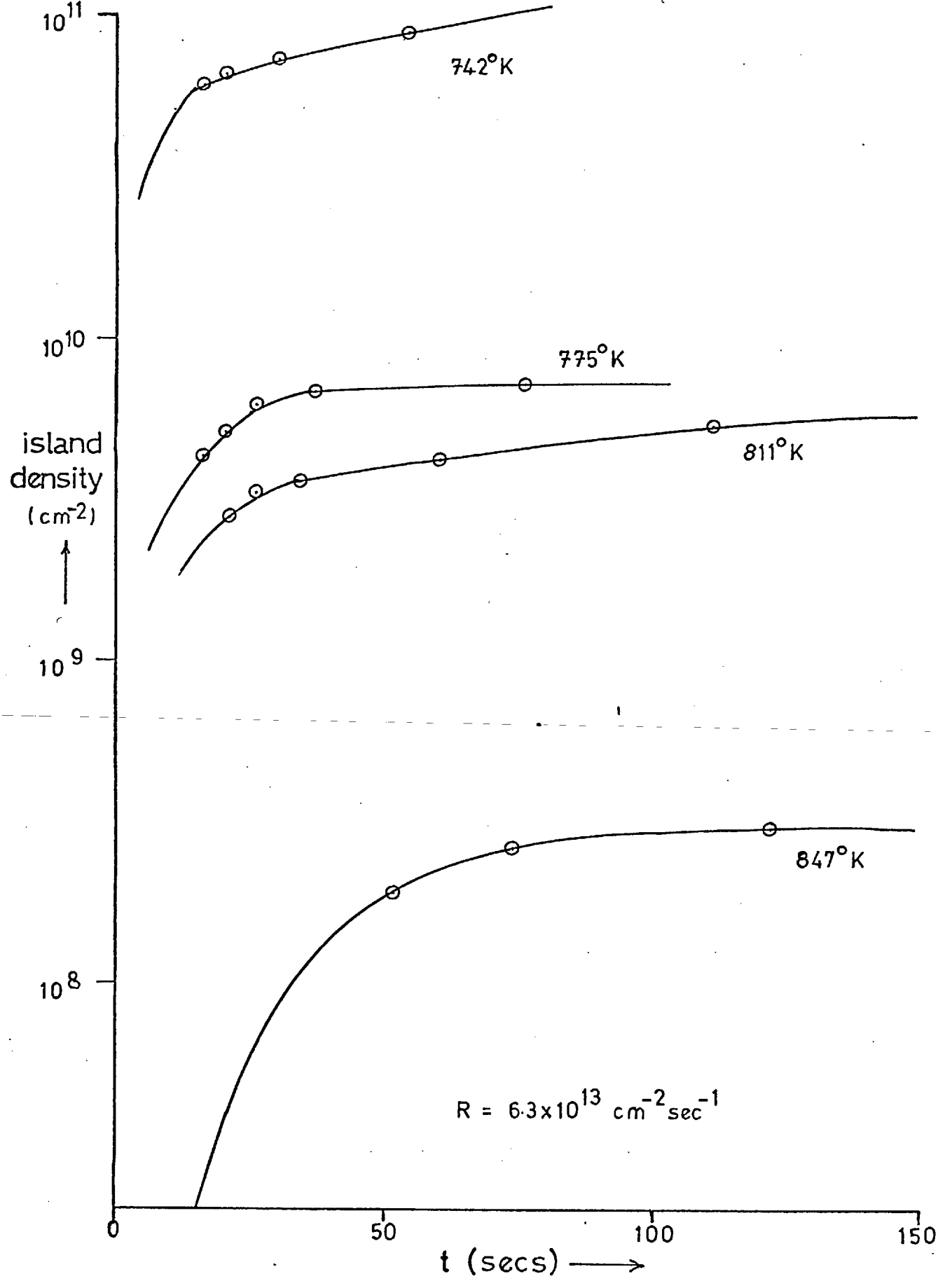

FIG. 4.9

TIME DEPENDENCE OF ISLAND DENSITY: BISMUTH ON CARBON

(POPPA 1967)

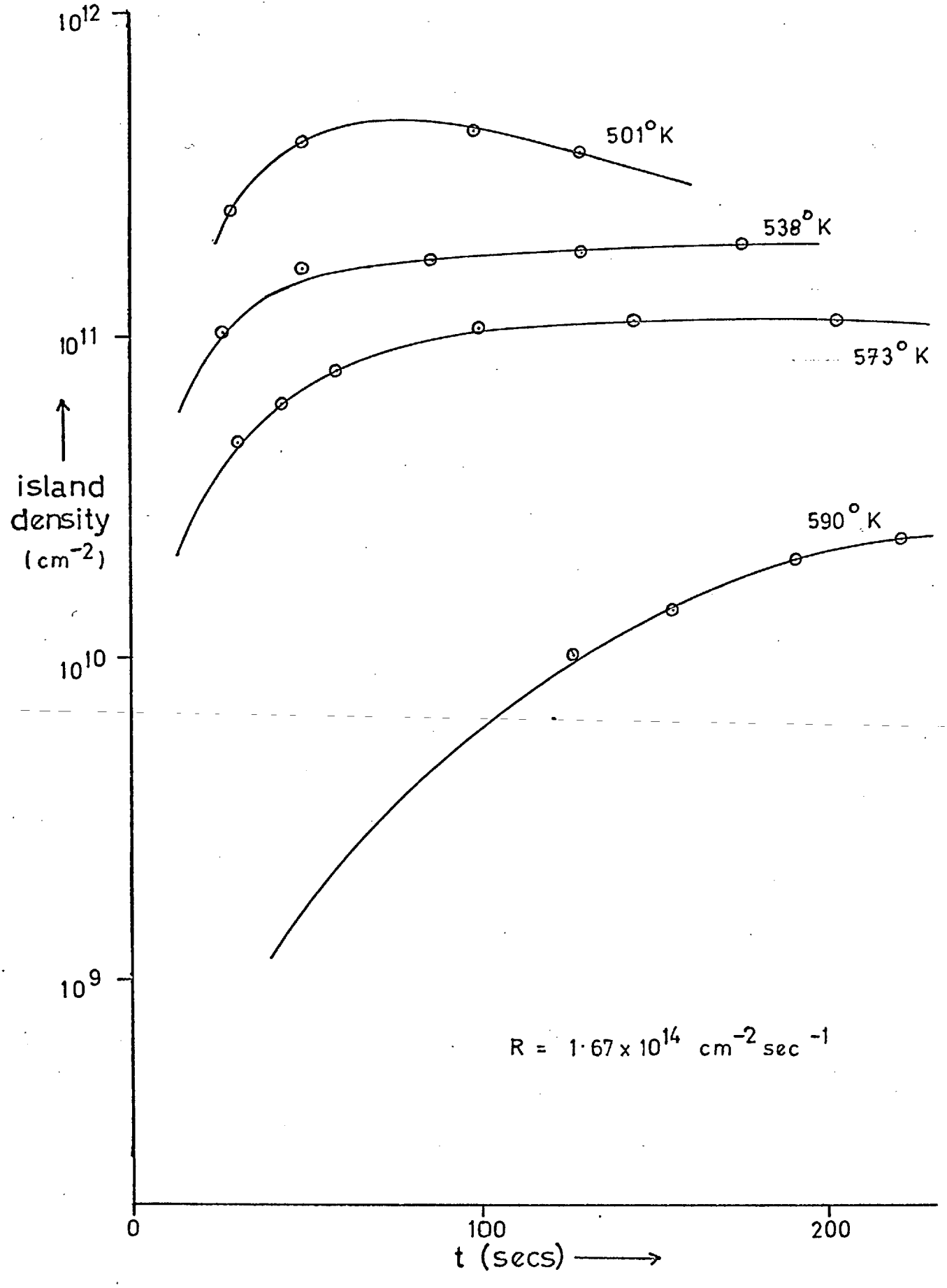

temperature for three different values of the fractional nucleation rate y.

Poppa's data was not presented in a really suitable form for the present analysis, so the plotted values are subject to error in translation. There is insufficient data to draw significant conclusions, but it is instructive to consider the values obtained.

4.2.7.1. Silver on carbon

The slope of the graph in Fig.4.10 for silver on carbon corresponds to an energy parameter of 3.0 eV. Poppa's range of incidence rates is so limited that it is difficult to estimate the critical nucleus size. If we use Poppa's value of $i^* = 2$, then eqn.(4n) for $x > 1$ (which is suggested by the shape of the curve in Fig.4.8) gives $E_2 + 2E_d = 12.0$ eV. The binding energy of a silver molecule is only 1.7 eV (Ackerman et al.,1960), so this suggests an $E_d$ value of approximately 5 eV which seems rather high.

4.2.7.2. Bismuth on carbon

The slope of the smaller gradient in Fig.4.11 for bismuth on carbon corresponds to an energy parameter of 0.70 eV. Again the shape of $n_s$ v. t curve (Fig. 4.9) suggests $x > 1$, and if we take Poppa's value of $i^* = 1$, then eqn.(4n) gives $E_d = 2.1$ eV.

There appears to be a transition in the graph, which corresponds to a change in critical nucleus size from $i^* = 1$ to $i^* = 3$ according to Poppa by a different means of analysis. It would be improper to evaluate the gradient of this region of the graph from essentially two points, but it seems that the minimum likely gradient corresponds to an energy parameter of 4.7 eV. Substi-

FIG. 4.10

$n_s(y)$ v. $1/T$ : silver on carbon

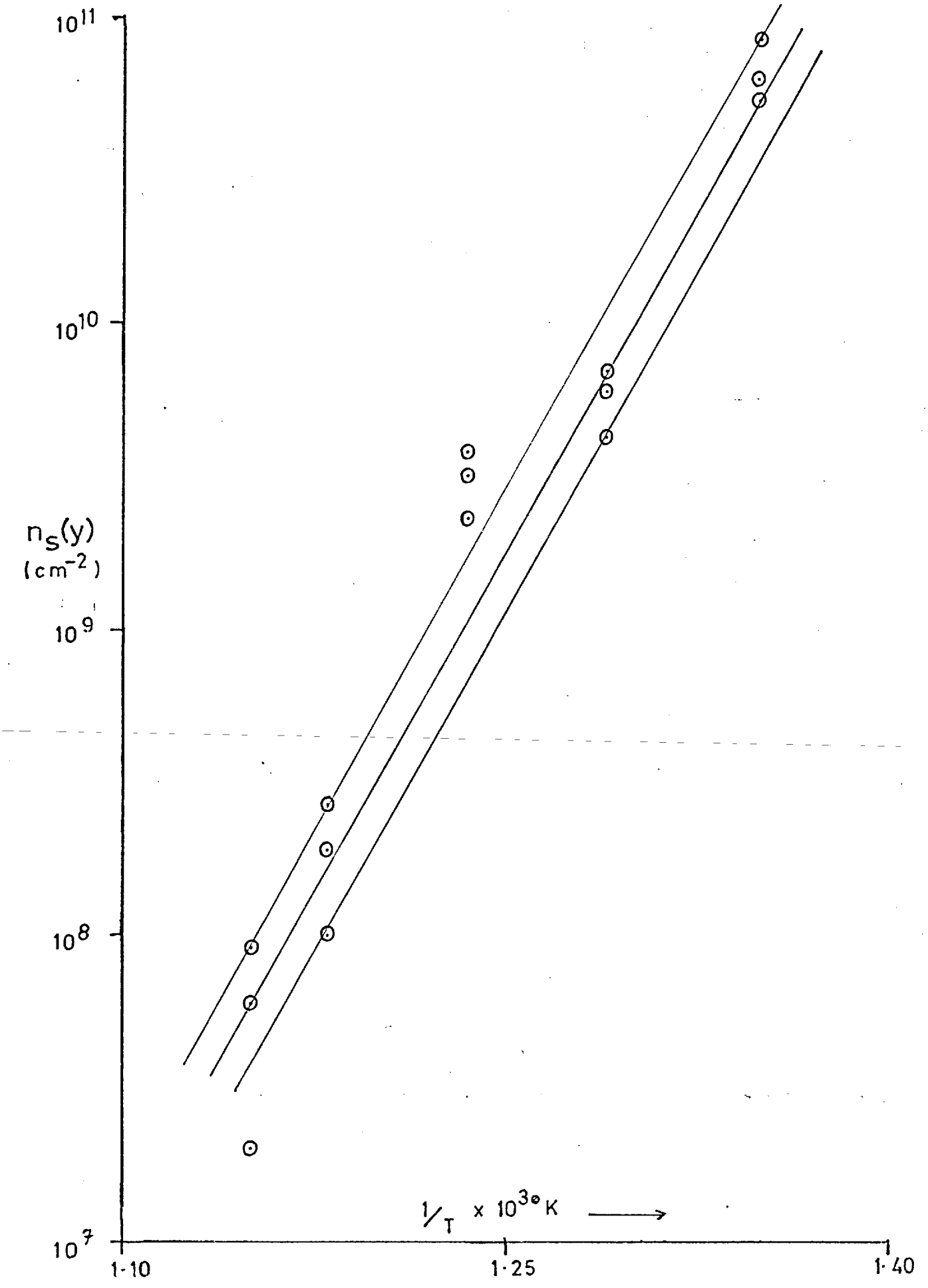

FIG. 4.11

$n_s(y)$ v. $^1/_T$ : bismuth on carbon

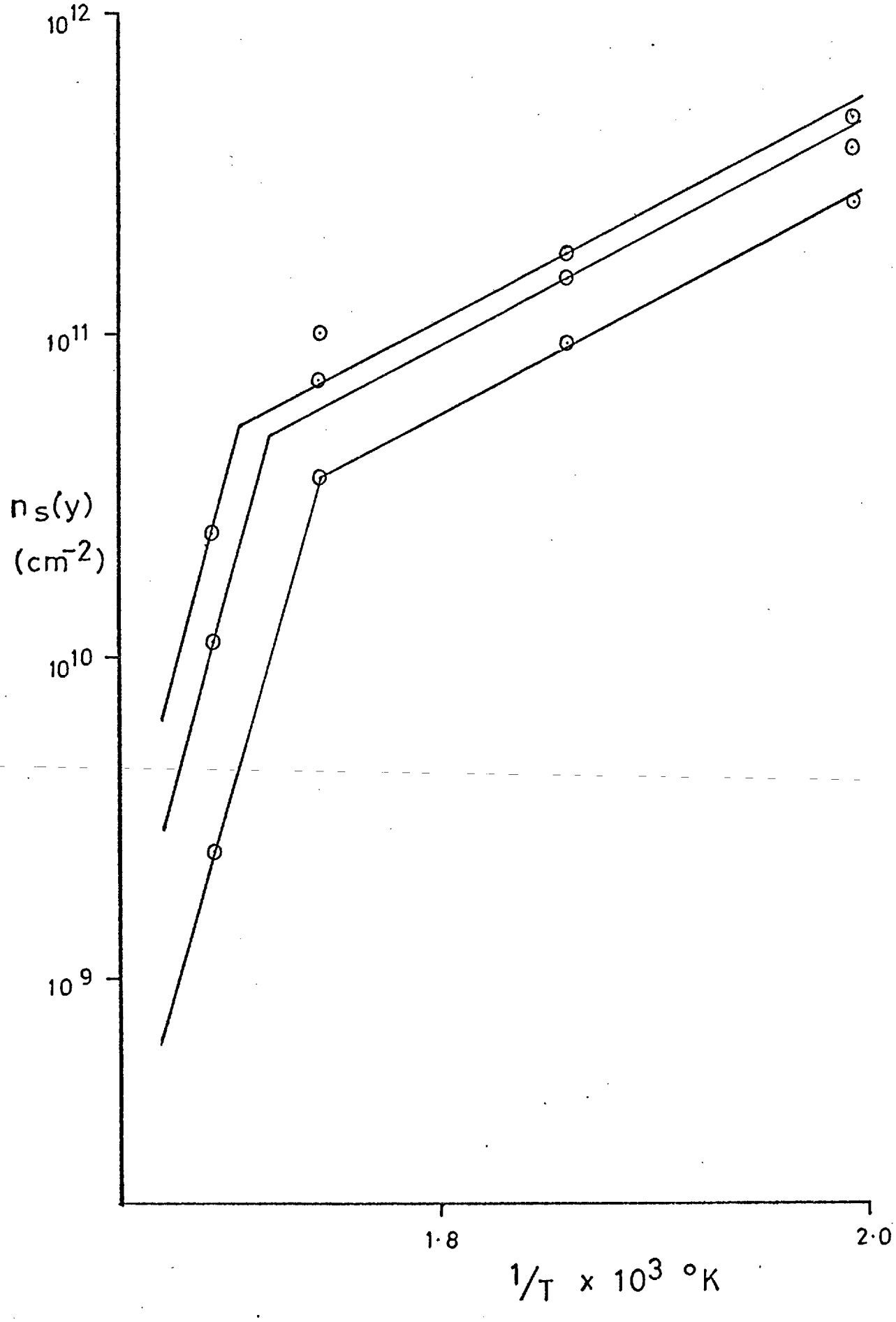

tuting into eqn.(4n) with $i^* = 3$ then gives $E_3 + 3E_d > 23.5$ eV.

4.2.8. The fractional nucleation rate model: conclusions

It has not been possible to rigorously check and confirm the predictions of the fractional nucleation rate model. However, there appear to be no experimental results which are inconsistent with its predictions.

4.3. THE CONDENSATION OF HIGH ENERGY BEAMS

This section is not obviously relevant to a study of adhesion, but the influences of high arrival energy and of electron bombardment on the nucleation process may be very important in determining the final adhesion of the film.

This work was carried out several months ago and was then interpreted and reported (Chapman & Campbell 1968) in terms of Lewis & Campbell's saturation island density model. It is now possible to analyse the data in terms of our new model, but the interpretation relies on a comparison with corresponding data for evaporated films, and we do not yet have $n_s(y)$ v. $1/T$ graphs for these.

It has already been shown (sect.4.2.5) that, provided the fractional nucleation rate is small, there is little difference between the analyses of the two models. We have therefore retained the analysis in terms of "saturation" densities, bearing in mind the shortcomings of this approach.

4.3.1. Introduction

In theories of thin film nucleation and growth, the energy with which atoms impinge on the substrate is not taken into account; it is usually assumed that the atoms are immediately

and completely thermally accommodated. This may be acceptable when the energy of the incident atoms is quite low, but becomes increasingly improbable as the incidence energy increases. Cabrera (1959) has shown theoretically that an atom should lose enough energy to the lattice to be captured if the incidence energy is less than twenty five times the adsorption energy. This condition will usually be satisfied in thermal evaporation experiments. The average kinetic energy of atoms from a source at 2000°K is only 0.2 eV. But when an atom is adsorbed, it gains as much in kinetic energy as it loses in potential energy; the adsorption energy of gold on rocksalt is ~0.5 eV $atom^{-1}$ (see Chapter II), so the impingement energy from a thermal source is ~0.7eV.

The nucleation behaviour of gold atoms, incident with beam energies 0.1-0.6 eV on to a rocksalt substrate, has been studied using a mechanical velocity distributor (Beavitt, Turnell, & Campbell, 1967); no sensible effect was found.

A study over the range 0-2 eV, using the same velocity distributor principle, is in progress (Chapman & Jordan, to be published). The method of operation of the distributor is shown in Fig.4.12; the relative displacement of an atom along the receiving substrate is equal to the displacement of the disc during the time of flight of the atom from the source. The experimental arrangement is shown in Fig.4.13.

The present report is concerned with the results of measurements of the growth of gold on rocksalt when the incident atoms, obtained by sputtering ejection, have mean energies ~20 eV. We have shown that island density measurements can be very informative and so these have been used for the present study of high incidence

re
th
be
th
th
th
th
Th
to
ve
at
ve
mu
wi
be

FIG.4.12

DIAGRAM OF DISC VELOCITY SELECTOR SYSTEM.

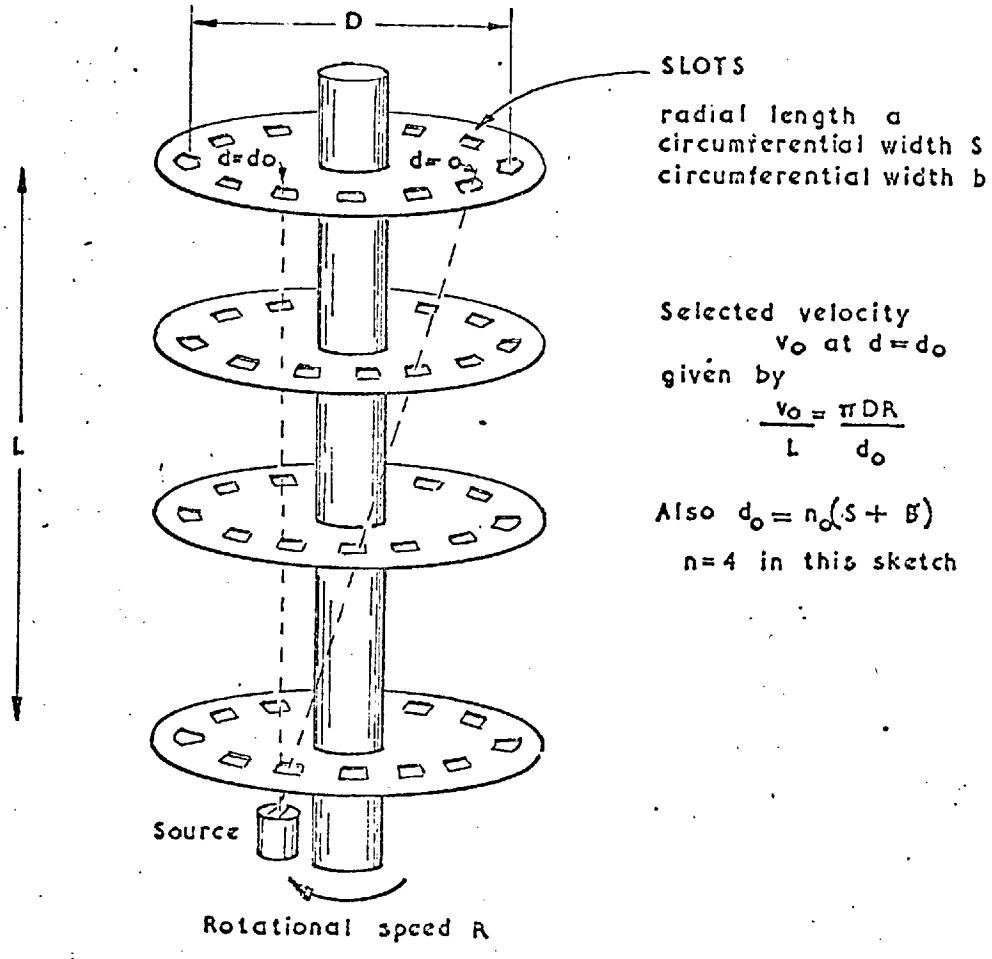

FIG. 4.13

DIAGRAM OF DISC TYPE VELOCITY SELECTOR

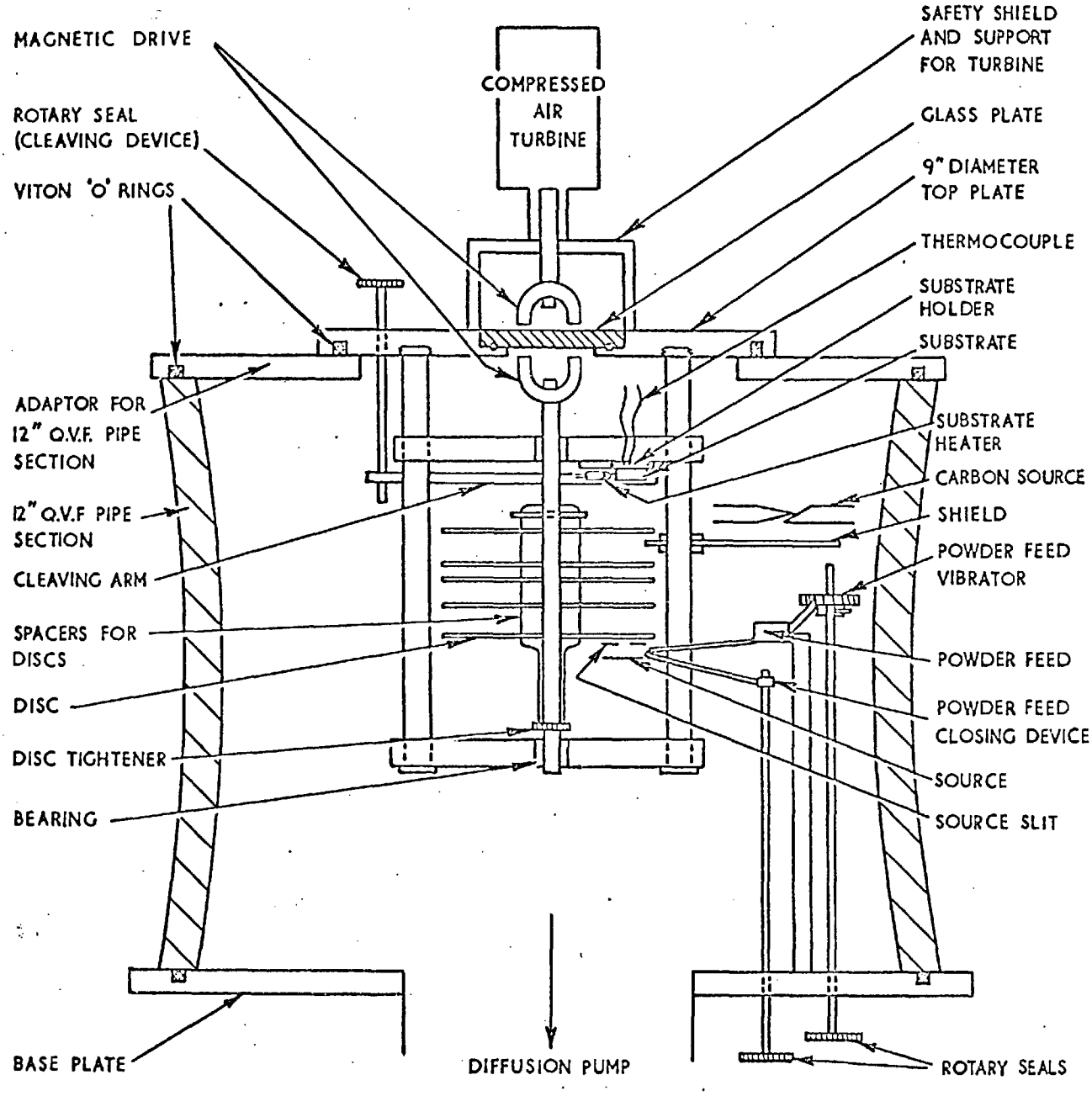

energy; the results are compared with those obtained using thermal evaporation sources when the incident atoms have energies ~0.3 eV. We have looked also at the orientations of the deposits, and have compared these with the orientations of corresponding evaporated deposits.

4.3.2. Experimental details

4.3.2.1. The high energy gold beam

The high energy beam was obtained by a sputtering technique. When a single crystal target is bombarded by fast heavy ions, atoms of the target are ejected anisotropically; material is preferentially ejected along the low index crystallographic directions of the target. The energies of ejection along specific directions from a gold target bombarded by argon ions have been measured by Thompson (1968) using a time-of-flight technique; the spectra of relative numbers against energy are shown in Fig.4.14 for two different directions of ejection. The ⟨110⟩ spectrum is from a gold crystal bombarded in a near ⟨100⟩ direction with 41 keV argon ions; the mean ejection energy is 22.7 eV. The ⟨100⟩ spectrum is from a crystal bombarded in a ⟨100⟩ direction with 43 keV argon ions; the mean ejection energy in this case is 93.5 eV, due mainly to the high energy "tail".

4.3.2.2. The experimental arrangement

The central part of the apparatus is shown in Fig.4.15 (note that the photograph is a mirror image of the schematic diagram). The gold single crystal target was mounted so that the ion beam was incident in the required direction; the orientation was checked by the Laüe X-ray reflection method. The target could be rotated about an axis collinear with the ion incidence direction,

FIG. 4.14

SPECTRA OF HIGH ENERGY SPUTTERED GOLD

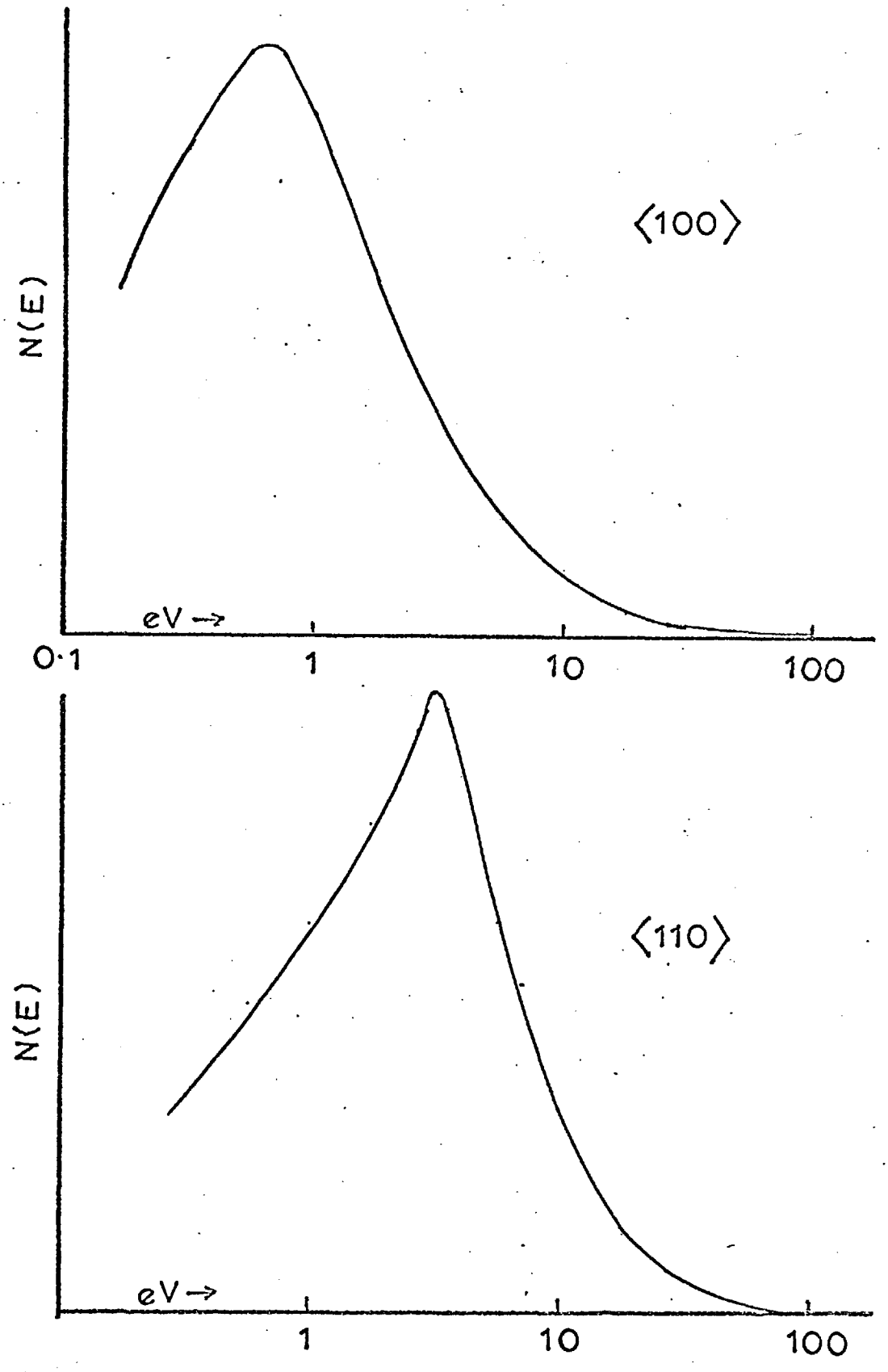

FIG. 4.15

APPARATUS USED FOR GROWTH OF GOLD SPUTTERED IN SELECTED CRYSTALLOGRAPHIC DIRECTIONS FROM A GOLD SINGLE CRYSTAL ONTO VACUUM CLEAVED ROCKSALT

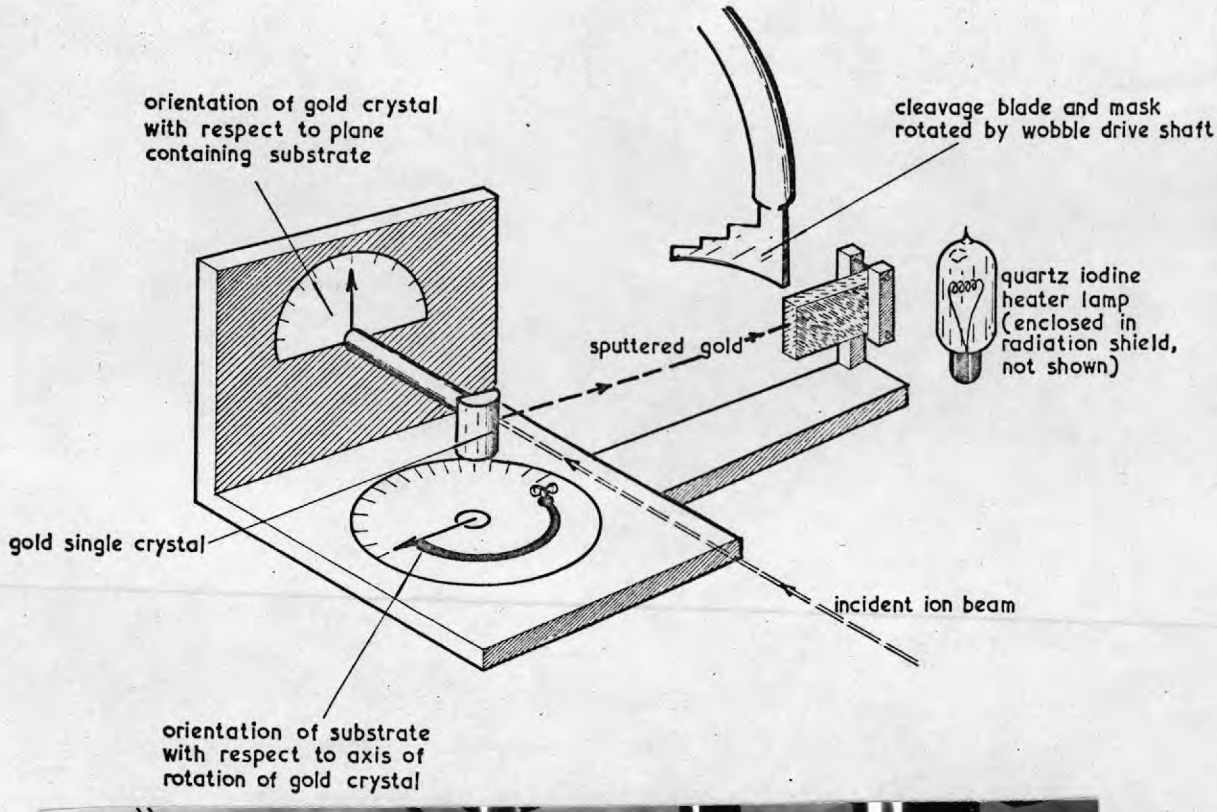


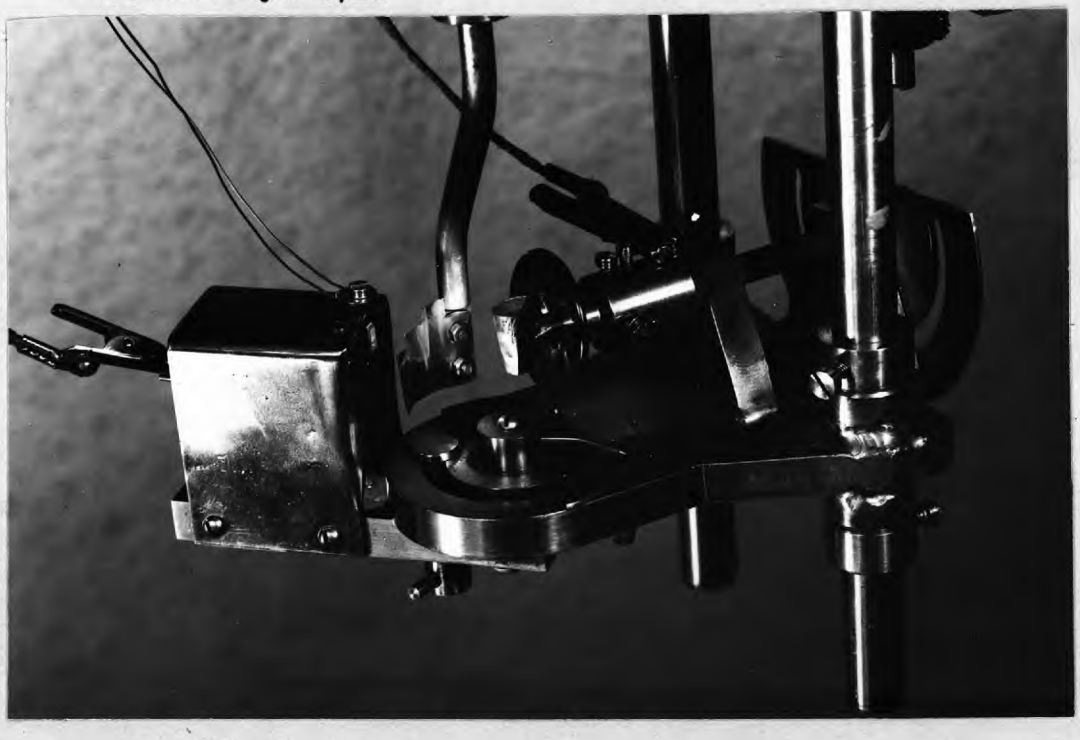

and the substrate could be rotated about a perpendicular axis through the target as shown, so that any ejection direction could be selected.

Harshaw rocksalt substrates were used, radiatively heated by a quartz-iodine lamp; the substrate temperature was measured by a chromel-alumel thermocouple. The substrates were clamped in a comparatively massive block, and the thermocouple was fixed to the block adjacent to the substrate. The energy flux at the substrate due to the incident sputtered beam was $\sim 10^{-5}$ cals $cm^{-2}$ $sec^{-1}$, so that surface heating was negligible.

In order to obtain a clean surface, the substrates were cleaved in vacuo immediately before deposition commenced. The cleavage blade, operated externally through a rotary seal, was combined with a stepped mask so that three different thicknesses of deposit on the same substrate could be obtained; in this way the island density at different stages of the experiment could be determined.

The incidence rate of gold at the substrate was measured by sputtering with large ion beam currents ($\sim 100 \mu A$) on to glass substrates at room temperature, measuring the thickness, assuming complete condensation, and further assuming that the sputtering rate was proportional to the ion current within the range used. An incidence rate of 1 Å $min^{-1}$ was produced by a few microamps beam current. The high energy ion beam was produced in a linear ion accelerator attached to the chamber containing the target assembly.

Experiments were carried out at pressures $\sim 10^{-6}$ torr. After heating the substrate to the required temperature, the gold

target was bombarded with a large ion current for several minutes to clean the surface. The ion current was then adjusted to the required value. The substrate was cleaved to commence deposition and masked off in sections at intervals, usually 1, 5, and 20 minutes, to obtain deposits of differnet thicknesses. After deposition, the substrates were cooled below 50°C before coating with carbon. The specimens were then examined by electron microscopy.

4.3.3. Results

Electron micrographs of a typical growth sequence are shown in Fig.4.16. The measured island densities are plotted as a function of time in Fig.4.17, where it can be seen that the density rapidly rises to a very high value, and then slowly increases. This is the quasi-plateau often mistaken for saturation, and in fact treated as saturation in the present case, as explained in sect.4.3.

The saturation values thus obtained for gold sputtered along the ⟨110⟩ direction are plotted aginst reciprocal substrate temperature in Fig.4.18. Incidence rates of 0.5 and 0.6 Å $min^{-1}$ were used, as shown. Values obtained by thermal evaporation deposition are shown for comparison; for these results the incidence rate was 8.4 Å $min^{-1}$.

According to Lewis & Campbell, in the complete condensation region when pairs of atoms are stable, the saturation island density $N_s$ is proportional to the square root of the incidence rate R (eqn.4d). If it assumed that the high energy results obey this rate dependence, and if the corresponding density values for an incidence rate of 8.4 Å $min^{-1}$ are thus calculated, the modified

FIG. 4.16

GROWTH SEQUENCE OF SPUTTERED GOLD ON ROCKSALT

| AFTER | 2½ mins | 10 mins | 22½ mins |
|---|---|---|---|
| DENSITY | $3{\cdot}2.\ 10^{11}\ cm^{-2}$ | $5{\cdot}2\ .10^{11}\ cm^{-2}$ | $6{\cdot}9.\ 10^{11} cm^{-2}$ |

(magnification: 60K)

FIG. 4.17

NUCLEATION DENSITY AND ESTIMATED THICKNESS FOR FILMS OBTAINED FROM HIGH ENERGY SPUTTERING EXPERIMENTS

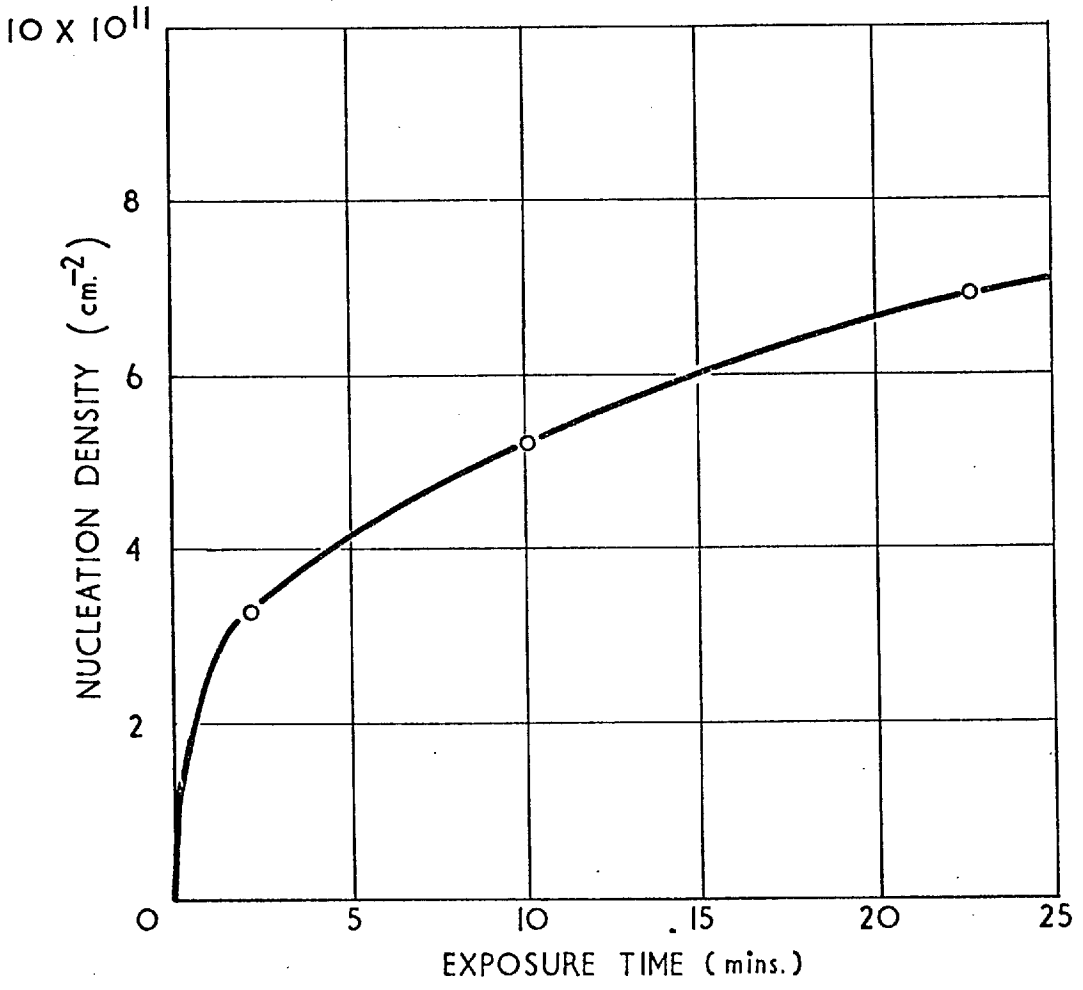

FIG. 4.18

EXPERIMENTAL VALUES OF SATURATION ISLAND DENSITIES OF GOLD ON ROCKSALT

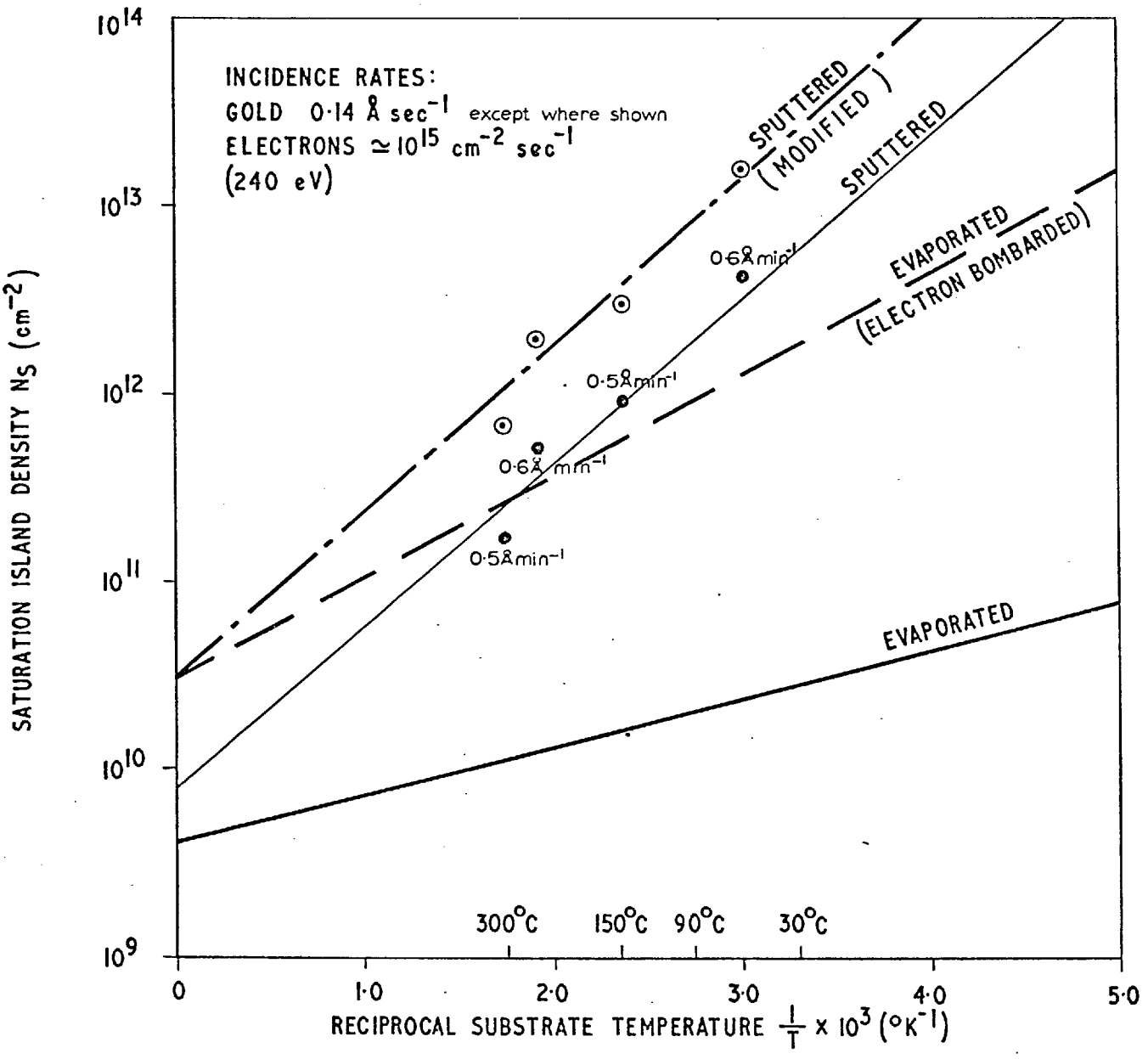

values shown in Fig.4.18 are obtained.

The fractional nucleation rate model predicts a rate dependence of $R^{2/3}$ for the same case (eqn.4n with $i^* = 1$), but the difference in the modified values would be small on a logarithmic scale although it would bring the points into better linearity. However, we will continue with the saturation model interpretation.

It can be seen that the effect of the high energy beam is to considerably increase the saturation island density, to increase the gradient of the line (which would correspond to a change in surface diffusion energy from 0.10 eV to 0.36 eV), and to shift the intercept at $1/T = 0$.

Because of the similarity of these results to those obtained by electron bombardment during thermal evaporation (Jordan & Stirland, to be published), the latter results also are shown in Fig.4.18; they were obtained at an incidence rate of 8.4 Å $min^{-1}$. Electron bombardment appears to produce, within the limits of experimental error, the same shift in the intercept at $1/T = 0$, and similar 'though less marked increases in saturation density and gradient ( corresponding to a surface diffusion energy of 0.22eV).

No experiments were carried out above 310°C because the rocksalt showed changes of surface structure at such temperatures.

The total volume of deposit was estimated by measuring the diameters and numbers of islands and assuming that each island was hemispherical. The condensation coefficient was then obtained from the ratio of condensed material to total incident material. In the unlikely event that the islands were spherical, the condensation coefficient would be twice the calculated value. It is

more likely that the island contact angle would be less than 90°, and hence that the condensation coefficient would be somewhat smaller than the calculated value.

The calculated condensation coefficients varied between 0.01 and 0.32, a typical value being 0.1; they showed no systematic variation with substrate temperature. Furthermore, there was no significant change in condensation coefficient during each experiment as the thickness increased. This apparently contradicts the theoretical prediction of the saturation model that at low temperatures when island density is controlled by surface diffusion, the condensation coefficient is equal to unity. This is discussed in the next section.

The high energy beam appears also to modify the orientation of the deposit. Fig.4.19 shows a typical sequence of transmission electron diffraction patterns obtained from three thicknesses of a specimen deposited at 150°C. It can be seen, particularly in the third and thickest film, that the orientation is predominantly the parallel orientation, i.e. $(001)_{Au}$// $(001)_{NaCl}$ with $[110]_{Au}$// $[110]_{NaCl}$ although the arcing of the 200 and 220 reflections shows that some misalignments are present. A gold deposit produced by evaporation, but otherwise under identical conditions, normally consists of two orientations, i.e. the parallel orientation together with a (111) orientation (e.g. Stirland 1966).

Further experiments have been carried out under different sputtering conditions, and produced similar results to those above. The gold single crystal target was bombarded along a ⟨111⟩ direction with 50 keV xenon ions. Atoms ejected along

FIG. 4.19

# DIFFRACTION PATTERNS OF HIGH ENERGY SPUTTERED DEPOSITS

substrate temperature 150°C
incidence rate 0·5Å $min^{-1}$

Deposition time

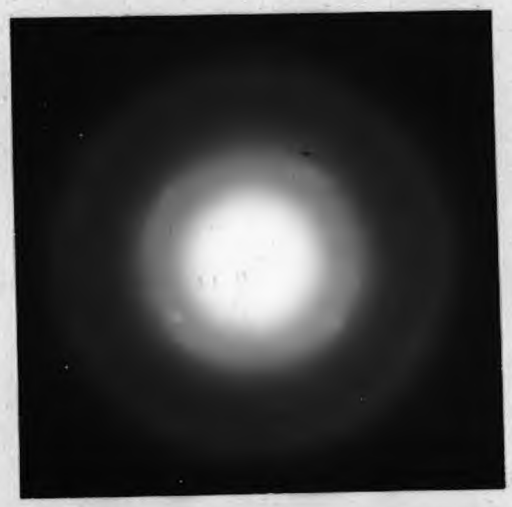

2·5 min

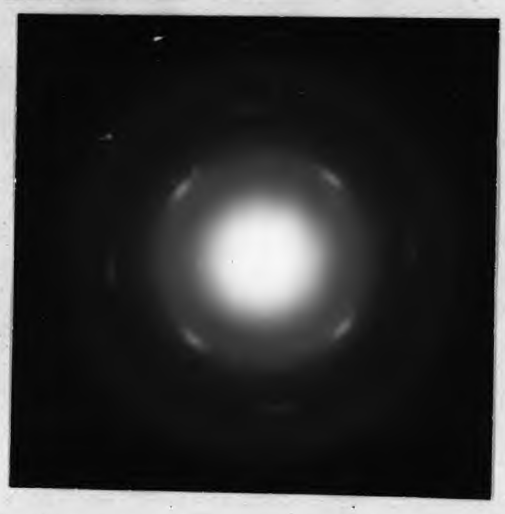

10 min

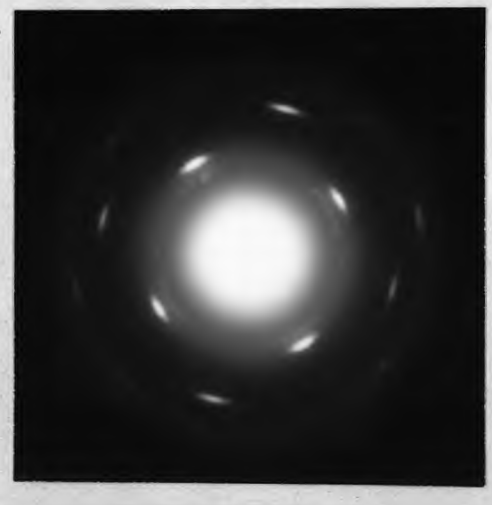

22·5 min
mean thickness 1·3Å

⟨100⟩ and ⟨110⟩ directions produced saturation densities of $7.0 \times 10^{11}$ $cm^{-2}$ and $7.2 \times 10^{11}$ $cm^{-2}$ respectively at deposition rates of 0.5 Å $min^{-1}$; the corresponding value for argon ⟨100⟩ bombardment/ gold ⟨110⟩ ejection is $9.2 \times 10^{11}$ $cm^{-2}$.

Unfortunately the ejection energy spectra for ⟨111⟩ bombardment are not known, but one would expect considerable differences between the ⟨100⟩ and ⟨110⟩ ejection directions, since these involve different contributions from each of the sputtering mechanisms involved.

Xenon bombardment also produced the same low condensation coefficients and orientation changes as were produced by argon ⟨100⟩ bombardment.

To summarise the results; compared with evaporation, the high energy beam appears to produce:

i. An increased saturation island density.

ii. A greater variation of saturation density with reciprocal substrate temperature.

iii. An increased intercept at $1/T = 0$.

iv. A low condensation coefficient.

v. A change in deposit orientation.

These results are discussed in the next section.

4.3.4. Discussion

It appears that the adatom behaviour has been altered, either directly or by modifying the interaction between adatom and substrate. Possible reasons for the different behaviour compared with evaporation deposition are described in the next section.

4.3.4.1. Thermal accommodation

It is assumed in nucleation theories that an incident atom

is immediately and completely thermally accommodated when it strikes the substrate surface. This may not be so, and the adatom may retain some of its incidence energy, producing a high effective temperature and hence enhanced diffusion and desorption probabilities. But it can be seen from eqn.(4d) that such diffusion enhancement would lead to smaller values of $N_s$, contrary to our observations.

Further evidence that enhanced diffusion and desorption are unlikely is provided by the experiments performed under different sputtering conditions with xenon as the bombarding species. Although the energies involved were unknown, they were likely to be different from those obtained with argon ⟨100⟩ bombardment; however, they produced very similar enhanced values of island densities. It would appear that we are dealing with a process which has an energy threshold below the energies used in any of the present experiments but which is almost independent of energy above the threshold. This would not be expected of a non-thermal accommodation model.

4.3.4.2. Reflection and penetration

We have so far assumed that incident material is adsorbed on the substrate surface. But some material may be immediately reflected back into the vapour phase or may penetrate the surface, and one would expect the proportions involved to be a function of arrival energy. The proportion that is adsorbed on the surface could display complete condensation behaviour, but the condensation coefficient would be equal only to that proportion so adsorbed. Contributing evidence for this proposal is that the observed coefficient did not appear to increase with

surface coverage as would be expected. Therefore loss of material by reflection or penetration could account, at least partly, for the low condensation coefficients obtained with the high energy beam. Some of the scatter in the calculated coefficients may be due to the method used for estimating the amount of material deposited, but we cannot suggest a complete explanation for the unsystematic coefficient variation.

Some penetration of the surface may be taking place. Nelson (1968, private communication) has suggested that an energy of only 1.5 eV is required for a gold atom to penetrate a rocksalt (100) surface down a ⟨100⟩ channel, plus a further 1 eV for each subsequent plane. If this is the case, then most of the sputtered beam would penetrate. However, other sources (e.g. Thompson 1968, private communication) suggest penetration energies one hundred times bigger. Using radioactive gold so that very small amounts could be detected, Lewis (1968, private communication) has shown that shallow penetration may occur even with thermal evaporation on to rocksalt.

But whether penetration, if it does take place, can affect nucleation behaviour is another matter. If gold penetrates the surface, diffuses around in the lattice, and eventually comes to the surface (in the surface)either substitutionally or interstitially, it could form a "special" adsorption site of the type discussed later. But we are unable to comment further on the likelihood of such diffusion and special site production.

4.3.4.3. Surface sites

Instead of modifying the intrinsic nucleation behaviour of the adatom, the action of the high energy beam may instead

be to modify the substrate surface and hence the energy parameters $E_a$ and $E_d$. We have already commented, both in Chapter II and in the present chapter, of the enormous changes that can be produced in these parameters by changes in surface topography or by surface charging. The equations of nucleation theories can be directly applied only if the modified parameters $E_a$ and $E_d$ apply to the whole surface, i.e. to every adsorption site on the surface. If eqn.(4d) can be applied, then the change in island densities corresponds to a change in surface diffusion energy from 0.10 eV to 0.36 eV $atom^{-1}$ and a change in the 1/T = 0 intercept value of $(RN_o/\nu_o)^{\frac{1}{2}}$ from $4 \times 10^{10}$ $cm^{-2}$ to $3 \times 10^{11}$ $cm^{-2}$. The fractional nucleation rate model would give a corresponding change in $E_d$ from 0.15 eV to 0.54 eV. But when the whole substrate is not modified, no quantitative conclusions can be drawn about changes in the nucleation parameters.

Electron bombardment of the substrate during evaporation has been found by Stirland (1966), Stirland (1968), and Jordan & Stirland, to produce both an increase in saturation density and a change in orientation. The results of the latter pair are very similar to the results of the present work, as was shown above, and suggest a similar mechanism. Palmberg, Rhodin & Todd (1967) have shown that electron bombardment before deposition produces the same change in epitaxy as was noted by the above gentlemen, provided that the substrate temperature was kept below 80°C. Stirland found that electron bombardment before deposition on a rocksalt substrate at 150°C produced an increase in island density, but no change in orientation.

Palmberg et al. have suggested that the effect of electron

bombardment is to dissociate the surface and produce surface vacancies or move substrate atoms from their normal positions. In either case, preferred nucleation sites would be formed, at which the adsorption energy is higher than at a normal site. The number of surface defects would be governed by the equilibrium between production rate and loss rate, the latter being temperature dependent and due to annealing-out of the defects. As the substrate temperature increases, so does the annealing rate and hence the number of defects decreases; the difference between island densities on bombarded and non-bombarded surfaces would therefore be expected to decrease with increasing substrate temperature, as is observed. Subsequent work by Rhodin & Palmberg (to be published) and by Townsend & Kelly (1968) has produced further evidence for the creation of surface defects by electron bombardment. The impact on the substrate surface of high energy neutral gold atoms, as in the present work, may produce similar damage. However, the surface damage in this case may result from associated charge effects, as is described in the following section (4.3.4.4).

But mere decoration of surface defects would not lead to the saturation density behaviour observed with electron bombardment by Jordan & Stirland, and with high energy bombardment in the present work; in both these cases, the defect production process continued simultaneously with condensate deposition. With an initially bare substrate, the defect production rate would quickly be balanced by the annealing rate, and an equilibrium density of defects would be set up. If bombardment was then stopped and gold evaporation immediately carried out, the defects

would be decorated and saturation behaviour would be observed. But the situation will be different if defect production continues during gold deposition. Then, as each defect site is removed from the defect production/annealing process by gold decoration, a fresh site will be produced elsewhere to maintain the equilibrium defect density. The fresh site will then be decorated, another site will be produced elsewhere, and so on. But this is inconsistent with the observations of saturation behaviour.

Saturation behaviour would be produced if the adsorption energy of a gold adatom at a defect was greater than that on a normal perfect rocksalt surface, and less than that at a stable gold island; having established an initial density of islands by decoration of defects, further adatoms would be preferentially adsorbed by the islands.

4.3.4.4. Charged material in the sputtered beam

There is a complication in the interpretation of the observed results because the sputtered beam contains not only neutral gold atoms but also an amount of charged material. There may be a few percent. of singly ionised gold atoms of low energy (Thompson 1968, private communication) and a much smaller number of multiply ionised gold atoms of quite high energy, perhaps as high as several keV (Kistemacker 1968, private communication). Furthermore, a small proportion of the argon ions bombarding the gold target may subsequently strike the substrate, as may the electrons which usually accompany sputtering processes. The incidence of so much charged material makes interpretation more difficult. Assuming, for the moment, that the bombardment does

not affect the substrate, we may be observing a dual nucleation process - of gold atoms and of gold ions. Because the ions would have a Coulomb interaction with the ionic rocksalt surface as well as a van der Waals' interaction (see Chapter II), both adsorption energy and diffusion energy would be increased, consistent with our observations. But for how long an ion could migrate across the surface without re-association with an electron is the pertinent question in this case. Re-association towards the end of a surface diffusion path would not affect the previous history of the ion, and so would not significantly alter its total diffusion path; late re-association may even be advantageous because otherwise the Coulomb repulsion between like gold ions would inhibit nucleation.

It may instead be that only the charged incident material is responsible for causing the surface defects discussed above. In this case, the high energy of the incident beam would not be directly affecting the nucleation process, serving only to produce the low condensation coefficients observed.

4.3.4.5. Orientation effects

The change in orientation may be due to an initial improved ordering of atoms in an island because a decorated defect in the surface produces a good foundation, or to a subsequent re-arrangement of multiply oriented islands when they are struck by incident energetic particles. Each configuration of an island is quasi-stable because a potential barrier discourages re-arrangement even into a configuration which is energetically more favourable; the collision of an incident particle may enable potential barriers to be surmounted because of the subsequent energy transfer.

The different effects of pre-bombardment observed by Palmberg et al. and by Stirland have been noted above. The former gentlemen acheived the single orientation below 80°C without simultaneous bombardment, which supports the "defect foundation" model; the latter's results at 150°C suggest that bombardment during deposition is necessary and hence support the "re-arrangement" model, although Stirland has suggested that the high density observed may have been due to decoration of carbonaceous material which had formed, under electron bombardment, from hydrocarbons in the vacuum system by "cracking" and subsequent cross-linking on the substrate. Maybe the electron-induced defects had annealed out at this elevated temperature, consistent with the observations of Palmberg et al.

Jordan & Stirland have produced much better singly oriented deposits with electron bombardment than in the present work. This would not be surprising on the "re-arrangement" model, since their electron energy input flux to the substrate was several thousand times larger than with the high energy beam.(The "high energy" of the sputtered beam is relative only to the energy of a thermal evaporation beam). On the other hand, Stirland suggests that the threshold for electron bombardment effects is at much lower energy inputs.

The evidence in favour of either model is not overwhelming, but the "defect foundation" model seems more likely, although we are unable to suggest a mechanism for the ordering effect.

4.3.5. Conclusions

It has been shown that poor thermal accommodation of high energy incident atoms would not lead to the changes in island

density behaviour which are observed. But lack of accommodation may be responsible for the low condensation coefficients.

There is evidence to suggest that the increased island densities may be due to the creation of "special" sites, with higher surface diffusion energy than usual. But whether the special sites are created by the impulse of high energy neutral atoms or by associated charge effects, has not been resolved. If the latter, then the high energy neutral material is having no effect on island densities. The density effects observed in the present work and the effects produced by electron bombardment may both be due to the production of surface sites of higher diffusion energy, but it has not been established that the same type of site is formed in both cases.

The changes in deposit orientation may be due to the ordering effect of a decorated special site, or to the re-arranging effect of impinging energetic particles on an already existing island. It is concluded that the former is more likely.

# CHAPTER V

# MECHANICAL METHODS

There have been several attempts to measure thin film adhesion energies by mechanically removing the film from the substrate. Many of the proposed methods, which have been reviewed by Campbell (1969), have been unsuccessful in removing the film, and many others have produced unsatisfactory results. Two adhesion tests which have gained some popularity are the "scratch test" of Weaver et al.(1958 et seq.) and the tape test originating from Strong (1935).

The scratch test consists of scribing the film with a fine smoothly rounded point under increasing loads, and taking the critical load which just penetrates to the substrate as a measure of the film adhesion. This method is discussed later in the chapter.

The tape test consists of pressing a length of adhesive tape against the film, and then tearing off the tape. The adhesion of the film is classified according to whether the film is wholly or partly removed from the substrate with the tape, or not removed at all. Obviously this is only a qualitative test.

Much of this chapter is concerned with an attempt to quantify the tape test, although in a very restricted range, and this has lead to some interesting results.

## 5.1 MECHANICAL STRIPPING

### 5.1.1. Method

The principle of the stripping method is shown in Fig.5.1. If a force F moves a distance dl in stripping a length dx of film of width w from its substrate, then equating the work done

FIG. 5.1

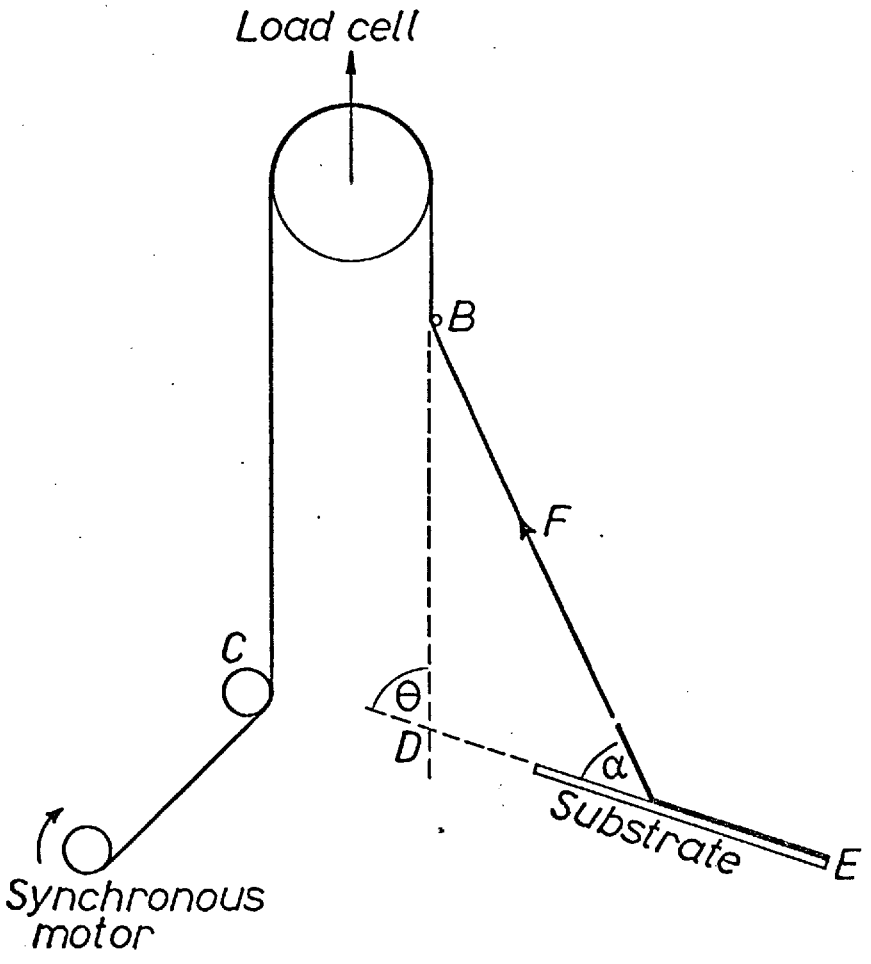


CONFIGURATION OF MECHANICAL STRIPPING APPARATUS

by the force to the work of removing the film,

$$F\,dl = S\,w\,dx \qquad \ldots.(5a)$$

where S is the stripping energy required to strip unit area of the film; this energy will exceed the adhesion energy by the amount of any extraneous work done in the removal process, and so it is a measure of adhesive performance, as discussed in Chapter I.

A consideration of the geometry of Fig.5.1. shows that:

$$dl = dx - dx \cos \alpha \qquad \ldots.(5b)$$

where $\alpha$ is the angle between the applied force and the substrate. Hence,

$$S = \frac{F}{w} ( 1 - \cos\alpha ) \qquad \ldots.(5c)$$

Thus the instantaneous stripping energy is directly related to the applied stripping force. But it is also possible, and often more convenient and more useful, to measure an average value of the stripping energy since it is clear from equation (5a) that:

$$S = \int \frac{F\,dl}{A} \qquad \ldots.(5d)$$

where A is the total area of film removed.

The experimental arrangement for carrying out such measurements is shown in Figs. 5.1 & 5.2. The stripping force is applied to the film via a thin string which passes over a pulley, whereby the force is measured, to a synchronous electric motor which winds the string at a constant rate $\dot{l}$. The two pivots B and C constrain the string so that the load on the pulley is always vertical and equal to twice the tension in the string. The pulley is suspended from a load cell (Coutant Ltd.) consisting of four piezoresistive silicon strain gauges in a bridge formation mounted on a cantilever. The off-balance bridge voltage, which is directly proportional to the applied load, is fed to a potentiometric

FIG.5.2

MECHANICAL STRIPPING APPARATUS.

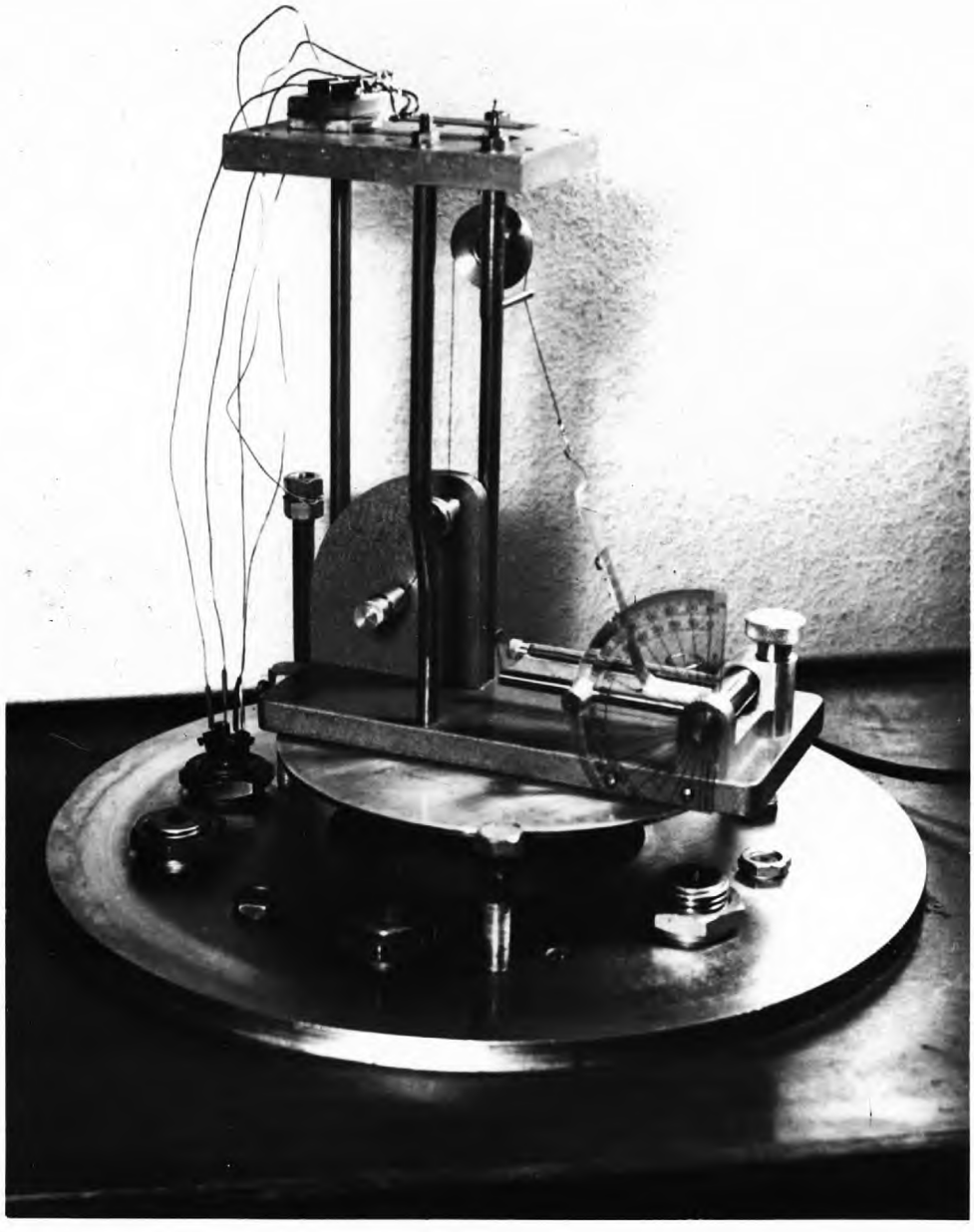

chart recorder.

The recorder actually traces the variation of F with time, but since the force moves at a constant rate $\dot{l}$ the recorded curve is easily translated into one of F $\dot{l}$ against time. The total area under the curve is directly proportional to $\int F\, dl$ and therefore to the work done in stripping the film.

5.1.2. Accuracy of the method

Both the pivots B and C and the pulley bearings have frictional resistances which impose limits to the meaningful sensitivity of the mechanical stripping apparatus.

The apparatus was first used to lift known masses at known constant rates, and the load cell output was continuously monitored. These observations enabled the apparatus to be calibrated for each standard mass; in addition, the constancy of the output could be checked and the calibration factors could be compared, which is equivalent to checking the linearity of the instrument. It was found that the cell output when lifting a given constant load, and thus working at a constant rate, varied.

The variation in deflection decreased from approximately 20% of mean at very small loads ( $<$ 0.5 gm.) to negligible amounts at larger loads. This variation is of the instantaneous load cell output, but the variation in integrated load outputs, i.e. the area under the recorded curves, was always much smaller and was typically less than 10%, even over very short integrating periods. The fluctuations were probably due to variations in frictional resistance at the pulley bearings as the pulley rotated.

It was found that the apparatus gave a very linear response over the whole range investigated, and any deviations from linearity were much smaller than those above, and could thus

be ignored.

It therefore appears that frictional effects are either small or proportional to the applied load; in neither case is the accuracy much impaired provided that the apparatus is calibrated with standard loads.

5.1.3 Application to the measurement of thin film adhesion

In the cases of intermediate layer formation or interdiffusion adhesion (secn.1.4), the adhesion process is not usually reversible, and thus the stripping method can be used to obtain useful indications only of interfacial adhesion energies.

The stripping force is transmitted to the film via a thin wire trapeze to spread the load, fastened to a length of adhesive tape which in turn is attached to the film as shown in Fig.5.3. Several tapes were evaluated for this purpose. Conventional "Sellotape" (Sellotape Products Ltd.) was found to be suitable and was used for most of the work.

In order to make any useful measurements, the film must be completely removed from the substrate. Therefore the tape-film adhesion must be greater than the film-substrate adhesion. This limits the systems which can be investigated by this method.

5.1.4 Results

5.1.4.1. Preliminary comparative results: supported film

Films of gold, silver, and copper were stripped from soda glass, borosilicate glass, and silica substrates in order to compare the adhesions of the various combinations. The stripped film was supported along its entire length by backing tape. Stripping was carried out in atmosphere and also in a vacuum of $\sim 10^{-5}$ torr. This preliminary work was extremely useful in gaining familiarity with the techniques and uniquities of the appar-

FIG. 5.3

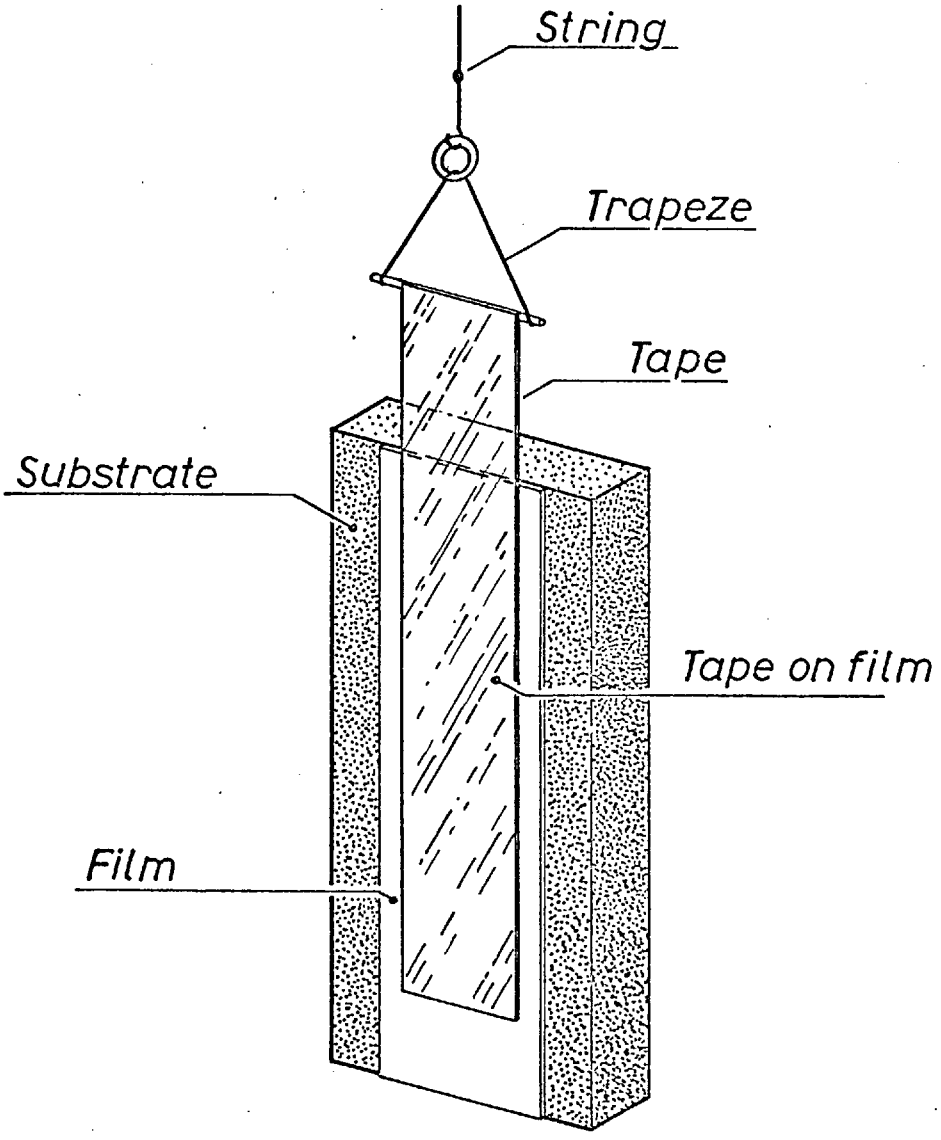


SAMPLE MOUNTING (A)

atus, but since insufficient detail was paid to several details, the actual values obtained are not reliable. It was observed, however, that all the films could be removed completely, and that in every case the values obtained for stripping at atmospheric pressure were considerably less than those for stripping in vacuum.

5.1.4.2. The influence of stripping angle: supported film

When a film is stripped from a substrate at a given angle, it may be expected that extraneous work will be associated with bending the film as it is removed. We would therefore expect the stripping energy to decrease with decreasing stripping angle. The relationship between these parameters was investigated.

It can be seen from Fig.5.1. that the stripping angle $\alpha$ decreases as stripping progresses. With the particular apparatus used, this decrease was from approximately $\theta$ to $\theta - 30^{\circ}$ over the length of the substrate, where $\theta$ is the angle of inclination of the substrate to the vertical. To gauge the effect of the changing stripping angle, experiments were carried out at various angles of $\theta$ . For this purpose, films of gold on soda glass substrates (Baird & Tatlock Ltd. D6/0150 3" x 1" microscope slides) were chosen. The surface of the substrate is obviously of great importance but investigation of substrate cleaning techniques suggested that many cleaning methods actually cause a deterioration of the substrate surface; Fig.5.4. shows the effect of some cleaning procedures (Blackburn & Campbell, private communication). It appeared that the best surface for our purposes was obtained merely by degreasing the glass. The substrates were therefore given the following treatment:

FIG. 5.4

EFFECTS ON GLASS OF VARIOUS SURFACE TREATMENTS

(Pt/C.replica) (X 10,000)


(a) Original glass surface.

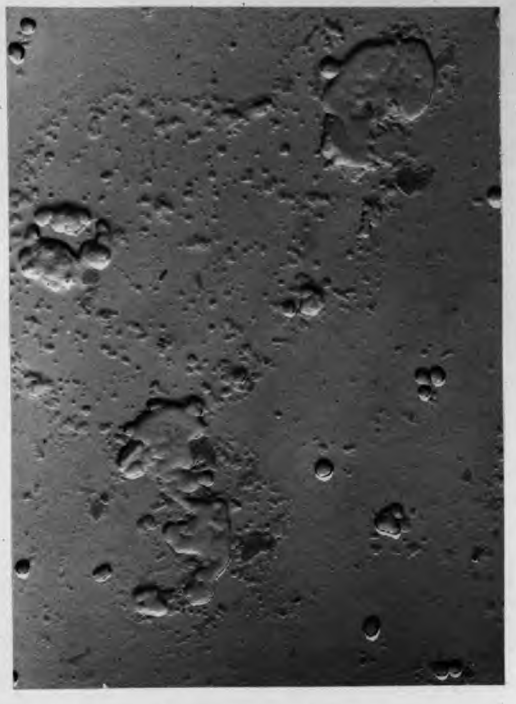

(b) 40 % H.F. sol$^{n}$. for 5mins.

(c) H. F. vapour at room temp. for 3 mins.

(d) Ground with 600 mesh carborundum

i. Washed for 10 minutes in an ultrasonic bath in "Decon" (Medical & Pharmaceutical Products Ltd.),

ii. Rinsed in 6 changes of deionised water,

iii. Washed for 10 minutes in an ultrasonic bath in isopropylalcohol and then polished dry with lens tissue to avoid drying marks.

The gold films were prepared by evaporating a given weight ($\pm$ 5%) of gold from a molybdenum boat in an oil-pumped vacuum system with liquid nitrogen trap at pressures $\sim 10^{-5}$ torr. The evaporation rate was not monitored, but evaporation took, typically, three minutes. The nominal thickness of the films, which covered most of the substrate, was 2000 Å.

The films were backed, along most of their length, with adhesive tape 1.3 cm wide. The tape tore a track of its own width in the film, but the number of ruptured cohesion bonds along each edge of the film was negligible compared with the number of ruptured gold-glass bonds and could therefore be ignored.

Stripping was carried out at a pressure $\sim 10^{-5}$ torr and a winding rate $\dot{l}$ of 8.8 micron $sec^{-1}$. A number of distinguishable glass substrates were each used several times, but no correlation was found between individual substrates and adhesion energies.

As $\theta$ decreased, the stripping force F increased as expected; angles of $\theta < 40^{\circ}$ produced values of F without the range of the load cell.

Results are shown in Fig.5.5. Each experimental point is an average of results from at least three films; the range of values shown indicates the expected error (R.M.S. deviation). These results show quite a large scatter and large R.M.S. deviations, but it is impossible to say how much of this was due to apparatus

FIG. 5.5

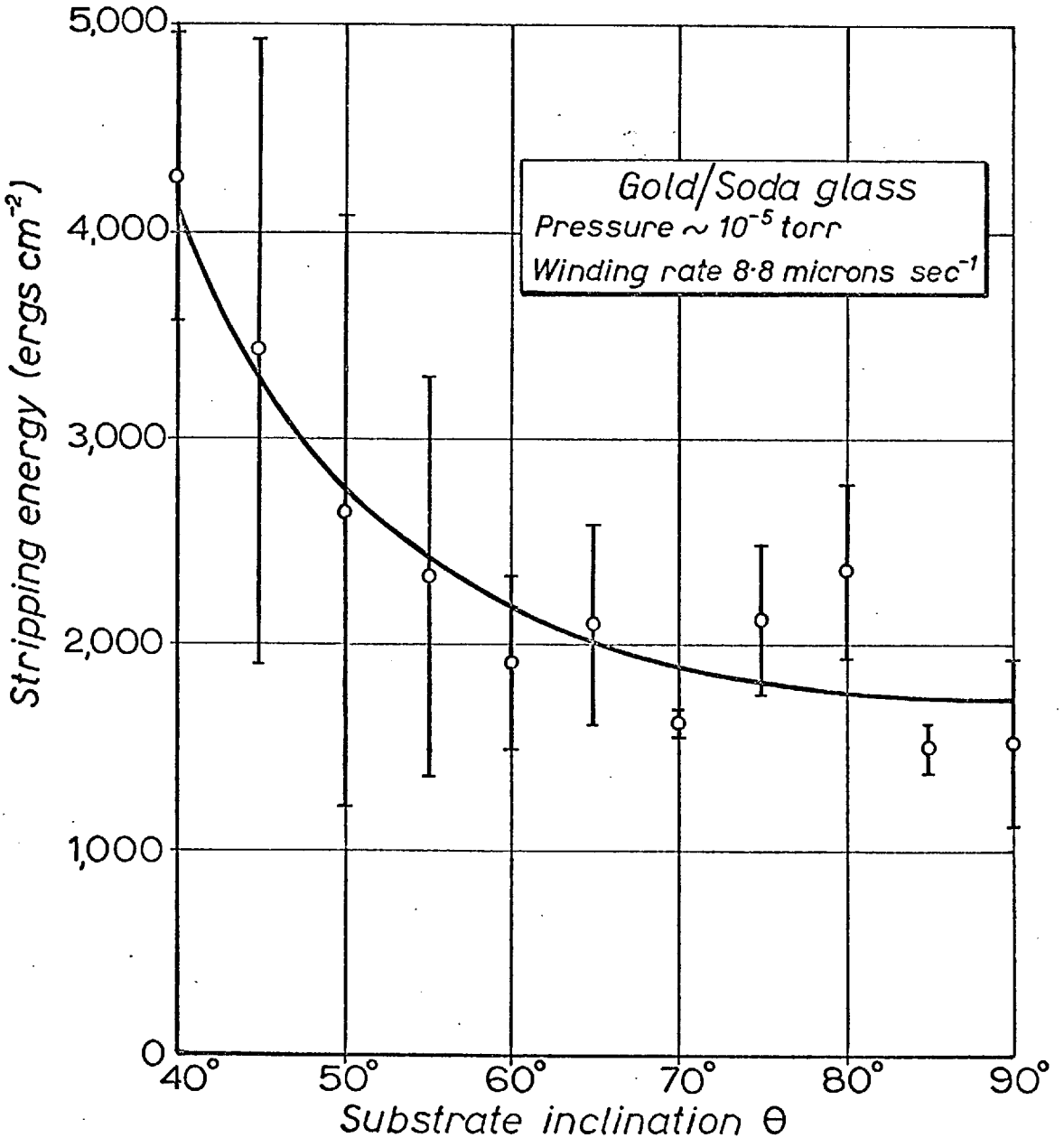


VARIATION OF STRIPPING ENERGY S WITH INCLINATION ANGLE θ

inconsistency and how much to genuine variations from sample to sample; during any one experiment, the stripping force showed deviations of as much as ± 50% of mean as stripping progressed.

A typical value of stripping energy obtained, 2000 erg $cm^{-2}$, corresponds to a bond energy of 1 eV, and is approximately double the value predicted in Table 2.5., which suggests that the experimental value obtained contains extraneous contributions. However, the value obtained is of the correct order of magnitude.

5.1.4.3. The influence of stripping rate: supported film

It can be seen from eqn.(5b) that the stripping rate $\dot{x}$ and the winding rate $\dot{l}$ are related via the stripping angle $\alpha$ :

$$\dot{l} = \dot{x}(1 - \cos\alpha)$$

We have seen that $\alpha$ decreases during the course of an experiment, and $\dot{x}$ will vary similarly. But this is not the only cause of stripping rate variation; both the load cell cantilever and the winding string are extensible, so that when the stripping force is increased, the stripping rate decreases, and vice versa. Therefore the change in stripping rate is not monotonic. However, this change of rate is small compared with the order of magnitude rate changes which were found necessary to produce significant variations in stripping energy, as shown in Fig.5.6. Each point is an average of at least four film samples - the range shown again refers to R.M.S. deviation. The substrate inclination angle $\theta$ was 90° in all cases, and stripping took place at $10^{-5}$ torr in an oil-pumped system.

Films of gold on glass were prepared and stripped as before except that fresh glass substrates were used for each sample. The constant load output variation (secn.5.1.2.) was less than 3% of mean deflection. Stripping speeds less than 500 Å $sec^{-1}$ were not attainable.

FIG. 5.6

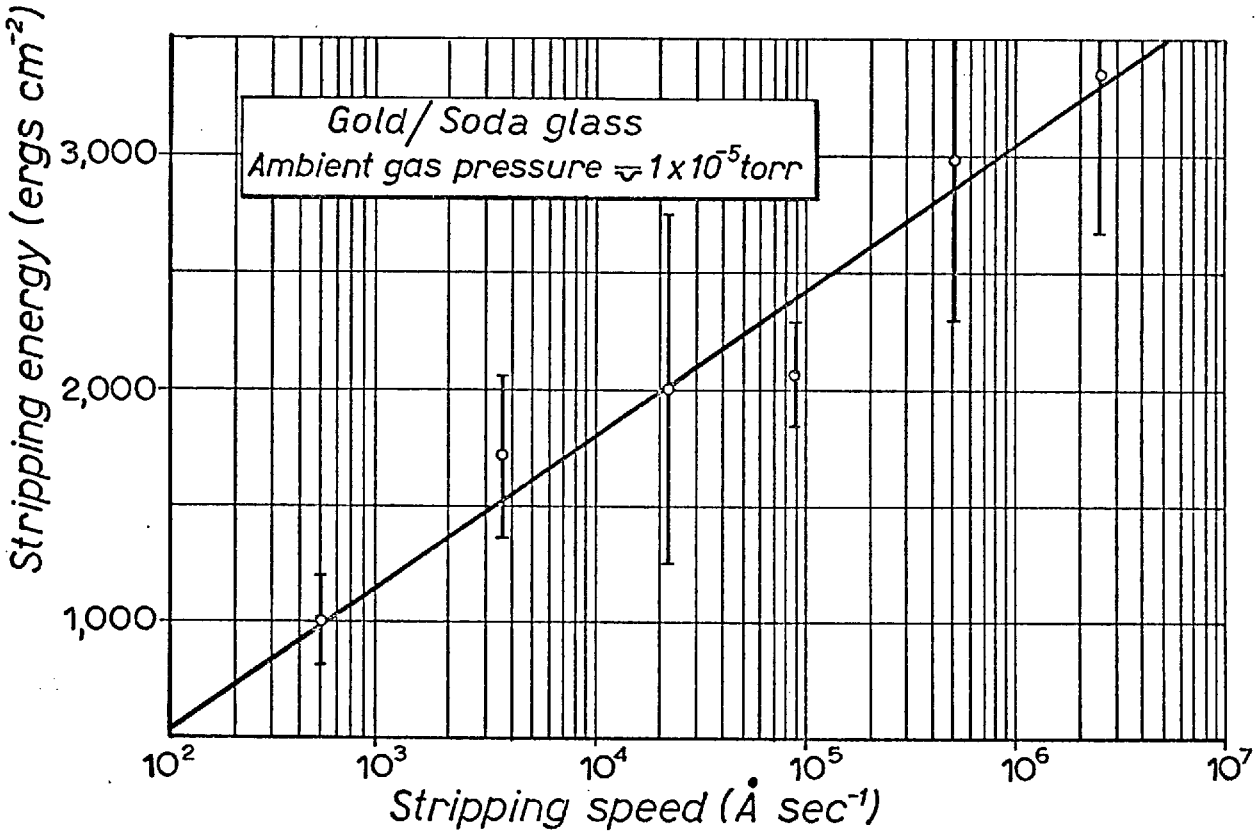


VARIATION OF STRIPPING ENERGY WITH STRIPPING RATE

5.1.4.4. The influence of the nature and pressure of the stripping environment: supported film

It had been observed (secn.5.1.4.1.) that stripping energy depended on the pressure of the surrounding gas during stripping. This effect was investigated further. Preparation and stripping conditions of the films were as before. Measurements were made in atmospheres of oxygen and of water vapour. The vacuum system was exhausted to $\sim 10^{-6}$ torr and then filled with gas to the required pressure. The substrate inclination $\theta$ was maintained at $90^{o}$, and the stripping speed was nominally 8.8 micron $sec^{-1}$. Results are shown in Fig.5.7. Although there is a large scatter which would make quantitative interpretation difficult, there is no doubt that an increased pressure of either oxygen or water vapour causes a decrease in stripping energy.

5.1.4.5. The influence of the adhesive tape and other considerations

The main criticism of the above results is that the backing tape may have influenced the results, for example by releasing stored strain energy during stripping. It had been suggested (Isler & Kilduff 1967, private communication) that stress-free backings could be produced using cross-linked silicone rubbers.

Stress in thin films can be measured by depositing on to thin glass substrates, taking the resulting deflection of the substrate/film combination as a measure of the stress ( e.g. Carpenter & Campbell 1967). A similar technique was used to measure the stress in silicone rubbers; all of these were found to produce very large stresses and their use was not considered further.

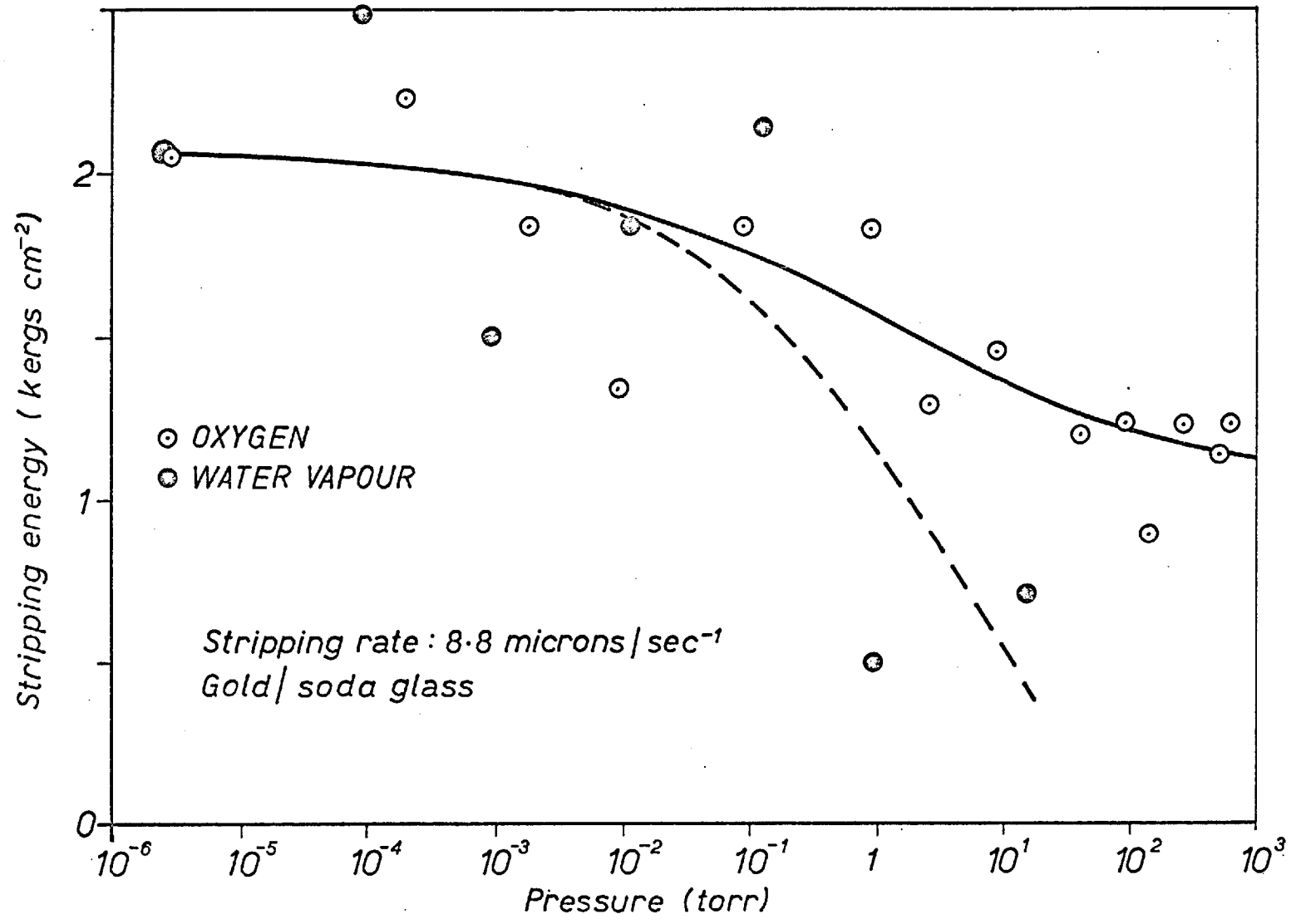


FIG. 5.7

VARIATION OF STRIPPING ENERGY WITH AMBIENT GAS PRESSURE

To avoid the risk of any spurious effects from the adhesive backing tape, it was decided to dispense with its use! This was acheived by attaching the tape to approximately the first centimetre of the film only, so that the stripping force to the remainder was transmitted through the film itself. This required films thick enough to transmit the stripping force without tearing or plastically deforming; the lower limit was found to be about 1500 Å. Some difficulty was encountered in stripping films more than 1 cm wide, as the width of the film stripped tended to decrease as stripping progressed. The area stripped could be measured whatever its shape, but it was obviously better to maintain a constant stripping width. This was found to be possible by stripping widths of approximately 5 mm. The mounting procedure is shown in Fig.5.8. A ½" width of tape was applied to one end of the film, and the tape and film were then scribed with a fresh razor blade (a fresh blade was essential to prevent dragging the film as it was scribed) to the shape shown. This had the further advantage that the beginning and end of stripping the unsupported film were each clearly defined by a discontinuous decrease in the required stripping force. Furthermore, the shorter length stripped reduced the variation in $\alpha$ during each experiment to less than 15°.

Further modifications to the equipment were made. It is well known in tensile testing that a rapidly varying applied force will cause fracture in a specimen more rapidly than a static force of the same magnitude. In order to obviate any vibration effects from the rotary pump during the stripping measurement, a sorption pump was introduced into the system as an alternative means of "backing" the diffusion pump. Since a sorption pump quickly saturates on

FIG. 5.8.

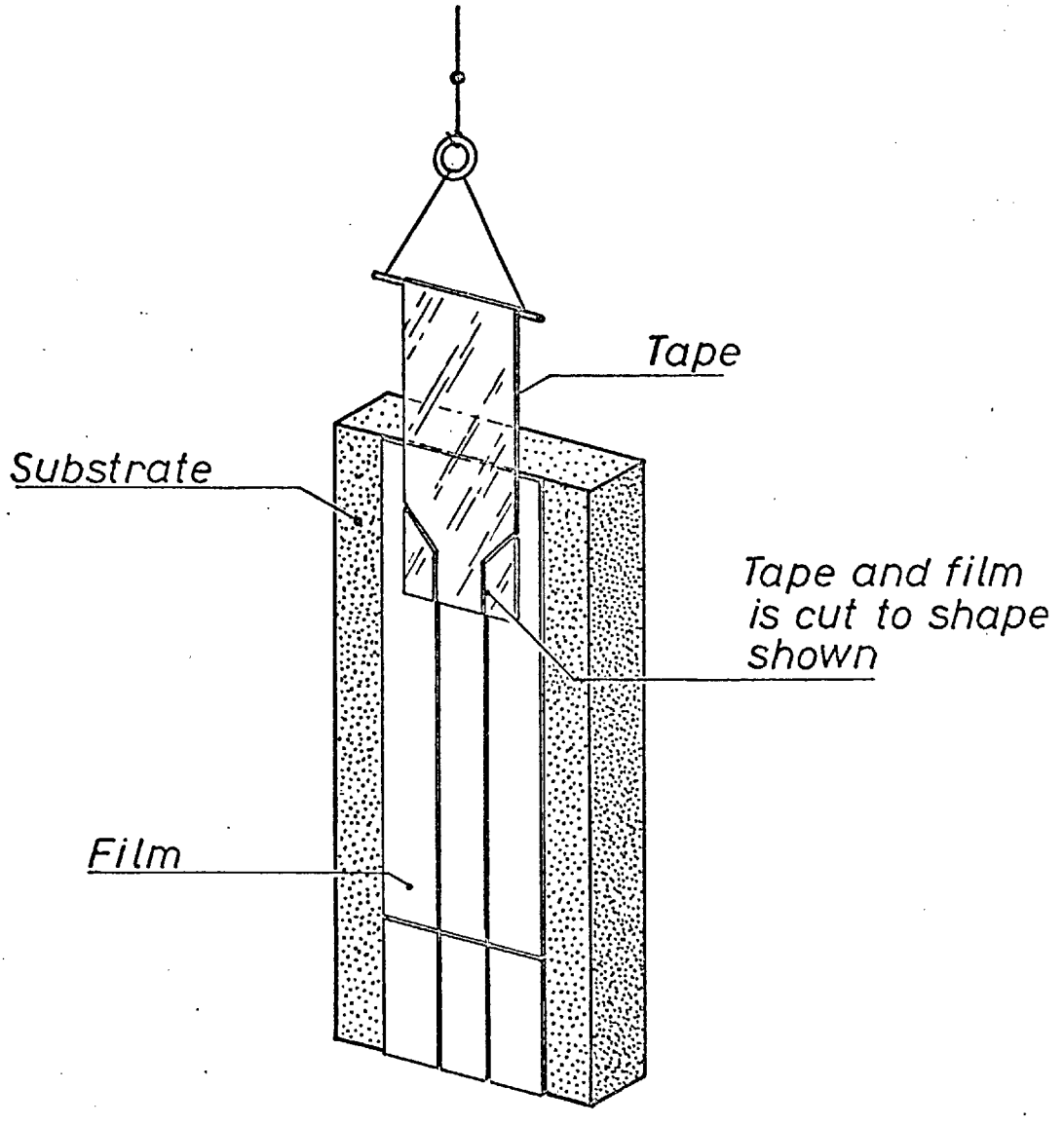


SAMPLE MOUNTING (B)

large gas loads, the rotary pump was used to prepump the system; the sorption pump was brought into use just before and during actual stripping.

In order to produce more consistent samples, groups of eight glass substrates were cleaned together, and evaporated on to simultaneously. The cleaning procedure was as before apart from the drying procedure: after the IPA wash, the substrates were placed in an IPA reflux condenser for 5 minutes to remove surplus water and residues, and then finally dried in an oven at 150°C for 10 minutes. This procedure avoided drying marks, which had been apparent to a limited extent before. Having been cleaned, the substrates were placed symmetrically on a turntable which was rotated above the source during evaporation to promote uniformity.

A further point which warranted investigation was the significance of stored energy in the string and cantilever. This stored energy is a function of stripping force, and if the stripping forces at the beginning and end of an experiment are different, the change in stored energy should be allowed for. The stored energy was measured as a function of stripping force by clamping the free end of the string and then noting the work done in producing a given force as winding proceeded. The results reported in secn.5.1.4.4. were examined from this point of view (indeed, the results given for oxygen are compensated for this effect), but the correction was always less than 8%.

Some preliminary familiarisation work with the revised equipment was carried out. The difference between the tape-backed film and the unsupported film was marked: the large stripping force fluctuations evident in the former were replaced

by much smaller fluctuations in the latter. Furthermore, the stripping energy was considerably smaller with the unsupported film, which suggests that considerable work had been done on the tape in previous experiments.

A typical record of the variation of stripping force with time is shown in Fig.5.9. The slack in the winding string is first taken up, then the force is large while the tape-backed film is being peeled, reducing as the tape width decreases (see Fig.5.8.) There is then a sharp decrease when the end of the tape and the beginning of the unsupported film is reached. The latter is then stripped, the stripping force again reducing suddenly as the end of the film is reached. Winding continues whilst a no-load baseline is recorded for a time equal to the significant stripping time. The difference in the areas under the two curves, after corrections for stored energy, is a measure of the net work done in removing the film.

An unfortunate consequence of the reduced stripping force of an unsupported film is that the baseline fluctuations due to frictional effects (secn.5.1.2.) are then comparatively large. It can be seen from Fig.5.9. that these were as much as 25% of the mean stripping force. However, these are only short term variations; if the area under the baseline is divided into four equal sections, it is found that the corresponding long-term fluctuations are less than 10% of the mean work of stripping.

Some electron microscopy was carried out at this stage. It was found that the original substrates were generally smooth, with occasional shallow craters. After stripping, the gold was almost completely removed from the substrate; any gold remaining was always found as small ($\sim$1000 Å) islands on very rough areas

FIG. 5.9

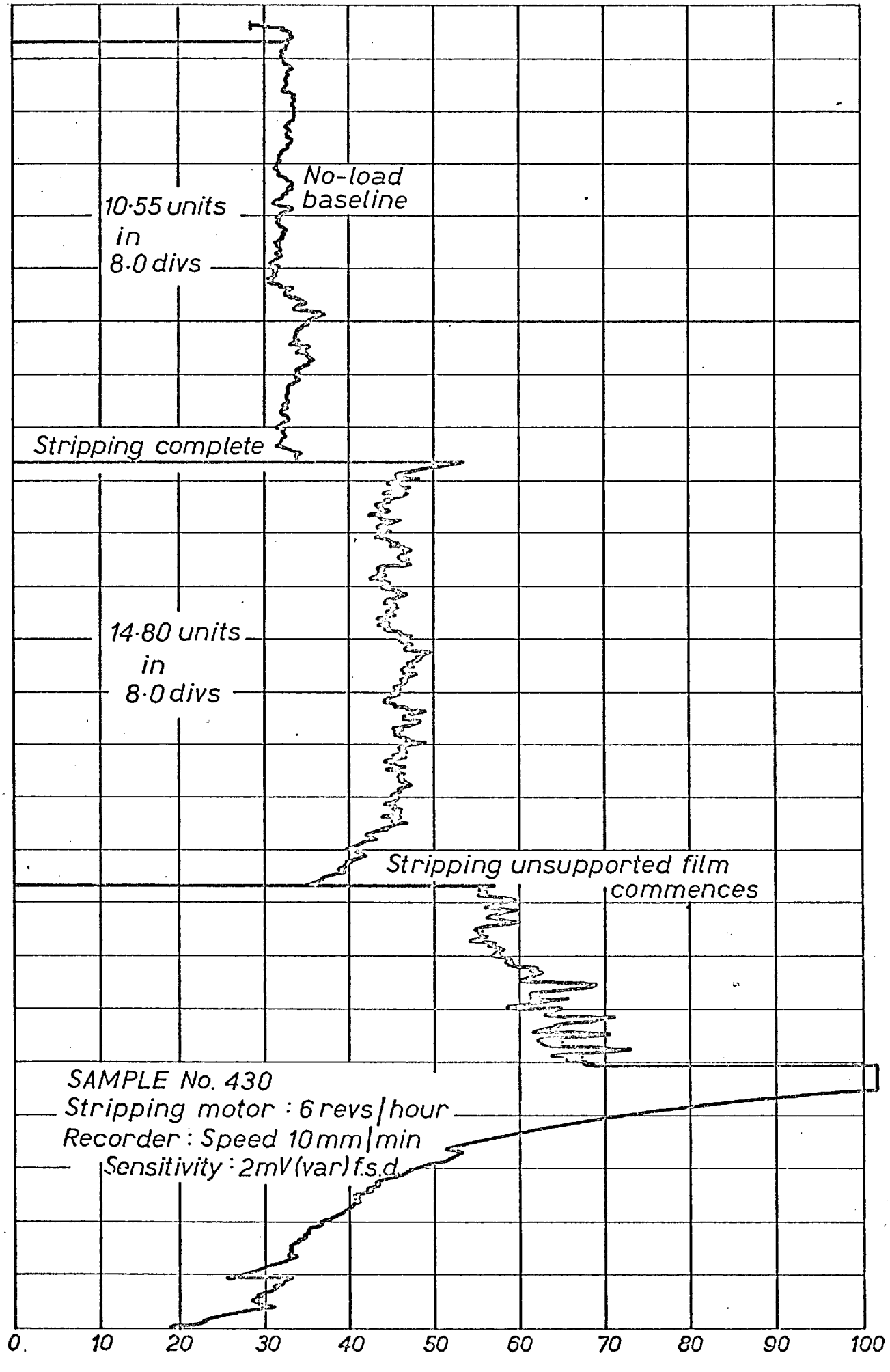
No-load baseline
10·55 units in 8·0 divs
Stripping complete
14·80 units in 8·0 divs
Stripping unsupported film commences
SAMPLE No. 430
Stripping motor : 6 revs/hour
Recorder : Speed 10 mm/min
Sensitivity : 2mV (var) f.s.d.
0
10
20
30
40
50
60
70
80
90
100

where mechanical interlocking is expected.

Fig.5.10. is a scanning electron (Cambridge Instruments 'Stereoscan') micrograph of a film of gold being stripped from a glass substrate. It can be seen that there is no sharp discontinuity in the bending of the film at the point of stripping, and that stripping takes place along the plane of contact, as expected for interfacial adhesion. The thickness of the film can be seen quite clearly.

Fig.5.11. is a micrograph of the scribed edge of the film remaining on the substrate after stripping. The irregularity of the edge of the remaining film is approximately one micron, which is negligible compared with the width ($\simeq$5 mm) of the film removed. No gold is visible on the stripped area.

It was easy to demonstrate the pressure effect on stripping energy during any experimental run simply by varying the pressure, and so it was soon found that the pressure effect was still evident, and was therefore associated not only with the supporting tape.

Ageing effects, over a period of several weeks, were looked for, but no trend could be found in the general scatter of results.

5.1.4.6. Pressure effect: unsupported film

There was insufficient time available to carry out a detailed investigation, and results are available for one set of eight samples only, whcih were stripped in air at various pressures. The films were of thickness 3100 $\pm$ 100 Å and were deposited at 14 Å $sec^{-1}$. The stripping rate was 53 micron $sec^{-1}$, and the substrate inclination angle $\theta$ was 90°. Results are shown in Fig.5.12. There does appear to be a genuine trend to a lower stripping energy at higher pressures, or to introduce a useful

FIG. 5.10

Stripping gold film from glass

x 5k

FIG. 5.11

Scribed edge

x 5k

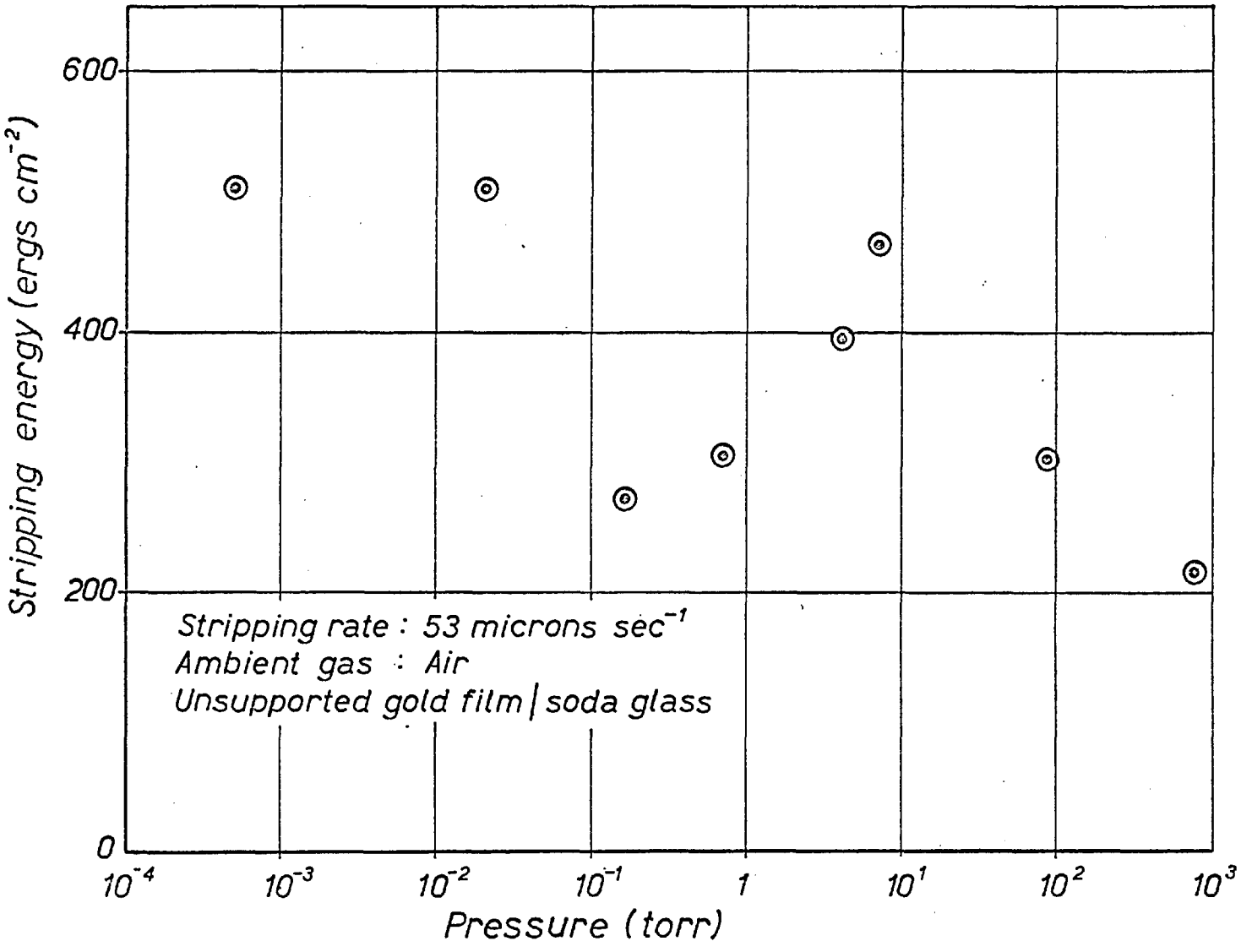


FIG. 5.12

VARIATION OF STRIPPING ENERGY WITH AMBIENT GAS PRESSURE

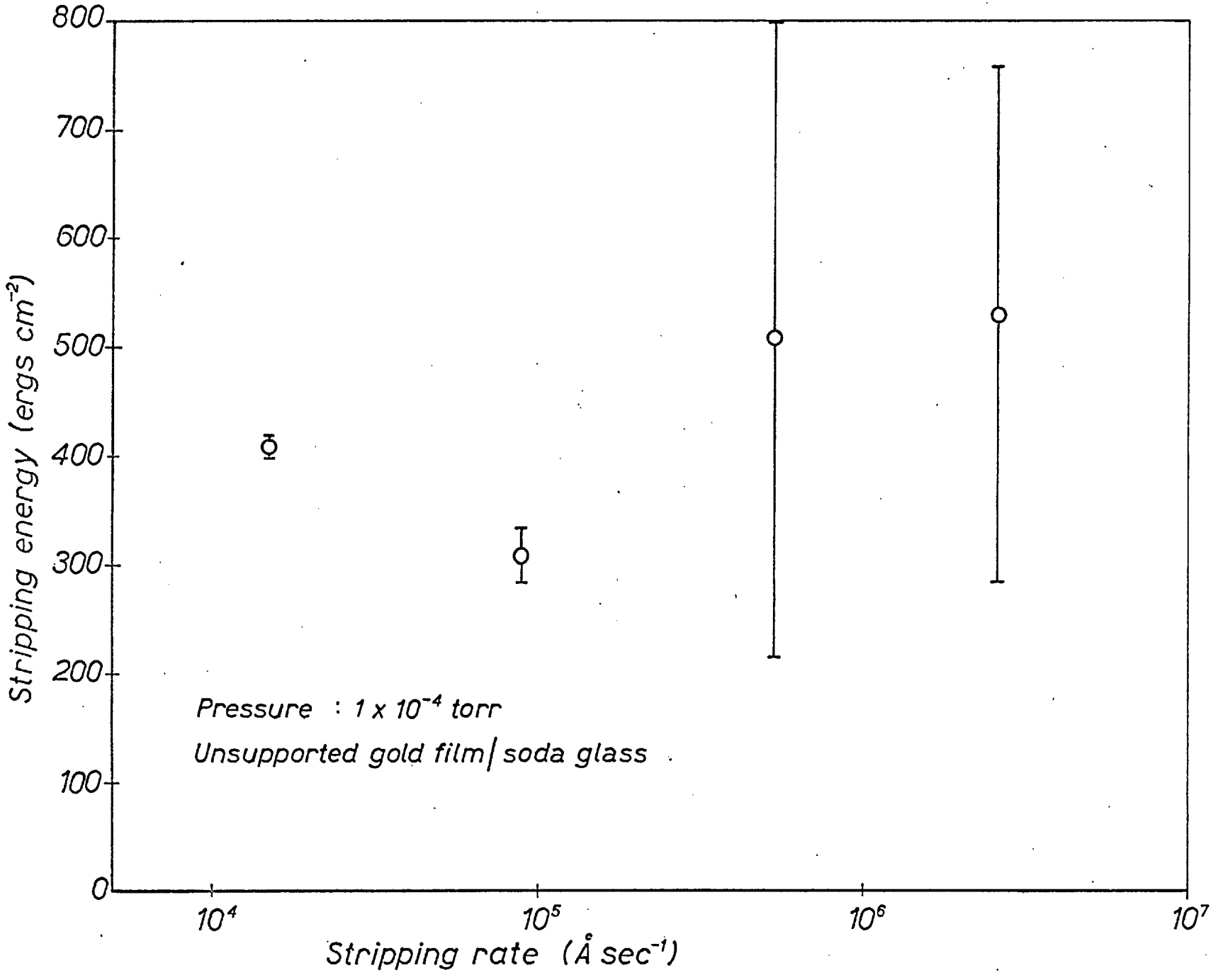


FIG. 5.13

VARIATION OF STRIPPING ENERGY WITH STRIPPING RATE

notation, $p\uparrow S\downarrow$.

5.1.4.7. Stripping rate effect: unsupported film

Measurements were carried out at different rates for a further set of eight samples. The thickness of the films was 3000 ± 100 Å, and stripping was carried out at $1 \times 10^{-4}$ torr. Four different stripping rates were used, and two samples were stripped at each rate. The results, shown in Fig.5.13., are quite inconclusive regarding speed dependence. Unfortunately, it was not possible to extend this investigation over a greater number of samples.

It was also observed at this late stage that dark bands were visible on the stripped film. It is possible that the bands, which were spaced at about 1 mm intervals, had always been present but they were rather difficult to see: local illumination had to be just right. Stress-induced ordering was suspected; the films were examined by glancing angle electron diffraction, but no deviation from the usual polycrystalline structure was found.

5.1.5. Discussion

The above results may be summarised as follows:

For supported films, $\theta\downarrow$ $S\uparrow$

$p\downarrow$ $S\uparrow$

$v\downarrow$ $S\downarrow$ where v is the stripping rate

For unsupported films, $p\downarrow$ $S\uparrow$

v S inconclusive

presence of bands on stripped film

Let us first consider the variation of stripping energy with substrate inclination angle $\theta$. Extraneous work associated with bending the film would be manifested by a decrease of the stripping energy S with decreasing $\theta$; however, S appears to

increase as $\theta$ decreases below a certain value. For an explanation of this, the mechanical properties of the film must be considered. The elastic limit of a gold film 2000 Å thick is reached when a force of approximately $1 \times 10^9$ dynes $cm^{-2}$ (Hoffman 1966), i.e. $2 \times 10^4$ dynes per cm width, is applied. If a force acting at $\alpha$ to the substrate strips a film of unit width, then

$$S = F \ (1 - \cos \alpha)$$

If $S = 2000$ erg $cm^{-2}$ (a typical value in the above results), then the elastic limit would be reached when $\alpha = 25^\circ$. If the film is inelastically strained, this will be a sink for further extraneous work, and thus an increase of S for $\alpha < 25^\circ$ would be expected. Since $\alpha$ changes from $\theta$ to $\theta - 30^\circ$ during each experiment, this should produce an effect when $\theta = 55^\circ$; from the graph, this appears to be occurring for rather larger values of $\theta$. This is surprising, since the backing tape would be expected to transmit a proportion of the applied stress; it is possible, however, that the tape was more ductile than the film.

It is also possible that the above effect masked a smaller decrease of S with $\theta$ due to film bending. In this case, however, one would expect S to initially decrease with $\theta$ before the inelastic effect becomes significant, which is not apparent. Since there was no significant variation of S with $\theta$ around $\theta = 90^\circ$, all further experiments were carried out at this angle.

The observed dependence on stripping rate and ambient gas pressure may be explained in the following ways:

Rate dependence: During the stripping process, the lattices of both film and substrate around the line of detachment undergo a strain cycle. These regions of strain may be only local or, more

likely, extend over a distance of several hundred angstroms. Provided that the strain is elastic, the lattices will return to their initial positions after stripping. But many lattice processes involve dissipative losses. Some of these processes lead to losses such as static dislocation losses, which consume work even when performed infinitely slowly. But more are rate dependent; the latter group includes losses due to thermo-elastic damping, grain boundary friction, and dynamic dislocation losses. And even a perfectly elastic process consumes net zero work only when it is reversible. A necessary condition for a reversible process is that it takes place infinitely slowly so that the system is in equilibrium at all times; the more slowly films are stripped, the more nearly one attains conditions of reversibility, and the less extraneous work is required.

Therefore, due to a combination of all the above effects, one would expect $v \downarrow S \downarrow$ . This in fact was observed in the case of the supported films. We cannot predict the precise shape of the $S = fn.(v)$ relation without a more detailed knowledge of the processes occurring. At very low stripping rates when the relaxation times of the lattice processes involved are very long compared with the interval between stripping adjacent atoms, the rate dependence should cease and one would thus expect constant stripping energy below a certain rate. This has not been observed within the range of stripping rates attainable in the present apparatus, but may obtain at lower rates.

Pressure dependence: When a bond is broken in absolute vacuum, the whole binding energy of that bond is absorbed as an increase in the energy of the system. However, at finite pressures, a gas-solid bond may instantaneously replace the solid-solid bond,

in which case only the difference in binding energies is absorbed, and hence the stripping energy could be considerably reduced. The probability of a gas atom being at the right place at the right time is obviously dependent on gas pressure. If S is the observed stripping energy and S', S'' and S''' are the equivalent stripping energies of the film-substrate, gas-substrate, and gas-film combinations respectively, then we may expect a relation of the form:

$$S = S' - \beta p S'' - \gamma p S'''$$

where p is the ambient gas pressure, and $\beta$ and $\gamma$ are constants; $\beta p$ and $\gamma p$ are probabilities and hence subject to the usual condition that they have a maximum value of unity above the critical pressure at which they (separately) first reach unity. The expression would lead to a dependence of the form shown in Fig. 5.14. If $\beta = \gamma$, and one would expect them to be very similar, there would be only one inflexion point.

The numerical scatter of experimental points on the graph of S against p is too great to draw any firm conclusions, but the observed dependence does not preclude the above explanation.

The Electrostatic Theory of Adhesion: Dependences of stripping rate and gas pressure have also been observed by Derjaguin and his colleagues at the U.S.S.R. Academy of Sciences, with such systems as stripping thick polymer films from various substrates and cleaving mica crystals. Derjaguin et al.(1957) have interpreted these results in terms of their electrostatic theory of adhesion. Although this theory was first communicated some while ago, it appears to have received little attention in the West, perhaps because the large majority of the published literature has been in Russian only. Some similar work has been carried out

FIG. 5.14

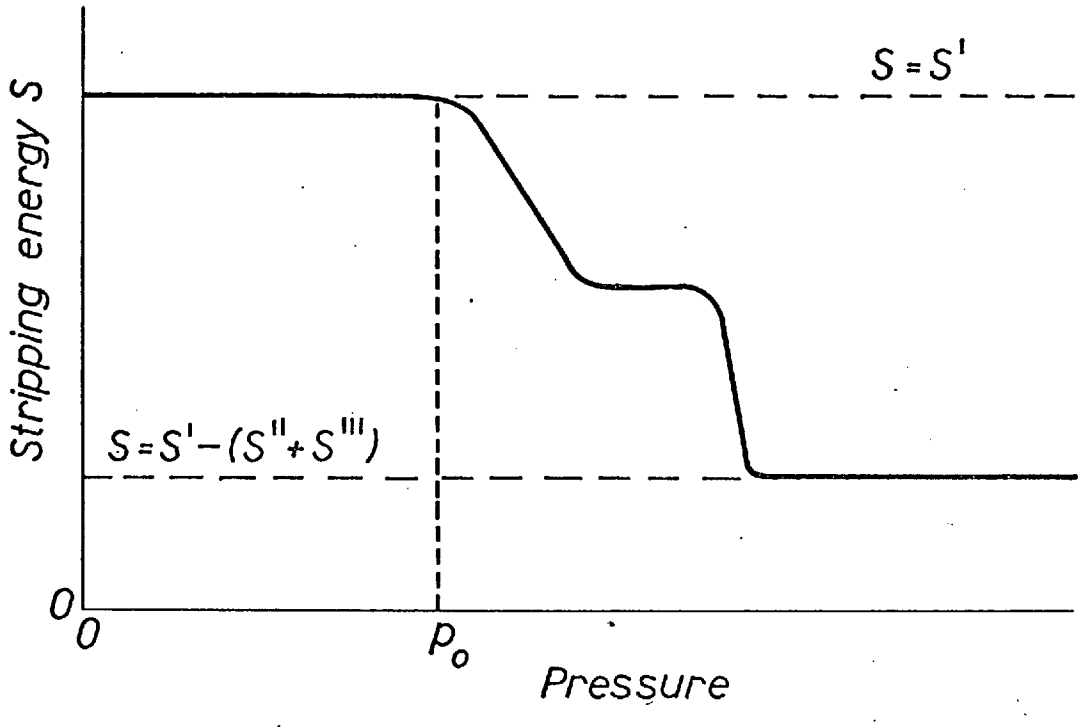


VARIATION OF STRIPPING ENERGY WITH GAS PRESSURE ACCORDING TO MODEL (b)

in the U.S.A. by Skinner et al.(1953), but this was of a comparatively limited nature; more recently Ryan & Grossman (1968) have published evidence of electrostatic effects in adhesion.

The electrostatic theory (Appendix 3) postulates the formation of a double electrical charge layer at the interface when two bodies are brought into contact, so that a potential difference which may vary from a few tenths to several volts is established. The work done in stripping a film from its substrate then includes the work of separating the charges; the energy of molecular bonding, for physisorption, is shown to be comparatively negligible in most cases.

The separation of the double charge layer is similar to separating the plates of a parallel plate condenser. The pressure dependence is explained in terms of a pressure-dependent discharge occuring across the plates, and the rate depeneence is explained in terms of charge leakage from the plates.

So far it has not been possible to directly confirm or refute the existence of a double charge layer in thin film systems. However, the existence of a contact potential between a metal and and insulator is not unlikely: Davies (1967) has been able to determine a work function of 4.3 eV for borosilicate glass by measuring the surface charge density produced by the contact of various metals on the glass. The attraction of the electrostatic theory is that it implies that, by attention to the surfaces, the adhesion across an interface may become a parameter that can be controlled.

5.1.6. Conclusions

It appears from a microscopic examination of the substrates that, in the mechanical stripping of gold from glass, rupture is generally occuring at the interface and hence that adhesion is

being measured. In a few cases, on untypical rough areas of the glass substrates where effective adhesion is greatly increased, rupture is occuring in the condensate but these instances contribute so little that they may be neglected. It therefore appears that the gold/glass system is an example of weak interfacial adhesion.

The stripping of supported films appears to be both rate and pressure dependent. The pressure dependence of unsupported films has also been demonstrated, but an examination of their rate dependence was inconclusive because of insufficient data.

Two accounts of the dependences have been given. It has not been possible to perform an experiment to differentiate between the two theories. Derjaguin et al. worked with thick polymer films using a falling weight technique, and obtained stripping energies in the range $10^4$ - $10^6$ erg $cm^{-2}$. Compared with such figures, physical molecular bonding energies of 500 erg $cm^{-2}$ are negligible and the electrostatic bonding is the only significant contribution to adhesion. But we have obtained much smaller values of stripping energy, $\sim$ 1000 erg $cm^{-2}$; under these circumstances molecular bonding is not negligible and adhesion is a cooperative process of both bonding mechanisms.

The distinction between the molecular and electrostatic forces is that the latter should lead to rate dependent stripping energies. Therefore the relative importance of these two mechanisms in contributing to the durability of thin film devices depends on conditions. Under circumstances where the film peels off very slowly over a long period, as in the case of a reflective aluminium coating from a mirror, the electrostatic contribution may well be negligible; but in the resistance to sudden stresses, this contribution may well be dominant.

The Russian evidence for electrostatic adhesion seems very strong, although several other authors (e.g. Huntsberger 1967) claim that electrostatic effects are negligible in adhesion. It is possible that the double charge layer may be more significant in influencing the electrical properties of the film.

Having been unable to substantiate or refute either of the proposed explanations of our observations, or to assess their relative magnitudes, we must conclude that either or both may be important.

## 5.2. THE SCRATCH TEST OF ADHESION

The scratch test was originally suggested by Heavens (1950). The method was later developed and an analysis given by Benjamin & Weaver (1960). The principle of the method was described at the beginning of the chapter.

In comparing the scratch test with the mechanical stripping method of measuring adhesion, it appeared that the best conditions for the scratch test to be quantitatively successful would be a comparison of the same material film on the same material substrate, with different deposition methods. So films of gold on glass were prepared both by evaporation and by R.F. sputtering. Both types of film could be removed by the mechanical stripping method, and the results indicated that the sputtered films adhered more strongly, as is usually found.

The scratch test was carried out by scribing the films with a smooth rounded steel tip of radius 25 microns under loads varying from 2.5 to 45 gm. In the case of the evaporated films, the gold was completely removed even under very small loads, as can be seen in Fig.5.15. The failure mechanism of the film appears to be initial shearing followed by stripping as the film is

pushed up ahead of the probe tip; the stripping action seems to occur in short sections, and the film is usually folded rather beautifully, as in Fig.5.16. The effect of the scratch test on the sputtered films was very different: for small loads, no effect was observed, but for large loads it appeared that the film was extruded from under the probe tip, thinning the film without exposing the substrate, as in Fig.5.17.

Since the failure mechanisms are so different, it would appear that the scratch test cannot be used quantitatively even in comparing different preparation methods of the same film. A more complete analysis of the scratch test has been carried out by Butler et al.(1969), and they have concluded that so many factors other than adhesion are involved in the scribing process that quantitative interpretation is not possible; they also found different failure mechanisms for different film materials.

# THE SCRATCH TEST

FIG. 5.15

2.5 gm

x 500

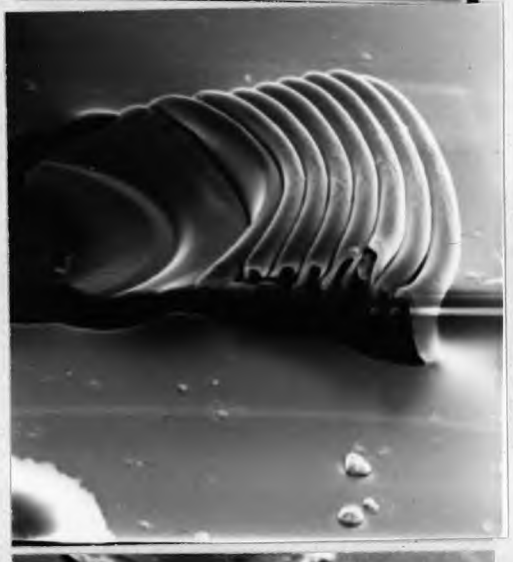

FIG. 5.16

10 gm

x 2k

FIG. 5.17

45 gm

x 2k

# CHAPTER VI

# CONCLUSIONS

It has been shown in the previous chapters that our knowledge of adhesion, and in particular thin film adhesion, is very limited. This is largely due to the difficulty of making meaningful quantitative measurements. Of the methods of thin film adhesion measurement discussed earlier, microcalorimetry is unsuitable because of practical limitations of the measuring apparatus, and there are practical and interpretation difficulties with the nucleation and growth methods. Although there are stringent limitations on the thin film systems that can be studied with the mechanical stripping method, it does appear to offer the only means at present of gaining any useful quantitative information about adhesion. The method may appear to be rather primitive, but it is its very simplicity that reveals its limitations, whilst more exotic experimental techniques cloak their faults in complexity. The results obtained with this method, particularly the pressure dependence of stripping energy, have been rather surprising and have suggested the existence of an electrostatic component in adhesion, not previously considered for thin films. This may be a very important effect not only in determining the durability of a device, but also, because of the interfacial double charge layer, in influencing the electrical properties of the film.

There are other experimental techniques which may become vitally important in adhesion and more general surface studies when the present problems of interpretation have been overcome; field emission and field ion microscopy, scanning electron microscopy, and low energy electron diffraction are examples of such

techniques. Electron paramagnetic resonance may also provide a means of adhesion measurement: Smith (1968, private communication) found that thin films of silver on rocksalt exhibited resonances not found in either of the materials separately; these resonances may have been due to interfacial properties. The effect was investigated further by Smith and the present author with copper films on rocksalt, but although anomalous resonances were again found, no interpretation could be offered.

The most promising topic for future work on adhesion appears to be a further investigation of electrostatic effects. A most interesting experiment would be to mechanically strip a film under conditions which should prevent discharge (Appendix 3.4) and then to measure the surface charge density on the substrate by a scanning probe technique (Davies, 1967a). And it becomes increasingly clear that adhesion, and electrostatic adhesion in particular, is closely related to the subject of static electrification, which is another familiar phenomenon not well understood.

A study of electrostatic adhesion, contact electrification, and related general surface phenomena is to be carried out in the Materials Science section of Imperial College and it is hoped that the present study of adhesion may eventually prove more fruitful than its original aims !

## PUBLICATIONS

The following papers have been published or accepted for publication:

| | |
|---|---|
| "A suspended disk vacuum gauge" | J.Sci.Inst.(J.Phys.E), 1968, Ser.2, Vol. 1, 45-51. (with A.R.Beavitt & D.S.Campbell) |
| "Condensation of high-energy atomic beams" | J.Phys.C (Solid St. Phys), 1969, Ser.2, Vol. 2, 200-209. (with D.S.Campbell) |
| "Fractional nucleation rate" | J.Phys.C (Solid St. Phys), 1969, to be published. (with M.R.Jordan) |
| "Adhesion of thin metallic films" | Proc.7th.Conf.Adhesion & Adhesives, ed. Alner, 1969 (Univ. of London), to be published. |

ACKNOWLEDGEMENTS

The work described in this thesis was undertaken whilst the candidate was at the Allen Clark Research Centre of the Plessey Company Ltd., on a joint university-industry Ph.D. project. Thanks are due to the Directors of the Plessey Co. for enabling the joint project to be carried out, and to the Ministry of Technology for supporting the work.

Thanks are due also to:

Professor J. C. Anderson, the university supervisor, and Dr. D. S. Campbell, the industrial supervisor, for their constant interest, encouragement, and assistance.

Dr. B. Lewis, Mr. D. J. Stirland, Dr. M. R. Jordan, and many other colleagues of the Plessey Co., for many valuable discussions and comments.

Dr. R. Little of Keele University for the microcalorimetry facilities.

Dr. R. S. Nelson and Mr. D. Holloway of A.E.R.E. Harwell for the use of the linear ion accelerator.

Dr. M. Smith of Warwick University for the E.S.R. facilities.

and most in every way, Gillian

# APPENDIX 1

## DIPOLE INTERACTIONS

### A.1.1. THE INTERACTION ENERGY OF TWO DIPOLES

In Fig.2.1 of the main text, let:

$A = (\ 0,\ 0,\ 0)$ $\qquad$ $C = (\ X,\ Y,\ Z)$

$B = (\ x_1,\ y_1,\ z_1)$ $\qquad$ $D = (\ X+x_2,\ Y+y_2,\ Z+z_2)$

The interaction energy W of the two dipoles is given by:

$$W = \frac{e^2}{AC} + \frac{e^2}{BD} - \frac{e^2}{AD} - \frac{e^2}{BC}$$

$$= \frac{e^2}{R}\left( \frac{\Sigma x_1 x_2}{R^2} + \frac{3}{2R^4}\left[ \left\{ \Sigma X(x_2 - x_1) \right\}^2 - \left\{ \Sigma X\, x_1 \right\}^2 - \left\{ \Sigma X\, x_2 \right\}^2 \right] \right)$$

where $\Sigma$ denotes summation over x, y, and z components, and $\underline{R}$ is the vector joining A & C. In the special case when $\underline{R}$ lies along the z - axis, then $\underline{R} = (0, 0, R)$ and

$$W = \frac{e^2}{R^3}\ (\ x_1 x_2 + y_1 y_2 - 2 z_1 z_2\ )$$

### A.1.2. THE ENERGY OF AN INDUCED DIPOLE

An atomic dipole can be represented by two charges +e and -e separated by a distance x, and hence having a dipole moment $\mu = ex$. If the dipole is induced by an electric field f, then

$$\mu = e\,x = \alpha\, f$$

where $\alpha$ is the polarisability. If the separation of the charges is now increased by a distance dx due to an increase df in the electric field, then work is done on the dipole system and hence its potential energy increases. The incremental energy change dW is given by:

$$dW = e\, f\, dx$$

$$= \alpha\, f\, df \qquad \text{from above}$$

Therefore the total energy of an atomic dipole induced by a field F is given by:

$$W = \int_0^F \alpha f \, df = \tfrac{1}{2} \alpha F^2 = \tfrac{1}{2} \frac{e^2 X^2}{\alpha}$$

where $\mu = e X = \alpha F$

A.1.3. SIMPLIFIED MODEL OF THE LONDON DISPERSION EFFECT

The London approach to the interaction problem (1937) is to treat each rotating dipole in an atom as the sum of three independent linear harmonic oscillators with equilibrium positions at the atom centre. Consider two such atoms, each represented by three such oscillators along the x, y, and z axes, with subscripts 1 & 2 referring to the two atoms.

The potential energy P of the two isolated sets of oscillators is given by secn.A.1.2:

$$P = \frac{\sum e^2 x_1^2}{2\alpha} + \frac{\sum e^2 x_2^2}{2\alpha}.$$

This expression is of typical form for oscillators of frequency $\nu_o$ given by:

$$\nu_o = \frac{1}{2\pi}\sqrt{\frac{e^2}{m\alpha}}$$

where m is the effective electron mass. The energy of each oscillator, in the ground state, is $\tfrac{1}{2} h \nu_o$.

If the two dipole systems are now allowed to interact, the total potential energy increases to a value P' given by, according to secn.A.1.1:

$$P' = \frac{\sum e^2 x_1^2}{2\alpha} + \frac{\sum e^2 x_2^2}{2\alpha} + \frac{e^2}{R^3}(x_1 x_2 + y_1 y_2 - 2 z_1 z_2)$$

It will now be shown that the effect of the interaction energy is equivalent to producing two different independent oscillating systems with modified frequencies. This is acheived by making a transformation of coordinates:

$$\underline{r_+} = \begin{cases} x_+ = \frac{1}{2^{\frac{1}{2}}}(x_1 + x_2) \\ y_+ = \frac{1}{2^{\frac{1}{2}}}(y_1 + y_2) \\ z_+ = \frac{1}{2^{\frac{1}{2}}}(z_1 + z_2) \end{cases}$$

$$\underline{r_-} = \begin{cases} x_- = \frac{1}{2^{\frac{1}{2}}}(x_1 - x_2) \\ \text{etc.} \end{cases}$$

The potential energy equation then becomes:

$$W = \frac{e^2}{2\alpha}\left[(1 + \frac{\alpha}{R^3})(x_+^2 + y_+^2) + (1 - \frac{\alpha}{R^3})(x_-^2 + y_-^2) + (1 - \frac{2\alpha}{R^3})z_+^2 + (1 + \frac{2\alpha}{R^3})z_-^2\right]$$

It can be seen from secn.A.1.2 that this is the energy of an assembly of six oscillators of frequencies given by (with the obvious notation):

$$\nu_x^{\pm} = \nu_y^{\pm} = \nu_0(1 \pm \frac{\alpha}{R^3})^{\frac{1}{2}} = \nu_0(1 \pm \frac{\alpha}{2R^3} - \frac{\alpha^2}{8R^6} \pm \ldots\ldots)$$

$$\nu_z^{\pm} = \nu_0(1 \pm \frac{2}{R^3})^{\frac{1}{2}} = \nu_0(1 \mp \frac{\alpha}{R^3} - \frac{\alpha^2}{2R^6} \mp \ldots\ldots)$$

The lowest energy state of the system is given by $W = \sum \frac{1}{2} h\nu$

$$\text{i.e.} \quad = \frac{h\nu_0}{2}\left[6 - \frac{\alpha^2}{R^6}(\frac{4}{8} + \frac{2}{2}) + \ldots\ldots\right]$$

But the first term $3\,h\nu_o$ is just the total zero-point energy of the systems in isolation. Therefore the interaction energy is

$$W = \frac{3\,h\nu_o\alpha^2}{4R^6}$$

ignoring terms in $\alpha^3/R^9$ and above, which is consistent with the original requirement (see Chapter II) that R must be much greater than the molecular size.

# APPENDIX 2

## THE CALVET MICROCALORIMETER

### A.2.1. THE INTEGRATING ACTION

Consider the flow of heat at rate $\phi_j$ between two surfaces at temperatures $\theta_{ij}$ and $\theta_{ej}$ connected by a thermocouple. If $\lambda$ is the proportion of the heat flow carried by the thermocouple, then:

$$\lambda \phi_j = C\ (\theta_{ij} - \theta_{ej})$$

where C is the thermal conductivity of the couple. But the e.m.f. $e_j$ ~~of~~ generated in the couple is also proportional to the temperature difference between its junctions:

$$e_j = \varepsilon\ (\theta_{ij} - \theta_{ej})$$

where $\varepsilon$ is the thermoelectric power. Hence:

$$e_j = \frac{\varepsilon\lambda}{C} \cdot \phi_j$$

If a surface is covered by an array of equivalent thermocouples connected electrically in series and very regularly arranged so that they each cover the same area of surface, the total e.m.f. E generated in the thermopile is proportional to the total heat flow $\Phi$ from the surface, since $\varepsilon, \lambda$, and C are the same for each thermocouple:

$$E = \sum_j e_j = \sum_j \frac{\varepsilon\lambda}{C} \cdot \phi_j = \frac{\varepsilon\lambda}{C} \cdot \Phi$$

A.2.2. THE CALORIMETER ELEMENT

The calorimeter element (Fig. A.2.1) consists of a reaction cell which fits snugly into a cylindrical socket, and a thermocouple array which is attached uniformly to the outer surface of the socket which is designated the "internal boundary", and to the co-axial inner surface of a socket in a massive metallic block, which is designated the "external boundary". The integrating action of the calorimeter depends on the uniform distribution of the thermojunctions on the boundaries. Spherical boundaries would be ideal, but such a calorimeter would be difficult to construct; therefore cylindrical boundaries and an overall cylindrical symmetry of the instrument are adopted. Since the ends of the internal boundary are non-representative of its surface, the boundary must be long compared with its radius. Calvet uses a boundary which is 8 cm long and 1 cm internal diameter; the reaction cell is the same diameter but only 3.8 cm long and is placed in the middle of the socket to reduce the heat loss from the non-representative surface.

The inner cylindrical socket is a silver tube of wall thickness 0.2 mm. Its outer surface, i.e. the internal boundary, is covered with a mica insulator of thickness 0.01 mm to eliminate electrical shorting between the thermojunctions. The surface of the insulator is uniformly covered with contact pads, one for each thermojunction; a minimum of insulated boundary surface is left uncovered. The contact pads are made of polished silver to reduce the radiative loss

FIG. A2.1
THE CALORIMETER ELEMENT

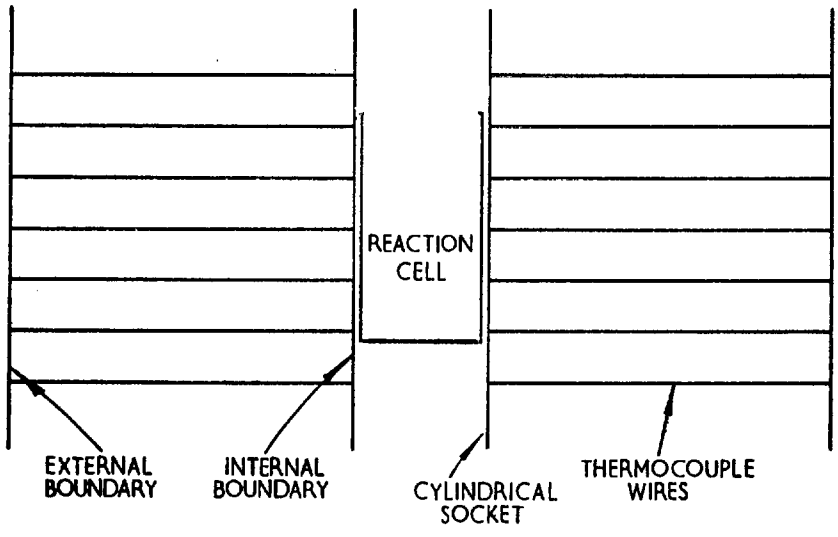


FIG. A 2.2
METHOD OF ATTACHMENT OF THERMOCOUPLES

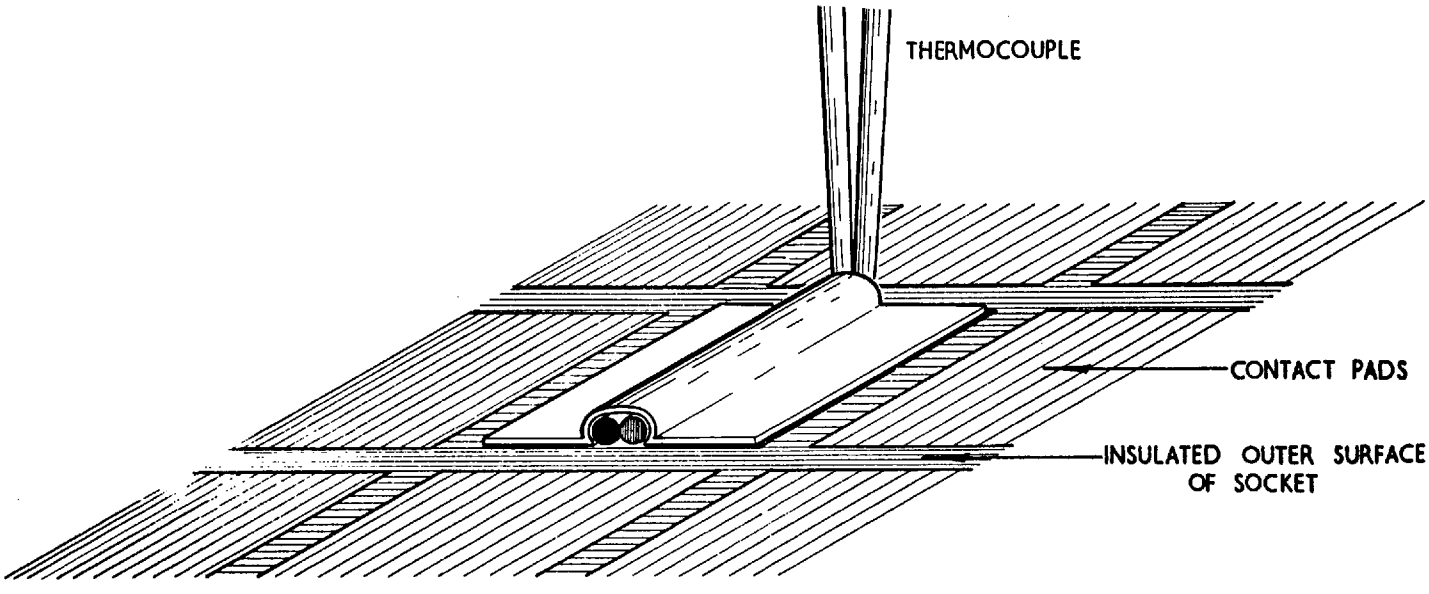

from the pad and to improve the thermal flow in the pad to the thermojunction and so increase the fraction of the total heat exchange between the boundaries which is conducted along the thermocouple wires. The thermojunctions are affixed to the contact pads with silver saddles (Fig. A.2.2.) which ensure a strong and thermally sound contact. The outer thermojunctions are similarly attached to the external boundary. Chromel-alumel thermocouples are normally used, with as many as one thousand thermojunctions.

### A.2.3. THE DIFFERENTIAL ARRANGEMENT

The purpose of the differential arrangement is effectively to control the temperature of the reference junctions of the thermocouples within much smaller limits than are produced by the thermostatic control of the calorimeter block, and hence to increase the meaningful sensitivity of the instrument.

The identical calorimeter elements are mounted symmetrically in a massive cylindrical metallic block (Fig. A.2.3.) with their thermopiles in opposition, so that corresponding external boundary thermocouple junctions are equally affected by any external thermal perturbations, and may therefore be considered to be at identical temperatures. The laboratory cell contains the reaction under investigation; the reference cell is used to eliminate temperature variations of the external boundary junctions.

Consider any corresponding pair of thermocouples. Let $\theta_e(t)$ be the (same) temperature of the external boundary junctions at time t. Let $\theta_{il}(t)$ and $\theta_{ir}(t)$ be the temperature of the internal boundary junctions of the laboratory and reference cell thermojunctions respect-

FIG. A2.3

THE DIFFERENTIAL ARRANGEMENT

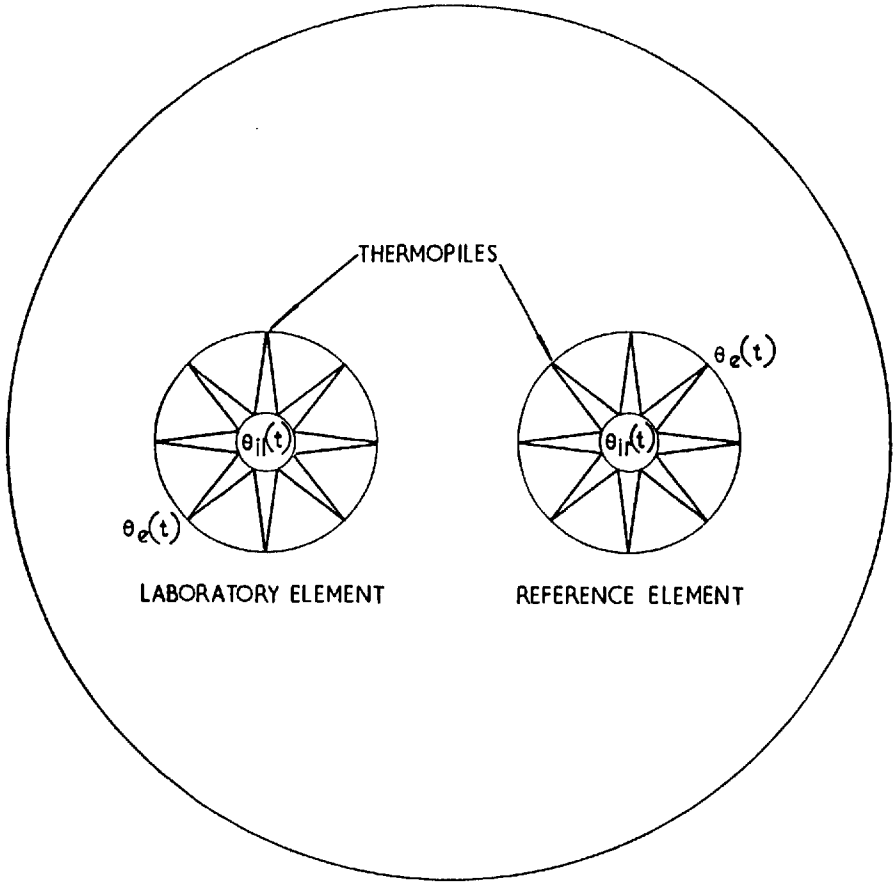

ively. Although no reaction occurs within the reference cell, it still undergoes temperature fluctuations due to the Peltier effect of the current in the thermopiles at the heterogeneous junctions.

At time t, e.m.f.s developed are given by:-

$$e_l(t) = \varepsilon\left[\theta_{il}(t) - \theta_e(t)\right]$$

$$e_r(t) = \varepsilon\left[\theta_{ir}(t) - \theta_e(t)\right]$$

$$\text{net e.m.f.} = \Delta e(t) = \varepsilon\left[\theta_{il}(t) - \theta_{ir}(t)\right]$$

Because of the temperature gradients between the internal and external boundaries, there is a heat exchange in both elements:-

$$dQ_{i\rightarrow e}(t) = p\left[\theta_i(t) - \theta_e(t)\right]dt$$

where p is the heat flow per unit time per unit temperature difference and is common to both elements due to their identical construction.

This heat flow causes a temperature change of the cells

$$d\theta_i(t) = -\frac{dQ(t)}{\mu}$$

$$= -\frac{p}{\mu}\left[\theta_i(t) - \theta_e(t)\right]dt$$

where $\mu$ is the heat capacity of the calorimeter cell.

Let $\theta'_i\ (t + dt)$ be the temperature the cell would have reached at time $(t + dt)$ if no heat exchange between the boundaries had taken place.

$$\theta_i(t + dt) = \theta'_i\ (t + dt) - \frac{p}{\mu}\left[\theta_i(t) - \theta_e(t)\right] dt$$

$$\therefore\ e(t + dt) = \varepsilon\left[\theta'_i\ (t + dt) - \frac{p}{\mu}\left\{\theta_i(t) - \theta_e(t)\right\} dt - \theta_e(t + dt)\right]$$

$$\therefore\ e(t + dt) = \varepsilon\left[\theta'_{il}(t + dt) - \theta'_{ir}(t + dt) - \frac{p}{\mu}\left\{\theta_{il}\ (t) - \theta_{ir}(t)\right\} dt\right]$$

$$= \varepsilon\left[\theta_{il}(t + dt) - \theta_{ir}(t + dt)\right]$$

independent of the value of $\theta_e(t)$, whether constant or variable.

The microcalorimeter has a lower limit of meaningful energy measurement because it is practically impossible to satisfy the assumption made above that corresponding points of the boundaries are at identical temperatures. The lower limit of the instrument is determined by the stability of the "experimental zero" - the net e.m.f. generated when both cells are unchanged. One is then restricted to such processes that the outputs involved are large compared with the fluctuations of the experimental zero. The need for thermostatting is clear; the central block diminishes external fluctuations appreciably, but the final variation between corresponding points will remain a function of the thermostat fluctuations.

A.2.4. OPTIMUM PERFORMANCE OF THE CALORIMETER

The design of the calorimeter for optimum sensitivity of the instrument will now be considered.

Let:

$W$ = the rate of energy production in the laboratory cell

$\theta_{il}$ = temperature of laboratory cell boundary

$\theta_{ir}$ = temperature of reference cell boundary

$\theta_e$ = temperature of external boundary

$n$ = no. of thermocouples in each calorimeter element

$\pi$ = Peltier coefficient

$I$ = current in circuit

$\varepsilon$ = thermoelectric power

$\rho$ = resistance of external measuring instrument and connecting wires

$\mu$ = heat capacity of cell

$S,S'$ = cross sectional areas of thermocouple wires

$r,r'$ = electrical resistivities of thermocouple wires

$c,c'$ = thermal conductivities of thermocouple wires

$l$ = common length of thermocouple wires

$p$ = heat loss from the calorimeter cell per second per degree temperature difference between the boundaries

$p_c$ = heat loss via thermocouples

$p_o$ = $p-p_c$

$R$ = $\frac{r}{S}+\frac{r'}{S'}$

$C$ = $cS + c'S'$

$\eta$ = effective resistance of thermojunctions

The heat W produced in the laboratory cell is somewhat modified by the Peltier and Joule effects at the thermojunctions, so that the net rate of energy production within the internal boundary is $W - n\pi I + nI^2\eta$. Some of this is lost as a heat flow to the external boundary, and some causes a change in the temperature of the cell. Hence,

$$W - n\pi I + n\eta I^2 = p\ (\theta_i - \theta_e) + \mu \cdot \frac{d\theta_i}{dt}$$

For slowly varying or constant output processes, the heat flux due to temperature variations of the calorimeter cells can be neglected. In the laboratory element,

$$W - n\pi I + n\eta I^2 = p\ (\theta_{il} - \theta_e) = p\ \Delta\theta$$

and the e.m.f. generated is

$$\underset{\rightarrow}{E} = n\varepsilon\Delta\theta = \frac{n\varepsilon}{p}\ (W - n\pi I + n\eta I^2)$$

In the reference element, the Peltier effect causes a temperature rise since the current traverses the thermoelectric junctions in the opposite sense; the Joule effect causes a heating as in the laboratory cell, being independent of current direction.

$$n\eta I^2 + n\pi I = p\ (\theta_{ir} - \theta_e) = p\Delta\theta'$$

and the e.m.f. generated is:

$$\underset{\leftarrow}{E} = n\varepsilon\Delta\theta' = \frac{n\varepsilon}{p}\ (n\pi I + n\eta I^2)$$

Therefore the net e.m.f. is given by

$$E_{net} = \underset{\rightarrow}{E} - \underset{\leftarrow}{E} = \frac{n\varepsilon}{p}\ (W - 2n\pi I)$$

Now

$$I = \frac{E_{net}}{\text{Total resistance}} = \frac{n\varepsilon\ (W-2n\pi I)}{p(\rho + 2n\ell R)}$$

$$\therefore \qquad I = \frac{n\varepsilon W}{p\ (\rho + 2n\ell R) + 2n^2\varepsilon\pi}$$

$$\therefore \qquad I \propto W$$

If the generated current is measured with a moving coil galvanometer, then the figure of merit is the current sensitivity, $\sigma_I$.

$$\sigma_I = \frac{I}{W} = \frac{\varepsilon}{p\rho_{/n} + 2\ell R p + 2n\varepsilon\pi}$$

It can be shown that the factor $2n\varepsilon\pi$ is very much smaller than any other in the denominator and may be neglected.

Since $p = p_o + \frac{nC}{\ell}$ the sensitivity becomes

$$\sigma_I = \frac{\varepsilon}{(p_{o/n} + C/\ell)\ (\rho + 2n\ell R)}$$

Calvet obtained the optimum values of $n, \ell$, S and S′ for maximum sensitivity by differentiating this expression with respect to $n, \ell$, S, and S′ and obtained the following relations:-

$$n = \left(\frac{\varrho p_o}{2RC}\right)^{\frac{1}{2}}$$

$$\ell = \left(\frac{\varrho C}{2 p_o R}\right)^{\frac{1}{2}}$$

$$S = \left(\frac{2 p_o r}{\varrho C}\right)^{\frac{1}{2}} \cdot \ell$$

$$S' = \left(\frac{2 p_o r'}{\varrho C'}\right)^{\frac{1}{2}} \cdot \ell$$

Using these equations, Calvet (1956) constructed a calorimeter element using iron-constantan thermocouples and the following dimensions:-

| | |
|---|---|
| Calorimeter cell | Height 8.0 cms, diam. 1.4 cms |
| No. of thermocouples (n) | 144 |
| Length of thermocouple wires ($\ell$) | 3.0 cms |
| Iron wire $r = 10.10^{-6}$ ohm.cm | Cross-section $S = 6.0\ 10^{-4}$ $cm^2$ |
| $c = 0.161$ cals $s^{-1} cm^{-1} {}^{o}C^{-1}$ | Diameter 0.3 mm |
| Constantan wire $r = 44.10^{-6}$ ohm.cm | Cross-section $S = 21.3\ 10^{-4}$ $cm^2$ |
| $c = 0.054$ cals $s^{-1} cm^{-1} {}^{o}C^{-1}$ | Diameter 0.3 mm |
| Thermoelectric power | $= 50 \mu V\ {}^{o}C^{-1}$ |

Using a galvanometer giving a deflection of 1 mm on a screen 1 m from the mirror for a current of $4.10^{-10}$ amps, the sensitivity of the calorimeter was such that a 1 mm deflection of the light-spot corresponded to an output of $0.8\ .10^{-7}$ cals $s^{-1}$

$$= 3.4\ 10^{-7} \text{ joules } s^{-1}$$

$$\simeq 1/3 \text{ microwatt}$$

In later versions, chromel-alumel thermocouples were used, and the number of couples was considerably increased.

The treatment above to obtain the optimum design parameters is not strictly valid since $p_o$ is assumed constant. In fact, $p_o$ is composed of terms for conduction, radiation, and convection through the inter-boundary space. The radiation term is a function of the materials used and their absolute temperatures, and the conduction term is inversely proportional to log ($\ell$ + constant). A more precise treatment would need to consider $p_o$ more thoroughly.

However, it has been assumed in Calvet's treatment that the loss $p_o$ is due to a radial heat flow between the boundaries, and end effects have been ignored. But in practice it appears (Lafitte 1968) that most of this loss is from the ends of the reaction cell and is thus dependent mainly on the reaction cell diameter. Therefore $p_o$ is, in the present design, almost independent of $\ell$, n, s, and S' and Calvet's treatment is sufficient.

# APPENDIX 3

## THE ELECTROSTATIC THEORY OF ADHESION

### A.3.1. INTRODUCTION

The electrostatic theory postulates the formation of a double electrical charge layer at the interface when two bodies are brought into contact, so that a potential difference which may vary from a few-tenths to several volts is set up across the interface. The work done in stripping a film from its substrate is then the work of separating the charge layers; the energy of molecular bonding, for physisorption, is shown to be comparatively negligible in most cases.

Consider a length dl of a film of unit width being stripped from its substrate (Fig.A3.1); treating this as a parallel plate condenser of separation h, the voltage V between the plates is given by

$$V = 4\pi\sigma h$$

where $\sigma$ is the surface density of charge, and the gas between the plates is assumed to have a dielectric constant of unity. Thus the potential difference is proportional to separation, and therefore increases linearly until discharge takes place at a voltage which is a function of separation and gas pressure. If discharge takes place at a separation $h_d$, then the stripping energy S is equal to the work done in establishing the condenser, i.e. of moving a charge $\sigma$ dl a distance $h_d$ against an electric intensity of $2\pi\sigma$.

$$\therefore \quad S = 2\pi\sigma^2 h_d \, dl$$

$$= 2\pi\sigma^2 h_d \quad \text{per unit area}$$

or in the equivalent form, since $V = 4\pi\sigma h$,

$$= \tfrac{1}{2} \sigma V_d$$

$$= V_d^2 / 8\pi h_d$$

FIG. A3.1
CHARGE DISTRIBUTION IN HETEROGENEOUS MECHANICAL STRIPPING.

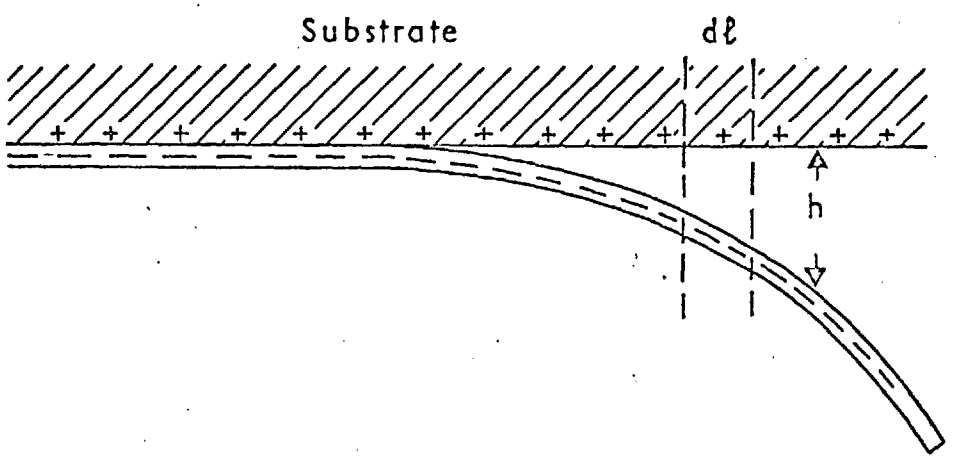

Initially the plate sepatation is the equilibrium adsorption distance $h_o$, but if $h_d \gg h_o$ as is usually found, the above expression may be taken as the stripping energy.

A.3.2. The discharge distance $h_d$.

The relation between $h_d$, $V_d$ and p can be found from the Paschen curve (Fig.A3.2) which is of the general form:

$$V_d = \frac{Bph}{C + \log ph}$$

This curve gives the relation between sparking potential, pressure, and electrode separation. B and C are constants. The discharge is started by the few ions always naturally present in the gap, and a large current is quickly built up by multiple collisions. As the gas pressure is reduced, the mean free path of the ions increases and the electric intensity needed to give an ion the energy to produce fresh ions by collision is reduced; so the sparking potential at first decreases. But as the m.f.p. becomes larger so the number of collisions per unit volume decreases and hence the total number of ions decreases. It then becomes more difficult to cause a spark at all, and so the sparking potential rises as pressure decreases. At very low pressures, the ionisation mechanism of sparking ceases to be operative and the discharge mechanism becomes one of field desorption of clumps of loosely adhering electrode material, which is pressure independent (Cranberg 1952).

To return to the practical problem of finding $h_d$ for the stripping system: the potential difference between the plates of the elementary condenser, $V = 4\pi\sigma h$, is also plotted on Fig.A3.2. The point G represents the initial condition, when the contact potential difference is $V_o$, the charge density is $\sigma_o$, and the

FIG.A3.2

PASCHEN GAS DISCHARGE CURVE (ARGON).

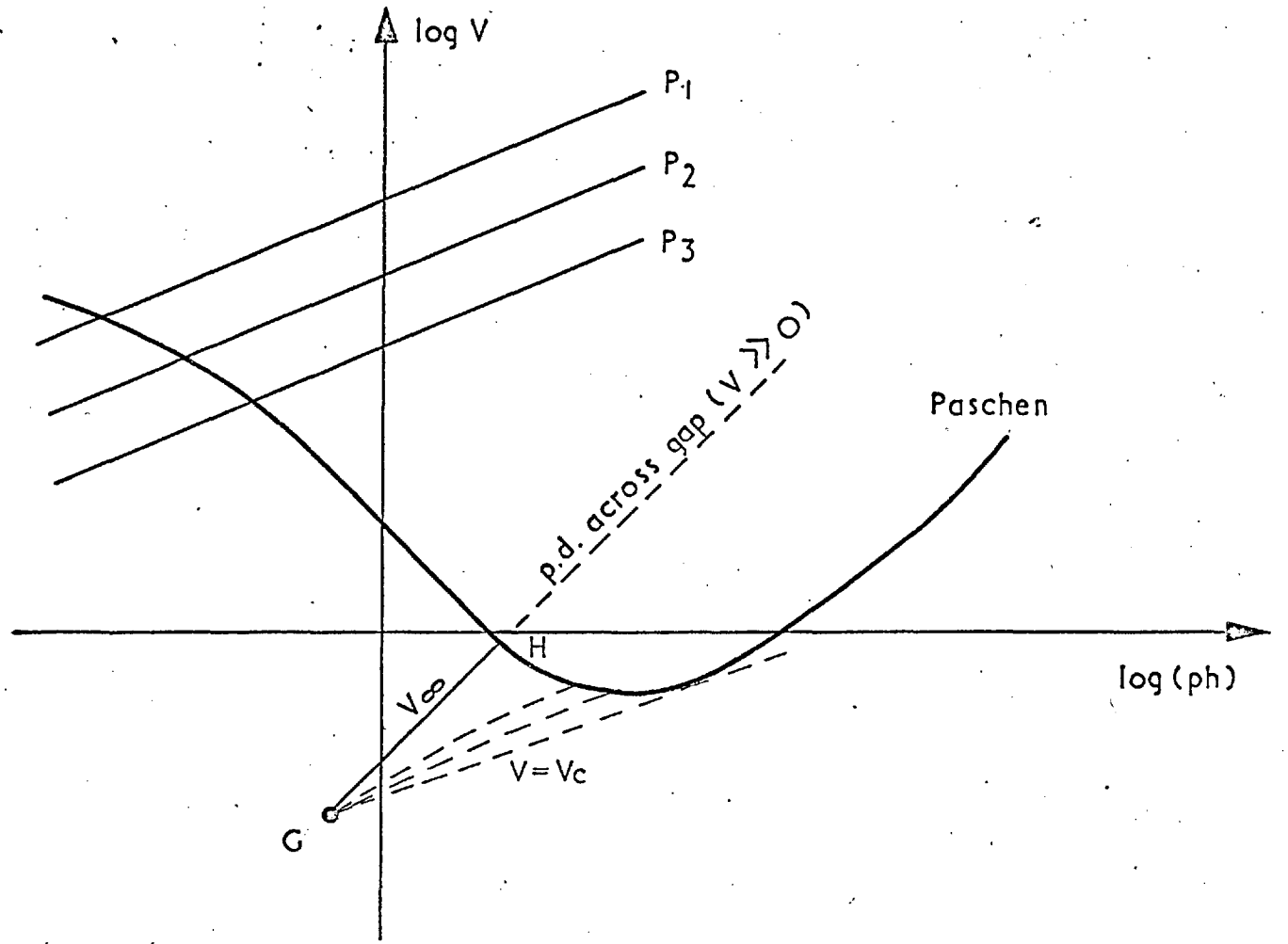

equilibrium separation, which will be a few angstroms, is $h_o$. For a given pressure p,

$$V = \frac{2\pi\sigma_o}{p} \cdot (ph)$$

$$\therefore \quad \log V = \log \frac{2\pi\sigma_o}{p} + \log (ph)$$

We thus obtain a straight line of unit gradient. The interplate potential increases until discharge occurs at a point given by the intersection of the above line with the Paschen curve, i.e. at H. If the discharge voltage is $V_d$ and the stripping energy S is given by

$$S = 2\pi \sigma^2 h_d$$

$$\text{then} \quad S = \frac{V_d^2}{8\pi h_d}$$

$$\text{since} \quad V_d = 4\pi h_d \sigma$$

A.3.3. Pressure Dependence

The effect of reducing gas pressure will be to displace the point G in Fig.A3.2, and therefore the line GH, to the left. The intercept with the Paschen curve will then give a greater spark potential $V_d$, since in all practical cases the intercept H will be on that part of the curve where (ph) $\downarrow$ $V_d$ $\uparrow$ (again using the convention introduced in Chapter V).

$$\therefore \quad p \downarrow \quad V_d \uparrow$$

$$\text{But} \quad S = \tfrac{1}{2} \sigma V_d$$

$$\therefore \quad V_d \uparrow \quad S \uparrow$$

$$\text{and hence} \quad p \downarrow \quad S \uparrow$$

At very low pressures, as was described above, gas ionisation ceases to be the dominant discharge mechanism. The discharge

potential is then given by the pressure-independent relation (Cranberg 1952):

$$\frac{V_d^2}{h_d} = \text{constant}$$

and since $$S = \frac{V_d^2}{8\pi h_d}$$

then the stripping energy is also constant and pressure-independent. Thus the electrostatic model predicts that the stripping energy will increase as the pressure decreases to a certain value, and then remain constant as the pressure is further decreased.

A.3.4. Rate Dependence

It has so far been assumed that the surface charge remains fixed. But it will in fact decay due to surface conductivity, field emission, and conduction in the gas. Clearly then, the remaining charge density $\sigma_h$ at a particular separation h will decrease as the time to reach this separation increases, i.e.

$$v \downarrow \quad \sigma_h \downarrow$$

But $$V_h = 4\pi\sigma_h h$$

$$\therefore \quad v \downarrow \quad V_h \downarrow$$

So from the starting point G on Fig.A3.2 will emerge a whole family of curves with steadily decreasing slope as the stripping rate v decreases. Similarly the intercept with the Paschen curve will change,

$$\therefore \quad v \downarrow \quad V_d \downarrow$$

and hence $$v \downarrow \quad S \downarrow$$

however, there will be a certain rate $v_c$ when the V.(ph) curve is tangential to the Paschen curve. Below this critical rate,

discharge cannot occur, and the work of stripping will be that of separating the condenser plates to infinity, i.e.

$$S_{v<v_c} = \int_0^\infty 2\pi\sigma_x \, dx$$

But $\sigma_x$ is also a function of v, and $v \downarrow \sigma_x \downarrow$ hence $S_{v<v_c}$ continues to decrease with further decrease of stripping rate.

Thus the model predicts that the stripping energy will decrease as the stripping rate decreases, with a discontinuity at a critical rate.

A.3.5. Theory & Experiment

Derjaguin and his colleagues have been able to correlate their theoretical predictions with experimental values determined by a mechanical stripping process, with some success. Having determined values of S under particular conditions, and using the equation

$$S = \frac{V_d^2}{8\pi h_d}$$

$$\text{i.e. } \log V_d = \tfrac{1}{2}\log 8\pi S + \tfrac{1}{2}\log h_d ,$$

they were able to plot work isobars corresponding to the pressures at which the values S were determined. Some isobars, at pressures $p_1$, $p_2$, and $p_3$ are shown in Fig.A3.2. If the Paschen curve for the ambient gas is known, its intercept with the work isobars will yield quantitative values for $V_d$ and $h_d$, and similarly the behaviour under different conditions can be predicted. The Russian results appear to correlate extremely well. They have also been able to observe electrons emitted during fast stripping processes, and even to analyse the velocities of the electrons.

## REFERENCES


Ackerman M., Goldfinger P., Stafford F.E., & Verhaegen G., 1962, Trans. Faraday Soc., 58, 478, 1926.

Argue G.R., Mercer E.E., & Cobble J.W., 1961, J.Phys.Chem, 65, 2041.

Attree R.W., Cushing R.L., Ladd J.A., & Pieroni J.J., 1958, Rev.Sci.Inst., 29, 6, 491.

Beavitt A.R., 1966, J.Sci.Inst., 43, 182.

Beavitt A.R., Turnell R.C., & Campbell D.S., 1967, Thin Solid Films, 1, 1, 3.

Benjamin L., & Benson G.C., 1962, Canad.J.Chem., 40, 4, 601.

Benjamin P., & Weaver C., 1959, Proc.Roy.Soc., A252, 418.

Benjamin P., & Weaver C., 1960, Proc.Roy.Soc., A254, 163.

Benjamin P., & Weaver C., 1963, Proc.Roy.Soc., A274, 267.

Bennett J.A., 1959, Structure & Props. of Thin Films, ed. Neugebauer, Newkirk, & Vermilyea (London: Wiley), 58.

Benzinger T.H., & Kitzinger C., 1962, Temp.Meas.Control Sci.Ind., 3, 3, 43.

de Boer J.H., 1950, Advances in Colloid Science, 3.

Böttcher C.J.F., 1943, Rec.trav.chim., 62, 325, 503.

Bowden F.P., & Tabor D., 1957, Proc.2nd.Conf. on Surface Activity, (London: Butterworth), FO 283.

Bozorth R.M., 1951, Ferromagnetism (New York: Van Nostrand), 460.

Butler D.W., Stoddart C.T.M., & Stuart P.R., 1969, Proc.7th.Conf. Adhesion & Adhesives (London: Univ. of London).

Cabrera N., 1959, Disc.Faraday Soc., 28, 16.

Calvet E., & Prat H., 1956, Microcalorimetrie (Paris: Masson).

Calvet E., & Prat H., 1963, Recent progress in microcalorimetry (Oxford: Pergamon).

Campbell D.S., 1969, Handbook of thin film technology, ed. L.I.Maissel & R.Glang (New York: McGraw Hill).

Carpenter R., & Campbell D.S., 1967, J.Mat.Sci., 2, 173.

Chapman B.N., & Campbell D.S., J.Phys.C (Solid St.Phys) Ser. 2, 2, 200.

Chavet I., 1963, J.Sci.Inst., 40, 8, 391.

Cranberg L., 1952, J.Appl.Phys., 23, 5, 518.

Davies D., 1967, Proc.Conf. Static Electrification (London: Institute of Physics), 29.

Davies D., 1967a, J.Sci.Inst., 44, 521.

Dekker A.J., 1963, Solid State Physics, (London: Macmillan).

Derjaguin B.V., Krotova N.A., Karassev V.V., Kirillova Y.M., & Aleinikova I.N., 1957, Proc.2nd.Conf. on Surface Activity (London: Butterworth), 3, BP 595.

Frenkel J., 1924, Z.Phys., 26, 117.

Halpern V., 1967, Brit.J.Appl.Phys., 18, 163.

Heavens O.S., 1950, J.Phys Radium, 11, 355.

Hodges D.J., & Acherjee B., 1965, Lab.Pract.(G.B.), 14, 7, 842.

Hoffman R.W., 1966, Physics of Thin Films, ed. Hass & Thun (New York: Academic Press), 260.

Huntsberger J.R., 1967, Treatise on Adhesion & Adhesives, ed. R.L. Patrick (London: Arnold), 1, 119.

Joyce B.A., Bradley R.R., & Booker G.R., 1967, Phil.Mag., 15, 138, 1167.

Leighton R.B., 1959, Princ. of Mod.Phys. (New York: McGraw Hill).

Lenel F.V., 1933, Z.physik.Chem., B23, 379.

Lewis B., 1967, Thin Solid Films, 1, 85.

Lewis B., 1968, Thin Solid Films, 2, 353.

Lewis B., & Campbell D.S., 1967, J.Vac.Sci.Tech., 4, 5, 209.

London F., 1937, Trans. Faraday Soc., 33, 8.

Mayer J.E., 1933, J.Chem.Physics, 1, 270.

Muller H., 1936, Proc.Roy.Soc., A154, 624.

Orr W.J.C., 1939, Trans. Faraday Soc., 35, 1247.

Palmberg P.W., Rhodin T.N., & Todd C.J., 1967, Appl.Phys.Letters, 10, 4, 122.

Pauling L., 1927, Proc.Roy.Soc., A114, 181.

Poppa H., 1965, J.Vac.Sci.Tech., 2, 1, 42.

Poppa H., 1967, J.Appl.Phys., 38, 10, 3883.

Richtmyer F.K., Kennard E.H., & Lauritsen T., 1955, Intro. to Modern Physics (New York: McGraw Hill).

Ryan J.A., & Grossman J.J., 1968, Science Journal, 4, 9, 41.

Skinner S.M., Savage R.L., & Rutzler J.E., 1953, J.Appl.Phys., 24, 4, 438.

Stirland D.J., 1966, Appl.Phys. Letters, 8, 12, 326.

Stirland D.J., 1966, Phil.Mag., 13, 126, 1181.

Stirland D.J., 1968, Thin Solid Films, 1, 447.

Strong J., 1935, Rev.Sci.Inst., 6, 97.

Thompson M.W., 1968, Phil.Mag., 18, 361.

Tian A., 1923, Bull.Soc.Chim.Belges, 33, 4, 427.

Townsend P.D., & Kelly J.C., Phys. Letters, 26A, 4, 138.

Van Vleck J.H., 1932, Electric & Magnetic Susceptibilities (Oxford: Clarendon), 225.

Verwey E.J.W., 1946, Rev.trav.chim., 65, 521.

Walton D., 1962, J.Chem.Phys., 37, 10, 2182.

Walton D., Rhodin T.N., & Rollins R., 1963, J.Chem.Phys., 38, 2698.

Weaver C., 1958, Proc. 1st.Conf. on Vacuum Techniques (London: Pergamon).

Westrum E.F., & Eyring L., 1952, J.Amer.Chem.Soc., 74, 2045.

Zachariasen W.H., 1932, J.Amer.Chem.Soc., 54, 3841.

Journal of Scientific Instruments (Journal of Physics E) 1968 Series 2 Volume 1

# A suspended disk vacuum gauge

**A R Beavitt,† D S Campbell and B N Chapman**
Allen Clark Research Centre, The Plessey Company Ltd., Caswell, Towcester, Northants.

MS *received 20 July 1967, in revised form 27 September 1967*

**Abstract** A wide range radiometer effect pressure gauge has been devised which gives a linear deflection with pressure over a theoretical range from 0·1 mtorr to less than 100 ptorr. The low pressure limit, set by photon pressure in radiometer effect gauges, has been extended by the utilization of specular reflection from the gauge surfaces. An expression has been derived for the deflection in absolute terms, and over a pressure range 0·4 $\mu$torr to 0·1 mtorr an ion gauge has been found to give good agreement with the calculated pressure.

## 1 Introduction

The design of the gauge described in this paper arose from a consideration of the radiometer effect errors of the disk evaporation ratemeter (Beavitt 1966). It was realized that a Knudsen-type gauge could be constructed since gas from suitably placed hot and cold surfaces impinging on, and diffusely reflected from, a disk vane would give a deflection proportional to the gas pressure. Several conventional type Knudsen gauges have been constructed (Knudsen 1910, Klumb and Schwarz 1944, Steckelmacher 1951): they are usually sensitive to vibration (Pirani and Yarwood 1961), cover a limited pressure range and are limited by radiation pressure. This last effect has been discussed by many authors including Steckelmacher (1951) and Schalkowsky and Marshall (1964). Klumb and Schwarz (1944) overcame the vibration and small pressure range problems by fixing vanes around a cylinder and using an annular heater system. More recently, the photon pressure limit has been reduced in various designs of radiometer effect gauge by using silica windows (Robinson 1962, Evrard and Beaufils 1965, Robinson 1965).

The gauge described here depends for its action on longitudinal Knudsen forces (see for example Poulis *et al.* 1964, Poulis, Massen and Thomas 1966); their experimental possibilities were investigated by Krupp *et al.* (1963). The photon pressure limit is lowered by specular reflections at the gauge surfaces by a theoretical factor of about $10^5$. Furthermore, the dynamical balancing of the disk vane makes it relatively insensitive to vibration and the unchanging geometry with deflection allows a very wide range of pressures to be covered. The simple construction of the vane means that this can be made very light, with consequent decrease in response time. The deflection depends on accommodation coefficient however, and there is therefore some dependence on the nature of the gas.

## 2 Construction

### 2.1 *Principle*

The gauge consists of a disk vane suspended above angled heater strips which are themselves mounted above a cooled reference surface (figure 1). Gas is scattered from the heater strips and base with a cosine distribution so that there is a net horizontal component of pressure at the vane due to the increased velocity of the hot gas. The separation of the vane and base from the heater strips can be seen to have no effect on the deflection (provided the vane and base diameter are large in comparison with the separation, and neglecting edge effects). Since the hot and cold surface horizontal components must be equal at zero temperature difference, and since the position of the base has no effect on the hot surface component, the cold surface component must be independent of base separation. This means that both the hot and cold surface components at the vane are limited by the heater strip geometry and do not change with vane–heater separation.

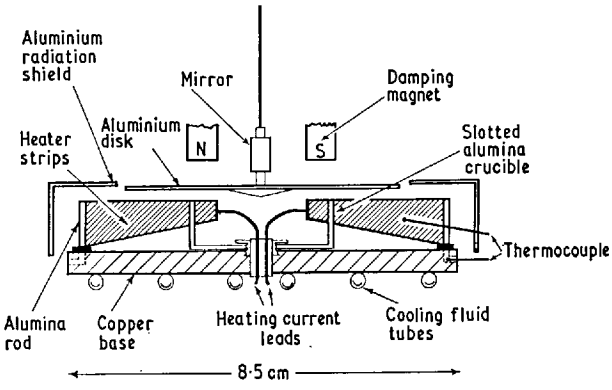


**Figure 1** Section through gauge

The vane and cooled reference surface are made flat and shiny so that the photon flux from the heater strips is specularly reflected and exerts little force on the vane. The heater strips are also made reflective to give a low emissivity. Gas is diffusely reflected from the vane however and the deflection is therefore independent of the vane temperature.

### 2.2 *Detail*

A disk construction was chosen rather than a cylindrical one, as a disk can be made lighter than a cylinder, and the two forms have been shown to have comparable sensitivities for impinging atoms.

† Now at the National Standards Laboratory, Chippendale, New South Wales, Australia.

Figure 2(*a*) shows the construction of the heater strips and cooled reference surface. The cooled reference surface consisted of a machined copper plate with cooling fluid tubes

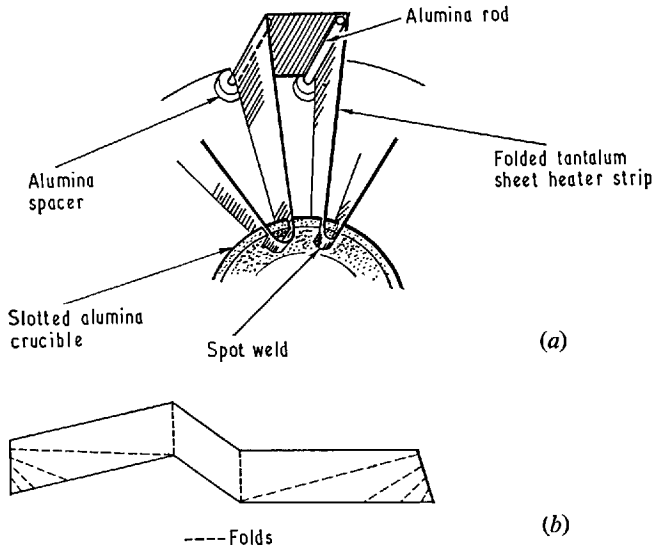


**Figure 2** (*a*) Arrangement of heater strips; (*b*) method of folding heater strips

soldered on the underside. Holes were drilled around the perimeter at an angle of 45° to take alumina rods for supporting the heater strips. The strips were supported at the centre by slots cut at 45° into part of a recrystallized alumina crucible (Morgan Refractories Ltd.). The heater strips were made from 0·002 in tantalum and folded in the manner shown in figure 2(*b*) to give a constant linear resistance (and therefore approximately linear temperature) even though the width was changed to preserve the same geometry at the centre and perimeter. The segments were joined up *in situ* by spot welding. The current leads were connected at opposite sides of the heater system, so that for a change in current the inductive forces on the vane were balanced. In addition, an a.c. heating current was used. The temperature difference between heater and base was measured with a platinum–rhodium thermocouple, with the hot junction spot welded to a heater strip.

To obtain a fast response time the disk vane must have a low inertia. Since the inertia of a disk varies as the fourth power of the radius, the thickness would ideally vary inversely with this power. An approximation to this condition was achieved by evaporation of aluminium through a star-shaped mask on to a revolving glass substrate. The substrate had previously been lightly smeared with Teepol (Shell Chemicals Ltd.) so that after marking out the centre (with a diamond scribe) and edge of the disk (with dividers) it could be floated off the substrate in water. A grid was used to lift the disk from the water and transfer it to an oven, where it was annealed for 30 minutes at 200°c between two flat plates. The disk used in these measurements was 6 cm in diameter, 10 $\mu$m thick in the centre and 0·9 $\mu$m thick at the edge. The evaporation time required was 15 minutes at a substrate distance of 5 cm with the use of a flash evaporation source. Disks have also been made from 0·002 in aluminium foil; the response time is longer but is still of practical length.

A 0·002 in × 0·0002 in JMC suspension alloy (Johnson Matthey & Co. Ltd.), 14 cm long, was attached to the vane by means of a Dural mounting (figure 3) with a mirror cemented to the stem for measuring small deflections. The vane was damped magnetically.

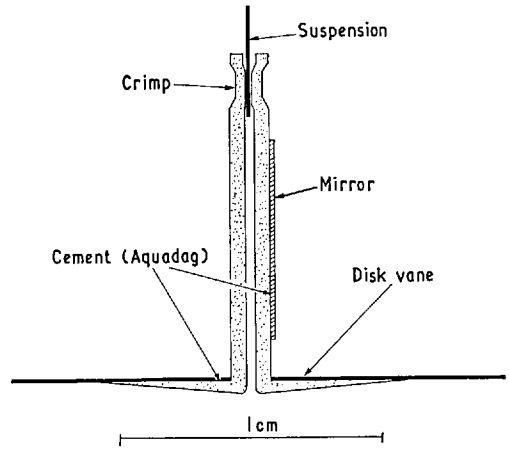


**Figure 3** Section through vane mounting

## 3 Theory

### 3.1 *Radiometer effect*

The force, and hence the couple, acting on the vane depends on the net horizontal component of momentum of the gas arriving. This component varies with the geometry of the system, with the temperatures of the heater strips and the base and with the pressure.

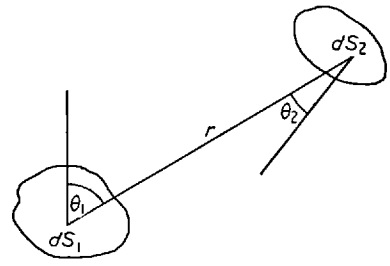


**Figure 4** Geometry for calculation of flux

According to Knudsen's cosine law, under conditions of molecular flow the momentum flux of molecules out of area $dS_1$ into $dS_2$ at distance $r$ (figure 4) into solid angle $d\omega$ in time $dt$ is

$$FdS_1 \cos\theta_1 \, d\omega dt = FdS_1 \cos\theta_1 \frac{dS_2 \cos\theta_2}{r^2} dt \qquad (1)$$

where $F$ is the momentum flux density.

Let $F_H$ and $F_C$ be the flux densities from the (hot) heater strips and (cold) base respectively. Then the turning couple on the vane is balanced by the restoring torque $C\chi$ of the suspension:

$$C\chi = JF_H + KF_C$$

where $J$ and $K$ are constants determined by the geometry of the system, $C$ is a constant determined by the suspension and $\chi$ is the angular deflection. However, when $F_H = F_C$, e.g. when the whole system is in equilibrium at ambient temperature, there is no turning couple and hence $J + K = 0$ and

$$C\chi = J(F_H - F_C). \qquad (2)$$

The geometrical constant $J$ is determined by Knudsen's cosine law, using expression (1). For the particular geometry used (heater strips at 45° to the vertical) this leads to a value

$J = 21{\cdot}4$, as shown in Appendix 1. Variation in the heater strip angle will alter the value of $J$ and it is shown in Appendix 2 that the optimum angle is 53°.

To calculate $F_H$ and $F_C$ consider a closed system. ~~The density of molecules is constant throughout and in particular~~ the number of molecules striking unit area in unit time is $p_i/(2\pi mkT_i)^{1/2}$ where $p_i$ and $T_i$ are the pressure and equivalent temperature of the incident gas. A similar expression holds for the numbers of molecules leaving at pressure $p_r$ and temperature $T_r$. Since these numbers must be equal

$$p_i/T_i^{1/2} = p_r/T_r^{1/2}. \tag{3}$$

The total change of momentum at a surface in time $dt$ is equal and opposite to the impulse of the force exerted by the molecules on the same area in the same time, i.e. to the impulse of the gas pressure. Momentum flux density $F$ and gas pressure $P$ can thus be related in the following manner.

Consider gas leaving a surface at an angle between $\theta$ and $\theta + d\theta$ to the normal (figure 5), i.e. into the solid angle

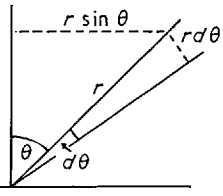


**Figure 5** Geometry for calculation of pressure equivalent of flux

$2\pi \sin\theta\, d\theta$ at $\theta$, in time $dt$. The momentum flux is $F\cos\theta \times 2\pi \sin\theta\, d\theta\, dt$ at $\theta$ and hence the flux perpendicular to surface is $2\pi F\cos^2\theta \sin\theta\, d\theta\, dt$ and the flux parallel to surface is $2\pi F\cos\theta \sin^2\theta\, d\theta\, dt$. The horizontal components are symmetrical with respect to the surface and mutually cancel. Therefore the net momentum flux away from the surface is

$$\int_0^{\pi/2} 2\pi F\cos^2\theta \sin\theta d\theta dt = \frac{2\pi F}{3} dt.$$

Similarly, the incident molecules provide a net flux of $\frac{2}{3}\pi F dt$ towards the surface. Hence the change of momentum is $\frac{4}{3}\pi F dt$ and the pressure $p$ is given by

$$p = \frac{d}{dt}(\text{momentum}) = 4\pi F/3. \tag{4}$$

$F_H$ and $F_C$ can be related to equivalent pressures $p_H$ and $p_C$ by similarly considering the effect of placing an elemental surface at the gas temperature in the path of the gas. The flux densities may then be expressed in terms of the system pressure $p_0$ and system temperature $T_0$ from equation (3):

$$\left.\begin{aligned} F_H &= \frac{3}{4\pi}p_H = \frac{3}{4\pi}p_0\left(\frac{T_{RH}}{T_0}\right)^{1/2} \\ F_C &= \frac{3}{4\pi}p_C = \frac{3}{4\pi}p_0\left(\frac{T_{RC}}{T_0}\right)^{1/2} \end{aligned}\right\} \tag{5}$$

where $T_{RH}$ and $T_{RC}$ are the temperatures of the beams from the hot and cold surfaces respectively. $T_{RH}$ and $T_{RC}$ are related to the thermal accommodation coefficients $\alpha_H$ and $\alpha_C$ of the two surfaces by the standard definitions

$$\left.\begin{aligned} \alpha_H &= \frac{T_{RH} - T_{IH}}{T_H - T_{IH}} \\ \alpha_C &= \frac{T_{RC} - T_{IC}}{T_C - T_{IC}} \end{aligned}\right\} \tag{6}$$

where $T_{IH}$ and $T_{IC}$ are the temperatures of the incident beams at the hot and cold surfaces respectively and $T_H$ and $T_C$ are the temperatures of the surfaces themselves.

When these values are substituted into equation (5), and hence into equation (2), the vane deflection is given by

$$C\chi = \frac{3Jp_0}{4\pi T_0^{1/2}}\left[\{\alpha_H T_H + (1-\alpha_H)T_{IH}\}^{1/2} - \{\alpha_C T_C + (1-\alpha_C)T_{IC}\}^{1/2}\right]. \tag{7}$$

In the case of complete thermal accommodation

$$\alpha_H = \alpha_C = 1$$

and the expression reduces to

$$C\chi = \frac{3Jp_0}{4\pi T_0^{1/2}}(T_H^{1/2} - T_0^{1/2}). \tag{8}$$

The thermal accommodation coefficient of the vane has not been introduced since this does not affect the horizontal momentum transferred to the vane, gas from the vane being emitted diffusely and thus symmetrically. However, the concept of 'slip' of gases (Smoluchowski 1911) is relevant. Of all molecules striking a surface, a fraction $f$ are adsorbed and subsequently diffusely re-emitted, whilst a fraction $1-f$ are specularly reflected with the same velocity; the latter fraction does not suffer a change of horizontal momentum at the vane and therefore transfers zero impulse. The turning couple on the vane is then due only to the adsorbed incident molecules and this reduces the equilibrium vane deflection $\chi$ by the fraction $f$ ($f$ is termed the 'slip' coefficient).

3.2 *Photon pressure*

The photon flux from a surface is the sum of emitted and reflected components. For the hot surface the effective photon pressure is given by (Roberts and Miller 1960)

$$P_H{}^{\nu} = \frac{4\sigma}{3c}\{\epsilon_H T_H^4 + (1-\epsilon_H)\epsilon_C T_C^4 + f(T_H^4, T_C^4)\}, \tag{9}$$

where $\sigma$ is the Stefan-Boltzmann constant, $c$ is the velocity of light and $\epsilon_H$ and $\epsilon_C$ are the emissivities of the hot and cold surfaces respectively. The first term represents the intrinsic emission, the second represents reflection of the flux from the cold surface (the reflection coefficient is related to emissivity by Kirchoff's law) and the last term represents background radiation. It is assumed that photons reflected at the hot surfaces and arriving at the vane come mainly from the base; this may not be valid, but will give an order of magnitude value of the photon pressure limit.

A similar expression holds for the photon pressure from the cold surface, so that the net pressure is given by

$$p_H{}^{\nu} - p_C{}^{\nu} = \frac{4\sigma}{3c}\epsilon_H\epsilon_C(T_H^4 - T_C^4). \tag{10}$$

From equations (2) and (5), since the geometry is unchanged the deflection $\chi^{\nu}$ due to photon pressure is given by

$$C\chi^{\nu} = \frac{3J\epsilon_V}{4\pi}(p_H{}^{\nu} - p_C{}^{\nu}) = \frac{J\sigma}{\pi c}\epsilon_H\epsilon_C\epsilon_V(T_H^4 - T_C^4). \tag{11}$$

The emissivity $\epsilon_V$ of the vane is introduced to account for the fraction of photon momentum transferred.

From equations (11) and (8) it can be seen that photon pressure produces an equal deflection to gas pressure when

$$p_0 = \frac{4\sigma\epsilon_H\epsilon_C\epsilon_V T_0^{1/2}}{3c}\left(\frac{T_H^4 - T_C^4}{T_H^{1/2} - T_C^{1/2}}\right) \qquad (12)$$

and this indicates the low pressure limit of the gauge.

## 4 Results

The gauge was set up in a mercury diffusion pumped system with cold trap. Before any measurements were made, the gauge without the vane was thoroughly degassed by raising the heater strips to 1500°c for several hours. The vane was then suspended 0·3 cm above the heater strips and the undamped period (approximately equal to the damped response time) measured. The undamped period was 25 seconds, and by comparison with an inertia bar the torsional constant was determined as $5 \times 10^{-3}$ dyn cm rad$^{-1}$.

Deflection of the vane was measured either relative to a zero position, defined when the hot and cold sources were at the same temperature, or by reading deflections at different hot source temperatures. In the latter case the response time was limited by the thermal inertia of the heater system.

The relationship between $\chi$ and temperature difference (equation (8)) was confirmed by measuring the deflections at constant pressure (figure 6). This relationship was used to correct measurements made at various pressures using the most convenient temperature difference to those at a standard temperature difference. To confirm the relationship between $\chi$ and pressure, the radiometer gauge was compared with a Bayard–Alpert ionization gauge. The system was evacuated to 0·1 $\mu$torr and then filled to the required pressure with various gases. In figure 7 the deflection $\chi$, corrected (by using figure 6) to a value of $(T_H^{1/2} - T_C^{1/2})/T_0^{1/2} = 0{\cdot}5$, has been plotted against ionization gauge readings that have been corrected for gauge sensitivities to the relevant gases (Craig and Harden 1964 unpublished). For comparison the theoretical pressure given by equation (8) has been plotted, assuming accommodation coefficients of unity.

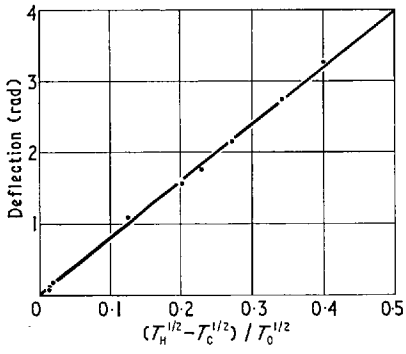


**Figure 6** Variation of deflection $\chi$ with temperature difference for constant pressure (16 $\mu$torr)

The actual largest temperature difference used was 572 degc with a liquid nitrogen cooled base. Hot source temperatures greater than 500°c caused the aluminium vane to wilt.

The smallest deflection measured was $4 \times 10^{-4}$ rad and the limit of detection with the optical lever used (2·3 m long) was about $10^{-4}$ rad. This corresponds to a pressure detection limit of 0·1 ntorr.

## 5 Discussion

The theory given in § 3.1 assumed a diffuse reflection of gas at the vane. Stickney (1962) found that various gases (at 10 $\mu$torr) were diffusely reflected from aluminium even when not energy-accommodated, and Smith (1964) found diffuse reflection (at 0·1 $\mu$torr) for pure nickel but some specular reflection from carbonized nickel.

Equation (7) shows a dependence of deflection on accommodation coefficients $\alpha_H$ and $\alpha_C$. Accommodation coefficients for different gases on high atomic weight metals vary between 0·3 and 1 (Leck 1957, p. 41) for contaminated surfaces but much lower values (cf. Wachman 1962) can be obtained for clean surfaces. When used at very low pressures the gauge surfaces could with advantage be coated with a low atomic weight material such as beryllium, to increase $\alpha$. A reasonable assumption from figure 7 is that the value of $\alpha$ is approximately 0·4. However, as has already been noted, this effect may also be due to the 'slip' of gas, so that the value of 0·4 may arise from a combination of both effects.

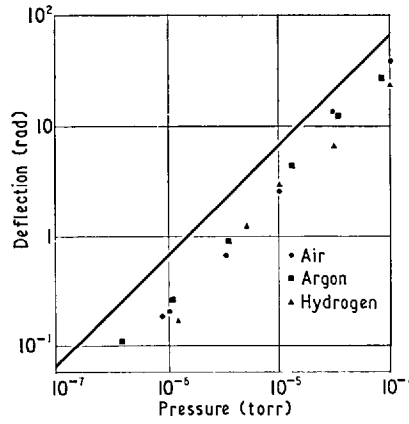


**Figure 7** Variation of deflection $\chi$ with pressure for constant temperature difference $((T_H^{1/2} - T_C^{1/2})/T_0^{1/2} = 0{\cdot}5)$

In the analysis it has been assumed that molecular flow conditions apply, i.e. that the gauge dimensions are much smaller than the molecular mean free path. According to Fredlund (1932) this condition prevails and hence the radiometer force is proportional to pressure if the mean free path is greater than 15 times the vane–heater spacing. This would impose a high pressure limit to the linear behaviour of the present design of 0·3 mtorr. Above this pressure the gauge would still operate but a different relationship would exist between deflection and pressure (cf. Krupp *et al.* 1963).

The theoretical photon pressure limit can be estimated by assuming values for the emissivity of the gauge surfaces and substituting them, together with the surface temperatures, in equation (12). The values of $\epsilon$ for unoxidized tantalum, copper and aluminium are approximately 0·2, 0·02 and 0·03 respectively; for $T_C = T_0 = 290°K$ and $T_H = 600°K$, the pressure limit is then 65 ptorr, compared with 1 $\mu$torr for a conventional Knudsen gauge operating at the same temperatures (Steckelmacher 1951). The values of emissivity are strongly dependent on the conditions of the surfaces; as the surfaces oxidize, the photon pressure limit increases and could be as much as three orders higher. However, reducing the base temperature reduces the photon pressure limit; with $T_C = 200°K$, using liquid nitrogen cooling, and $T_H = 470°K$, the limit is reduced to 25 ptorr.

Measurements of angular deflection down to $10^{-10}$ rad are possible with an optical lever amplifier (Jones 1961) but thermal fluctuations would limit deflection measurements of the vane described to about $10^{-5}$ rad. McCombie (1953) gives an expression for the smallest possible couple measurement $\Delta F$ occupying a time $S$ at temperature $T$:

$$\overline{\Delta F^2} = 2\kappa kT/S$$

where $\kappa$ is the damping constant. Fluctuation values much smaller than $10^{-5}$ rad would be possible with a feedback system owing to the reduction in $\kappa$.

## 6 Conclusions

It has been shown that a wide range radiometer pressure gauge can be made from a thin disk suspended over heated surfaces. Comparison of the radiometer gauge with a Bayard–Alpert ionization gauge shows that they are in good agreement provided that the thermal accommodation coefficient of gas on the gauge surfaces is taken to be approximately 0·4.

**Acknowledgments**

The authors are indebted to Mr. R. W. Allen for his invaluable assistance with the appendixes and for preparing the computer programme and carrying out the integration. Thanks are due also to the Ministry of Technology for support in this project and the Directors of the Plessey Company for permission to publish.

## Appendix 1: Calculation of geometrical constants

*Introduction*

In § 3.1 it has been shown that the turning couple on the vane is given by

$$C\chi = J(F_H - F_C).$$

Thus in calculating the turning couple constant $J$, it is necessary to consider the flux from only either the hot (heater) surface or the cold (base) surface. The evaluation of either involves complex integrals. This has been carried out for both surfaces, giving the same result, but as there are fewer terms in the expression relating to the cold surface, numerical evaluation is shown for this case only.

The principle of the method of calculation is that the heater strips and base may be replaced by equivalent vertical surfaces, which considerably simplifies the geometry.

*Equivalent surfaces*

According to Knudsen's cosine law the momentum flux $dF$ of molecules out of area $dS_1$ into $dS_2$ at distance $r$ (figure 4) in time $dt$ is given by

$$dF = FdS_1 \cos\theta_1 d\omega_2 dt \tag{13a}$$

where $d\omega_2$ is the solid angle subtended by $dS_2$ at $dS_1$ and $F$ is the momentum flux density.

Substituting for $d\omega_2$:

$$dF = FdS_1 \cos\theta_1 \frac{dS_2 \cos\theta_2}{r^2} dt \tag{13b}$$

$$= Fd\omega_1 dS_2 \cos\theta_2 \, dt \tag{13c}$$

where $d\omega_1$ is the solid angle subtended by $dS_1$ at $dS_2$. Thus the flux from $dS_1$ into $dS_2$ can be discussed in terms of $d\omega_1$ and $\theta_2$.

Consider one sector of the vane-heater–base assembly between adjacent heater strips (figure 8). The solid line of the heater strip represents the top horizontal edge. With this arrangement the vane, radius $R_2$, turns anticlockwise. The heater strips extend from radii $R_1$ to $R_3$. Angles $\phi$ are measured anticlockwise from a vertical reference plane plane through the top edge of a heater strip. The total angle between adjacent strips is $\Phi$.

Consider area $dS_v$ of the vane between $\phi$ and $\phi + d\phi$ and between $R$ and $R + dR$:

$$dS_v = Rd\phi dR. \tag{14}$$

The momentum flux out of each elemental area of the heater strips and base imparts an impulse to $dS_v$. From equation (13c), each elemental area can be replaced by any other area emitting the same momentum flux density and subtending the same solid angle at $dS_v$. Therefore each heater strip inclined at $\theta$ to the vertical can be replaced by its equivalent projection on to the reference plane.

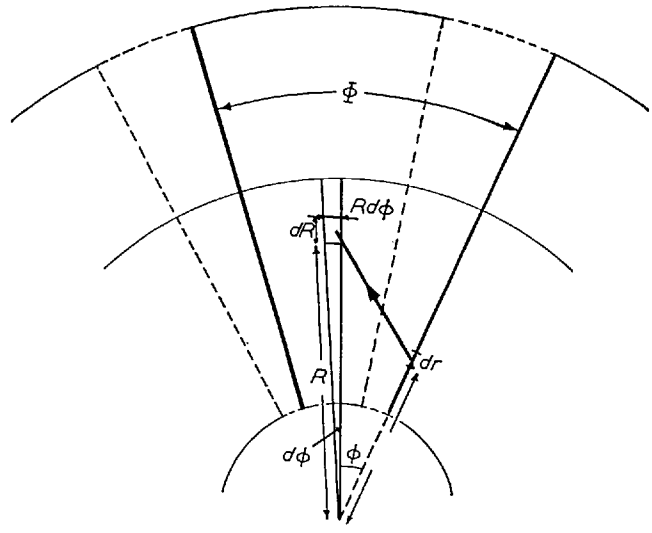


**Figure 8** Top view of gauge showing geometrical terms used in calculation

Figure 9 is a representation of the equivalent geometry. Consider an elemental area $dS_H$ of the equivalent heater between radii $r$ and $r + dr$, and between $l$ and $l + dl$ from the top of the heater:

$$dS_H = dldr. \tag{15}$$

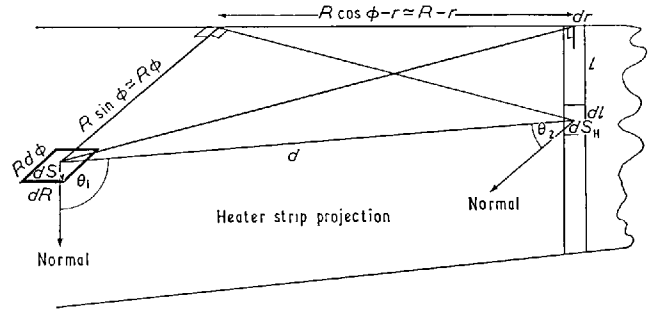


**Figure 9** Diagram showing equivalent geometry (horizontal view)

From equation (13b) the flux $dF$ out of $dS_H$ into $dS_v$ in time $dt$ is given by

$$dF = FdS_v \cos\theta_1 \frac{dS_H \cos\theta_2}{d^2} dt \tag{16}$$

where $F$ is the momentum flux density and $d$ is the distance between $dS_H$ and $dS_v$.

From figure 9 it can be seen that

$$\left.\begin{aligned} \cos\theta_1 &= l/d \\ \cos\theta_2 &= R\phi/d \\ \text{and} \quad d^2 &= R^2\phi^2 + (R-r)^2 + l^2. \end{aligned}\right\} \tag{17}$$

The impulsive force $X$ on $dS_v$ is equal to the rate of change of momentum. Therefore, by substituting in equation (16):

$$X = \frac{dF}{dt}$$

$$= FRd\phi dR\frac{l}{d}dldr\frac{R\phi}{d}\frac{1}{d^2}. \tag{18}$$

The component of this force in the horizontal plane perpendicular to the radius through $dS_v$ is $Xr\sin\phi/d$ (from figure 8) $\simeq Xr\phi/d$ and therefore the turning couple on $dS_v$ at radius $R$ due to the equivalent elemental flux source at $r$ is

$$\frac{XRr\phi}{d} = \frac{FR^3rl\phi^2dld\phi drdR}{\{R^2\phi^2 + (R-r)^2 + l^2\}^{5/2}} \tag{19}$$

which will be written as

$$\{F, \phi\}dld\phi drdR. \tag{20}$$

So far the flux from only one source has been considered. In fact $dS_v$ receives from two real hot surfaces (the heater strips) and one real cold surface (the cooled base). These will be shown to be equivalent to four hypothetical surfaces. The turning couple exerted on $dS_v$ is then the sum of integrals of expressions (19) for each surface.

*Evaluation of integration limits*

The remainder of the calculation is concerned with the evaluation of the integration limits and with the integration process. The integration limits depend on the position of $dS_v$, and two separate geometries need to be considered.

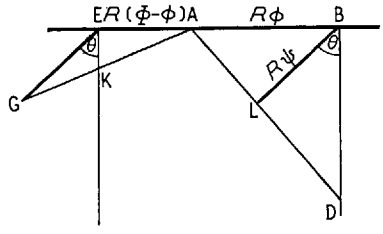


(*a*)

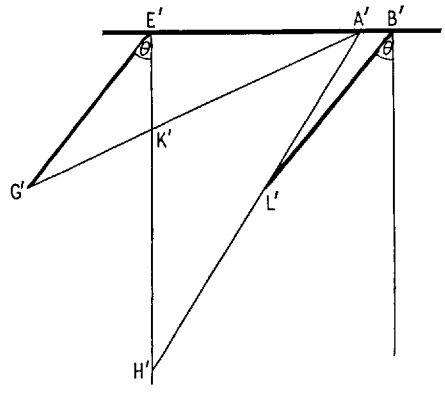


(*b*)

**Figure 10** Vertical sections of gauge geometry: (*a*) $\Phi \geqslant \phi \geqslant \psi\sin\theta$, (*b*) $0 \leqslant \phi < \psi\sin\theta$

(*a*) $\Phi \geqslant \phi \geqslant \psi\sin\theta$

Consider the vertical plane through $dS_v$ perpendicular to the radius (figure 10(*a*)). Arcs of circles are approximated to straight lines, which is acceptable when the total number $N$ of heater strips is large. A is the position of $dS_v$, BL is the real heater strip at $\theta$ to the vertical, and BD is its equivalent. The real heater strips are wedge-shaped, tapering to zero width at the centre of the system. Hence

$$\mathrm{BL} = R\psi \tag{21}$$

where $\psi$ is the angle of the heater strip wedge. Using the sine rule in triangle ABL to find $\angle$ BAL,

$$\mathrm{BD} = R\phi\tan\angle\,\mathrm{BAL}$$

$$= \frac{R\phi\psi\cos\theta}{\phi - \psi\sin\theta} \tag{22}$$

which is linearly proportional to $R$. Therefore every element of the vane along the segment between $\phi$ and $\phi + d\phi$ 'sees' the same equivalent heater. There are actually small end corrections but these can be shown to be negligible.

Only the momentum flux from the front surface of BL so far been considered, but similarly the back of the heater EG can be replaced by its equivalent EK and the base GL by two vertical surfaces at the base temperature, extending from K to $\infty$ and from D to $\infty$. By a calculation similar to that for BD

$$\mathrm{EK} = \frac{R(\Phi - \phi)\psi\cos\theta}{(\Phi - \phi) + \psi\sin\theta}. \tag{23}$$

Since the coefficients of $F_H$ and $F_C$ in the expression for total turning couple (equation (2)) are equal, it is necessary to calculate the individual turning couple for the surfaces of one temperature only. The cold surfaces are chosen since they involve fewer integrals. From equation (19) the turning couple $C_C\,d\phi drdR$ due to the momentum flux $F_C$ from the two elementary strips of the two cold surfaces is given by

$$C_Cd\phi drdR = \int_u^\infty\{F_C,\phi\}dld\phi drdR - \int_v^\infty\{F_C,(\Phi - \phi)\}dld\phi drdR \tag{24}$$

where $u = r\phi\psi\cos\theta/(\phi - \psi\sin\theta)$

and $v = r(\Phi - \phi)\psi\cos\theta/\{(\Phi - \phi) + \psi\sin\theta\}$.

(*b*) $0 \leqslant \phi < \psi\sin\theta$

In this case there are three hot and one cold equivalent surfaces (figure 10(*b*)). By the usual trigonometric methods

$$\mathrm{E'K'} = \frac{R(\Phi - \phi)\psi\cos\theta}{(\Phi - \phi) + \psi\sin\theta}$$

$$\mathrm{E'H'} = \frac{R(\Phi - \phi)\psi\cos\theta}{\psi\sin\theta - \phi}$$

and using parallel notation to that in geometry (*a*) above,

$$C'_Cd\phi drdR = \int_x^y\{F_C,(\Phi - \phi)\}dld\phi drdR$$

where $x = r(\Phi - \phi)\psi\cos\theta/\{(\Phi - \phi) + \psi\sin\theta\}$

and $y = r(\Phi - \phi)\psi\cos\theta/(\psi\sin\theta - \phi)$. (25)

The total turning couple $JF_C$ exerted on the whole of the vane by the whole of the cooled base is therefore given by

$$JF_C = N\int_0^{R_2}\int_{R_1}^{R_3}\left\{\int_{\psi\sin\theta}^{\Phi}C_Cd\phi + \int_0^{\psi\sin\theta}C'_Cd\phi\right\}drdR. \tag{26}$$

The first integration of expressions (19) with respect to $l$ is accomplished by writing the integral in the form

$$\int\{l/(a^2 + l^2)^{5/2}\}dl.$$

This is simply integrated by the substitution $l = a\tan\alpha$, and becomes

$$-1/3(a^2 + l^2)^{3/2} + \text{const.}$$

Carrying out the first integration over the appropriate limits with respect to $l$ algebraically, since numerical integration with $\infty$ as one limit is inaccurate, the turning couple constant $J$ is finally given by

$$J = N\int_0^{R_2}\int_{R_1}^{R_3}\frac{R^3 r}{3}\left\{-\int_{\psi\sin\theta}^{\Phi}\phi^2\left\{(R-r)^2+R^2\phi^2+\left(\frac{r\phi\psi\sin\theta}{\phi-\psi\sin\theta}\right)^2\right\}^{-3/2}d\phi+\int_0^{\Phi}\phi^2\left[(R-r)^2+R^2(\Phi-\phi)^2+\left\{\frac{r(\Phi-\phi)\psi\cos\theta}{(\Phi-\phi)+\psi\sin\theta}\right\}^2\right]^{-3/2}d\phi+\int_0^{\psi\sin\theta}(\Phi-\phi)^2\left[(R-r)^2+(\Phi-\phi)^2+\left\{\frac{r(\Phi-\phi)\psi\cos\theta}{\psi\sin\theta-\phi}\right\}^2\right]^{-3/2}\right\}drdR. \qquad (27)$$

The right-hand side of equation (27) has been evaluated numerically, for the particular geometry used, by computer methods. A copy of the programme used is available from the authors. A six-point Gaussian integration was used; the accuracy of this was checked with a test integral and found to be very satisfactory.

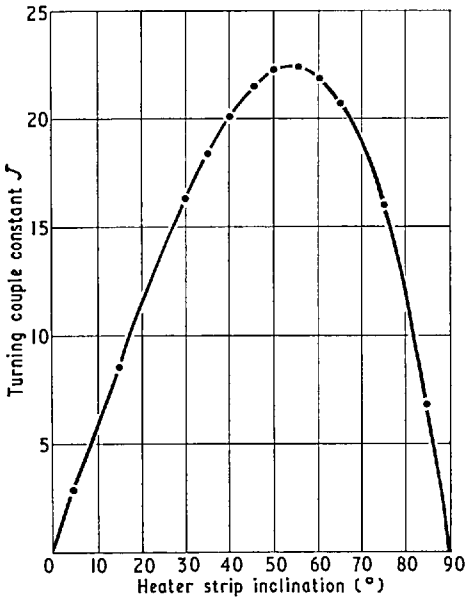


**Figure 11** Turning couple constant $J$ as a function of heater strip inclination $\theta$

The gauge constructed had the following dimensions: no. of heater strips $N = 24$ (hence angular separation $\phi = 0{\cdot}262$ rad); heater radii $R_1 = 1{\cdot}5$ cm, $R_3 = 4{\cdot}0$ cm; vane radius $R_2 = 3{\cdot}0$ cm; width of wedge-shaped heater strips at 4·0 cm radius 1·0 cm (hence angle of wedge $\psi = 0{\cdot}250$ rad); inclination of heater strips $\theta = \frac{1}{4}\pi$. For this geometry, the equilibrium equation for the suspended system is

$$C\chi = 21{\cdot}4(F_H - F_C)$$

and the momentum flux can be related to surface temperatures and pressure, as is shown in § 3.1.

**Appendix 2**

*Optimum inclination of heater strips*

Although the constructed gauge had heater strips fixed at 45° to the vertical, the turning couple constant $J$ has been calculated for varying angles $\theta$ of the heater inclination, all other values being as specified in the previous section. The results are shown in figure 11. The maximum turning couple is produced when the heater inclination is very nearly 53°.

**References**

Beavitt A R 1966 *J. Sci. Instrum.* **43** 182–5
Evrard R and Beaufils P 1965 *Le Vide* **20** 116–20
Fredlund E 1932, *Ann. Phys., Lpz.* **14** 617–43
Jones R V 1961 *J. Sci. Instrum.* **38** 37–45
Klumb H and Schwarz H 1944 *Z. Phys.*, **122** 418–36
Knudsen M 1910 *Ann. Phys., Lpz.* **32** 809–42
Krupp H Robens E Sandstede G and Walter G 1963 *Vacuum* **13** 297–301
Leck J H 1957 *Pressure Measurement in Vacuum Systems* (London: Institute of Physics)
McCombie C W 1953 *Rep. Progr. Phys.* **16** 266–320
Pirani M and Yarwood J 1961 *Principles of Vacuum Engineering* (London: Chapman and Hall)
Poulis J A Pelupessy B Massen C H and Thomas J M 1964 *J. Sci. Instrum.* **41** 295–301
Poulis J A Massen C H and Thomas J M 1966 *J. Sci. Instrum.* **43** 234–7
Roberts J K and Miller A R 1960 *Heat and Thermodynamics* (London: Blackie) p 496
Robinson N W 1962 *Le Vide* **17** 571–9
Robinson N W 1965 *Vacuum* **15** 27–32
Schalkowsky S and Marshall T Jr. 1964 *Rev. Sci. Instrum.* **35** 908–9
Smith J N Jr. 1964 *J. Chem. Phys.* **40** 2520–7
Smoluchowski M 1911 *Ann. Phys., Lpz.* **4** 983–1004
Steckelmacher W 1951 *Vacuum* **1** 266–82
Stickney R E 1962 *Phys. Fluids* **5** 1617–24
Wachman H Y 1962 *Amer. Rocket Soc. J.* **32** 2–12

J. PHYS. C (SOLID ST. PHYS.), 1969, SER. 2, VOL. 2. PRINTED IN GREAT BRITAIN

# Condensation of high-energy atomic beams†

B. N. CHAPMAN‡ and D. S. CAMPBELL§

Allen Clark Research Centre, The Plessey Company Limited, Caswell, Towcester, Northants.

*MS. received* 25*th June* 1968

**Abstract.** This paper presents the results of measurements of the growth of gold on rocksalt when the incident atoms, obtained by sputtering ejection, have energies of approximately 20 ev atom$^{-1}$. The results are compared with those obtained using thermal evaporation sources, when the incident atoms have energies of the order of 0·3 ev atom$^{-1}$.

The effect of the high arrival energy is manifested in an increased saturation island density (numbers of discrete groups of atoms per unit substrate area) and a change in the orientation of the deposit. The results are discussed in terms of incomplete thermal accommodation and production of atypical adsorption sites on the substrate.

## 1. Introduction

In theories of thin film nucleation and growth, the energy with which atoms impinge on the substrate surface is not taken into account; it is usually assumed that atoms are immediately and completely thermally accommodated. This may be acceptable when the energy of the incident atoms is quite low, but becomes increasingly improbable as the incidence energy increases. Cabrera (1959) has shown theoretically that an atom should lose sufficient energy to the lattice to be captured if the incidence energy is less than twenty-five times the adsorption energy. This condition will usually be satisfied in thermal evaporation experiments since the average kinetic energy of atoms from a source at 2000 °K is only 0·2 ev. When an atom is adsorbed, it gains in kinetic energy as much as it loses in potential energy; the adsorption energy of gold on rocksalt is approximately 0·5 ev atom$^{-1}$, so the impingement energy from a thermal source is about 0·7 ev atom$^{-1}$.

The nucleation behaviour of gold atoms, incident with beam energies 0·1–0·6 ev onto a rocksalt substrate, has been studied using a mechanical velocity distributor (Beavitt *et al.* 1967); no sensible energy effect was found. A study over the range 0–2 ev, using the same velocity distributor technique (Jordan and Chapman, to be published) is in progress. The present paper is concerned with the condensation of beams of gold atoms with incidence energies of approximately 20 ev atom$^{-1}$ on to rocksalt substrates.

The three important energy parameters which control the nucleation and growth of a film are:

(i) The adsorption energy $E_a$ between an adatom and the substrate.

(ii) The surface diffusion energy $E_d$, which is the energy an atom requires to jump from one adsorption site on the substrate to an adjacent site.

(iii) The cohesion energy $E_b$ between adjacent adatoms on the substrate.

A feature of nucleation which is sensitive to these parameters is the saturation island density (Lewis and Campbell 1967). During the initial stages of formation of a film, the number of 'islands' or discrete groups of atoms increases to a saturation value $N_s$ which is a function of substrate temperature. This is shown in figure 1, where saturation density measurements for thermally evaporated gold on vacuum-cleaved rocksalt have been plotted against corresponding reciprocal substrate temperatures. At low temperatures the island density is determined by surface diffusion, and the slope of the straight line obtained gives the surface diffusion energy $E_d$. At higher temperatures re-evaporation becomes important,

† This is an expanded version of a paper presented at the 2nd Conference on Thin Films held by the Institute of Physics and Physical Society at the University of Southampton, 22nd April, 1968.

‡ Now at Electrical Engineering Department, Imperial College, London.

§ Now at The Plessey Company Limited, Components Group, Bathgate, Scotland.

and the slope of the line is governed by the adsorption energy $E_a$ as well as $E_d$. Thus two regions are obtained. The intercept at $1/T = 0$ of the extrapolated low-temperature region is also of importance, and is governed by the incidence rate $R$, the density of adsorption sites $N_0$, and the vibrational frequency $\nu_0$ for surface diffusion.

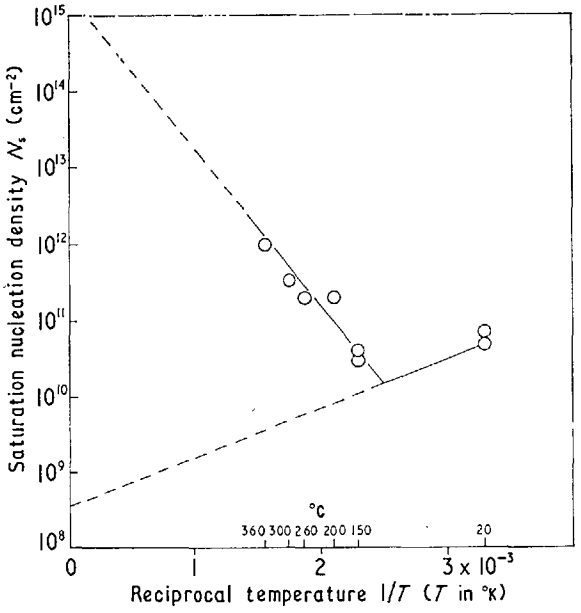


Figure 1. Temperature variation of saturation island density $N_s$ for evaporated gold on vacuum-cleaved rocksalt.

Island density measurements can thus be very informative and so have been used for the present study of high incidence energy. We have looked also at the orientations of the deposits and have compared these with corresponding evaporated deposits.

## 2. Experimental details

### 2.1. *The high-energy gold beam*

The high-energy beam was obtained by a sputtering technique. When a single-crystal target is bombarded by fast heavy ions, atoms of the target are ejected anisotropically, material being preferentially ejected along the low-index crystallographic directions of the target. The energies of ejection along specific directions from a gold target bombarded by argon ions have been measured by Thompson (1968) using a time-of-flight technique; the spectra of relative numbers against energy are shown, for two different directions of ejection, in figure 2. The ⟨110⟩ spectrum is from a gold crystal bombarded in a near ⟨100⟩ direction with 41 kev argon ions, the mean ejection energy being 22·7 ev. The ⟨100⟩ spectrum is from a crystal bombarded in a ⟨100⟩ direction with 43 kev argon ions; the mean ejection energy in this case is 93·5 ev, due mainly to the high energy 'tail'.

### 2.2. *The experimental arrangement*

The central part of the apparatus is shown in figure 3. The gold single-crystal target was mounted so that the ion beam was incident in the required direction; the orientation was checked by the Laüe x-ray reflection method. The target could be rotated about an axis collinear with the ion incidence direction, and the substrate could be rotated about a perpendicular axis through the target as shown, so that any ejection direction could be selected.

Harshaw rocksalt substrates were used, radiatively heated by a quartz-iodine lamp, and the substrate temperature was measured by a chromel–alumel thermocouple. The substrates were clamped in a comparatively massive block, and the thermocouple was fixed to

the block adjacent to the substrate. The energy flux at the substrate surface due to the incident sputtered beam was approximately $10^{-5}$ cal $cm^{-2}$ $s^{-1}$, so that surface heating was negligible.

In order to obtain a clean surface the substrates were cleaved *in vacuo* immediately before deposition commenced. The cleavage blade, operated externally through a rotary seal, was combined with a stepped mask so that three different thicknesses of deposit on the same substrate could be obtained; in this way the island density at different stages of the experiment could be measured.

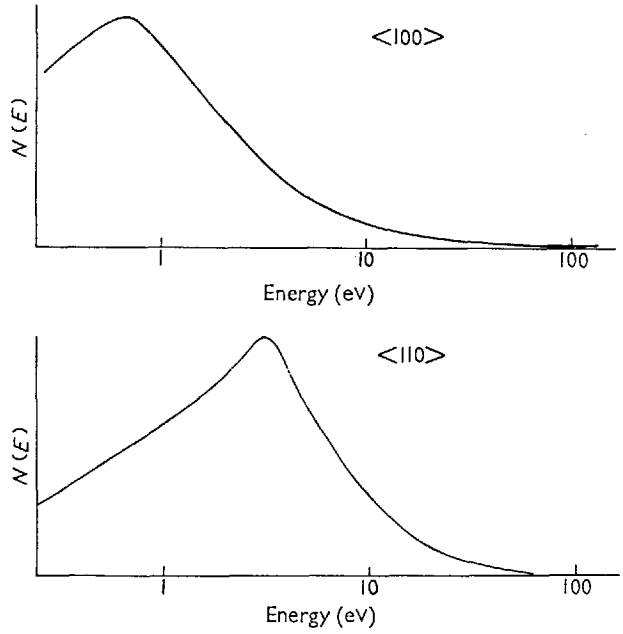


Figure 2. Energy spectra of gold sputtered in different ejection directions from a single crystal target.

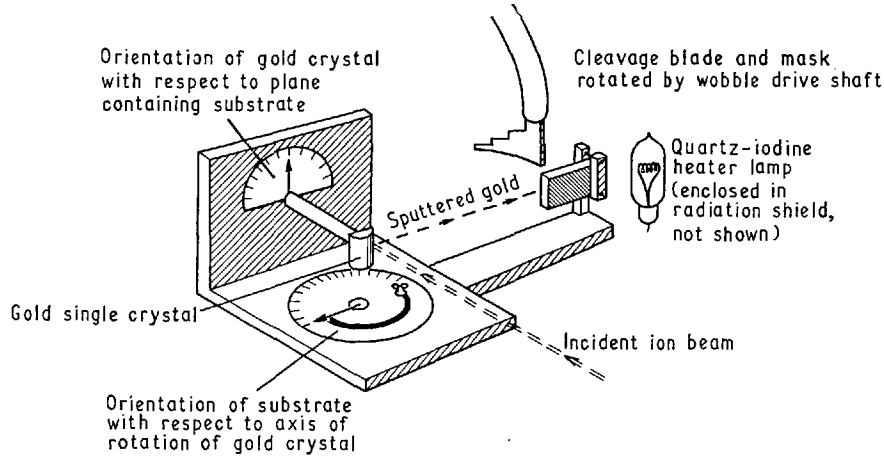


Figure 3. Apparatus used for the growth of gold sputtered in selected crystallographic directions from a gold single crystal onto vacuum-cleaved rocksalt.

The incidence rate of gold at the substrate was measured by sputtering with large ion beam currents ($\sim 100\ \mu A$) on to glass substrates at room temperature, measuring the thickness, assuming complete condensation, and further assuming that the sputtering rate was proportional to ion current within the range used. An incidence rate of 1 Å $min^{-1}$ was

produced by a few microamps beam current. The high-energy ion beam was produced in a linear ion-accelerator attached to the chamber containing the target assembly.

Experiments were carried out at a pressure of about $10^{-6}$ torr. After heating the substrate to the required temperature, the gold target was bombarded with a large ion current for a few minutes to clean the surface. The ion current was then adjusted to the required value, gold incidence rates being typically 0·5 Å $min^{-1}$. The substrate was cleaved to commence deposition and masked off in sections at intervals, usually 1, 5 and 20 minutes, to obtain deposits of different thicknesses. After deposition, the substrates were cooled below 50 °c before coating with carbon. The specimens were then examined by electron microscopy.

## 3. Results

*Saturation island densities*

Electron micrographs of a typical growth sequence are shown in figure 4 (plate). The measured island densities are plotted as a function of time in figure 5; the density rapidly rises to a very high value, and then slowly increases. Thus there appears to be saturation behaviour, as predicted.

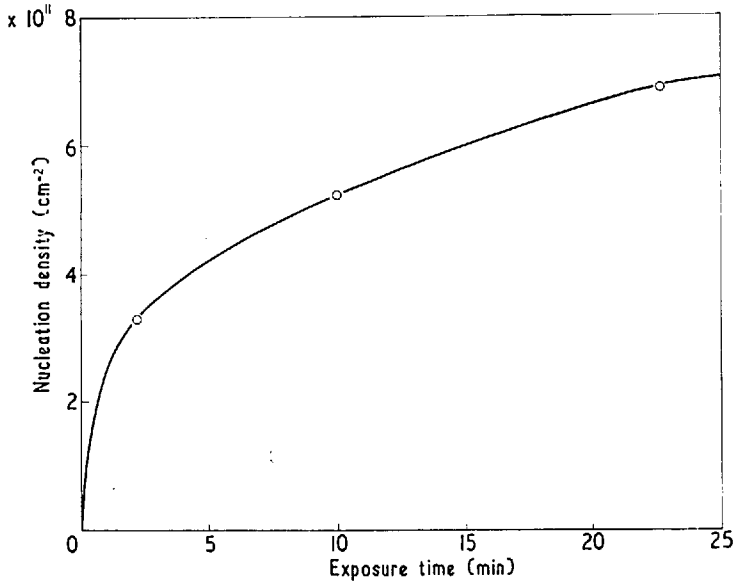


Figure 5. The change of island density with deposition time.

The saturation values obtained for gold sputtered along the ⟨110⟩ direction are plotted against reciprocal substrate temperature in figure 6; incidence rates of 0·5 Å $min^{-1}$ or 0·6 Å $min^{-1}$ were used, as shown. Values obtained by thermal evaporation deposition are shown for comparison; for these results, the incidence rate was 8·4 Å $min^{-1}$.

According to Lewis and Campbell (1967), in the low-temperature region when pairs of atoms are stable, saturation island density $N_s$ is proportional to the square root of the incidence rate $R$:

$$N_s = \left(\frac{N_0 R}{\nu_0}\right)^{1/2} \exp\left(\frac{E_d}{2kT}\right). \tag{1}$$

If it is assumed that the high-energy results obey this dependence on $R$, and if the corresponding density values for an incidence rate of 8·4 Å $min^{-1}$ are thus calculated, the modified values shown in figure 6 are obtained.

It can be seen that the effect of the high-energy beam is to considerably increase the saturation island density, to increase the gradient of the line (which would correspond to a change in surface diffusion energy from 0·10 ev to 0·36 ev), and to shift the intercept at $1/T = 0$.

Because of the similarity of these results to those obtained by electron bombardment during thermal evaporation (Jordan and Stirland, to be published), the latter results also are shown in figure 6; they were obtained at an incidence rate of 8·4 Å $min^{-1}$. Electron bombardment appears to produce, within the limits of experimental error, the same shift in the intercept at $1/T = 0$, and similar though less marked increases in saturation density and gradient (corresponding to a surface diffusion energy of 0·22 ev).

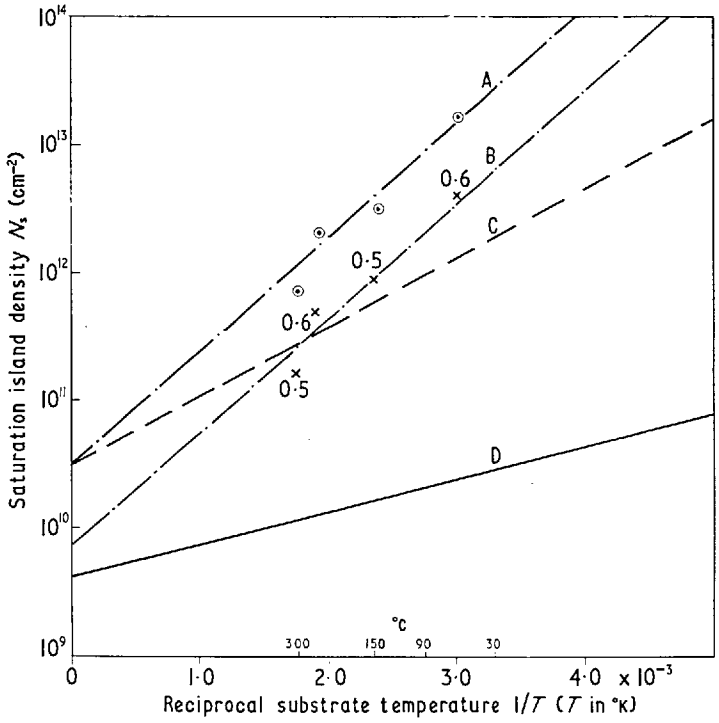


Figure 6. Experimental values of saturation island densities of gold on rocksalt. Curve A, sputtered (modified results); curve B, sputtered (high energy); curve C, evaporated (electron bombardment) electron flux approximately $10^{15}$ $cm^{-2}s^{-1}$ (240 ev); curve D, evaporated. Incidence rates, gold 0·14 Å $s^{-1}$ except where shown by numbers at × : these rates are in Å $min^{-1}$.

No experiments were carried out above 310 °c because the rocksalt showed changes of surface structure at such temperatures. The region of the $N_s$ against $1/T$ plot where the slope is expected to become negative, was not reached.

The total volume of deposit was estimated by measuring the diameters and numbers of islands and assuming that each island was hemispherical. The condensation coefficient was then obtained from the ratio of condensed material to total incident material. In the unlikely event that islands were spherical, the condensation coefficient would be twice the calculated value. It is more likely that the island contact angle would be less than 90°, and hence that the condensation coefficient would be somewhat less than the calculated value.

The calculated condensation coefficients varied between 0·01 and 0·32, a typical value being 0·1; they showed no systematic variation with substrate temperature. Furthermore, there was no significant change in condensation coefficient during each experiment as the thickness increased. This apparently contradicts the theoretical prediction that, at low

temperatures, when saturation island density is controlled by surface diffusion, the condensation coefficient is equal to unity. This is discussed in the next section.

The high energy appears also to modify the orientation of the deposit. Figure 7 (plate) shows a typical sequence of transmission electron diffraction patterns obtained from three thicknesses of a specimen deposited at 150 °c. It can be seen, particularly in the third and thickest film, that the orientation is predominantly the parallel orientation, i.e.$(001)_{Au}\|(001)_{NaCl}$ with $[110]_{Au}\|[110]_{NaCl}$ although the arcing of the 200 and 220 reflections shows that some misalignments are present. A gold deposit produced by evaporation, but under otherwise identical conditions, normally consists of two orientations (e.g. Stirland 1968), i.e. the parallel orientation together with a (111) orientation.

Further experiments have been carried out under different sputtering conditions and produced similar results to those above. The gold single-crystal target was bombarded along a ⟨111⟩ direction with 50 kev xenon ions. Atoms ejected along ⟨100⟩ and ⟨110⟩ directions produced saturation densities on substrates at 150 °c of $7{\cdot}0\times10^{11}$ cm$^{-2}$ and $7{\cdot}2\times10^{11}$ cm$^{-2}$ respectively at deposition rates of 0·5 Å min$^{-1}$, these densities being equivalent to $2{\cdot}9\times10^{12}$ cm$^{-2}$ and $3{\cdot}0\times10^{12}$ cm$^{-2}$ respectively at a deposition rate of 8·4 min$^{-1}$, again assuming a $R^{1/2}$ dependence. The corresponding value, for argon ⟨100⟩ bombardment and ⟨110⟩ ejection, of $3{\cdot}9\times10^{12}$ cm$^{-2}$ (figure 6) is the same, within the limits of experimental error.

Unfortunately the ejection energy spectra for ⟨111⟩ bombardment are not known, but one would expect considerable differences between the ⟨100⟩ and ⟨110⟩ ejection directions, since these involve different contributions from each of the several sputtering mechanisms involved.

Xenon bombardment also produced the same low condensation coefficients and orientation changes as were produced by argon ⟨100⟩ bombardment.

To summarize the results; compared with evaporation, the high-energy beam appears to produce:

(i) An increased saturation island density.
(ii) A greater variation of saturation density with reciprocal substrate temperature.
(iii) An increased intercept at $1/T = 0$.
(iv) A low condensation coefficient.
(v) A change in deposit orientation.

These results are discussed in the next section.

## 4. Discussion

Using a set of assumptions which appear to be justified for evaporation deposition, Lewis and Campbell (1967) derived equation (1) for conditions of complete condensation. However, we have used an entirely different deposition method and have obtained different experimental results. We conclude that the adatom behaviour has been altered, either directly or by modifying the interaction between adatom and substrate. Possible reasons for the different behaviour compared with evaporation deposition will now be discussed.

### 4.1. *Thermal accommodation*

It is assumed in nucleation theories that an incident atom is immediately and completely thermally accommodated when it strikes the surface of the substrate. This may not be so, and the adatom may retain some of its incidence energy, producing a high effective temperature and hence enhanced diffusion and desorption probabilities. However, it can be seen from equation (1) that diffusion enhancement would lead to smaller values of $N_s$, contrary to our observations. Furthermore, enhancing the desorption rate would, according to the Lewis–Campbell model, reduce the temperature of the transition from complete to incomplete condensation; this transition corresponds to a change from positive to negative slope respectively on the lg $N_s$ against $1/T$ graph. No such change is apparent from our observations.

Further evidence that enhanced diffusion and desorption are unlikely is provided by the experiments performed under different sputtering conditions, with xenon as the

bombarding ion species. Although the energies involved were unknown, they were likely to be different from those obtained with argon ⟨100⟩ bombardment and ⟨110⟩ ejection; however, they produced similar enhanced values for island densities. It would appear that we are dealing with a process which has an energy threshold below the energies used in any of the present experiments, but which is almost independent of energy above the threshold. This would not be expected of a non-thermal accommodation model.

### 4.2. *Reflection and penetration*

We have so far assumed that incident material is adsorbed on the substrate surface. However, some material may be immediately reflected back into the vapour phase or may penetrate the surface, the proportions involved being a function of arrival energy. The proportion that is adsorbed on the surface could display complete condensation behaviour, but the condensation coefficient would be equal only to that proportion so adsorbed. Contributing evidence for this proposal is that the observed coefficient did not appear to increase with deposit thickness, whereas, in the case of initially incomplete condensation of adatoms, the coefficient would increase to unity as the saturation density was established. It therefore appears that initially complete condensation of the proportion adsorbed is taking place. As the arrival energy is increased, one would expect the proportion adsorbed to decrease. So loss of material by reflection or penetration could account, at least partly, for the low condensation coefficients obtained with the high-energy beam. Some of the scatter of condensation coefficient results may be due to the method used for estimating the amount of material deposited, but we cannot suggest a complete explanation for the unsystematic coefficient variation.

Some penetration of the surface may be taking place. Nelson (1968, private communication) has suggested that an energy of only 1·5 ev is required for a gold atom to penetrate a rocksalt (100) surface down a ⟨100⟩ channel, plus a further 1 ev for each subsequent plane. If this is the case, then most of the sputtered beam would penetrate. Other sources, however (e.g. Thompson 1968, private communication), suggest penetration energies a hundred times bigger. Using radioactive gold so that very small amounts can be detected, Lewis (1968, private communication) has shown that shallow penetration may occur even with ordinary evaporation on to rocksalt.

But whether penetration, if it does take place, can affect nucleation behaviour is another matter. If gold penetrates the surface, diffuses around in the lattice, and eventually comes to the surface (*in* the surface) either substitutionally or interstitially, it could form a 'special' adsorption site of the type discussed later. But we are unable to comment further on the likelihood of such diffusion and special site production.

### 4.3. *Surface sites*

Instead of modifying the intrinsic nucleation behaviour of the adatom, the action of the high-energy sputtered beam might be to modify the substrate surface, and hence the energy parameters $E_a$ and $E_d$. The equation for saturation density (equation (1)) can be directly applied only if the modified parameters $E_a$ and $E_d$ apply to the whole surface, i.e. to every adsorption site on the surface. If equation (1) can be applied, then the change in island densities corresponds to a change in surface diffusion energy $E_d$, from 0·11 to 0·36 ev atom$^{-1}$ and a change in the $1/T = 0$ intercept value $(RN_0/\nu_0)^{1/2}$, from $4 \times 10^{10}$ cm$^{-2}$ to $3 \times 10^{11}$ cm$^{-2}$. This latter change could be interpreted as due to a change in $\nu_0$.

However, when the whole surface is not modified, equation (1) cannot be directly applied and no conclusions can thus be drawn about changes in the nucleation parameters.

Electron bombardment of the substrate during evaporation has been found by Stirland (1966, 1968) and Jordan and Stirland (to be published), to produce both an increase in saturation density and a change in orientation. The results of the latter are very similar to the results of the present work, as was shown above, and suggest a similar mechanism. Palmberg *et al.* (1967) have shown that electron bombardment before deposition produces the same change in epitaxy as was noted by the above gentlemen, provided that the substrate temperature was below 80 °C. Stirland found that electron bombardment before deposition

on a rocksalt substrate at 150 °c produced an increase in island density, but no change in orientation.

Palmberg *et al.* have suggested that the effect of electron bombardment is to dissociate the surface and produce surface vacancies or move substrate atoms from their normal positions. In either case, preferred nucleation sites would be formed, at which the adsorption energy is higher than at a normal adsorption site. The number of surface defects would be governed by the equilibrium between production rate and loss rate, the latter being temperature dependent and due to annealing-out of the defects. As the substrate temperature increases, so does the annealing rate, and hence the number of defects decreases; the difference between island densities on bombarded and non-bombarded surfaces would therefore be expected to decrease with increase of substrate temperature, as is observed. Subsequent work by Rhodin and Palmberg (to be published) and by Townsend and Kelly (1968) has produced further evidence for the creation of surface defects by electron bombardment. The impact on the substrate surface of high-energy neutral gold atoms, as in the present work, may produce similar damage.

But mere decoration of surface defects would not lead to the saturation island density behaviour observed with electron bombardment by Jordan and Stirland, and with high-energy bombardment in the present work; in both these cases the defect production process continued simultaneously with condensate deposition. With an initially bare substrate, the defect production rate would quickly be balanced by the (temperature-dependent) annealing rate, and an equilibrium density of defects would be set up. If defect-producing bombardment were then stopped and gold thermal evaporation immediately carried out, the defects would be decorated and saturation behaviour would be observed. But the situation will be different if defect production continues during gold deposition. Then, as each defect site is removed from the defect production/annealing process by gold decoration, a fresh site will be produced elsewhere to maintain the equilibrium defect density. The fresh site will then be decorated, another site will be produced elsewhere, and so on. But this is inconsistent with the observations of saturation behaviour.

However, saturation behaviour would be produced if the adsorption energy of a gold adatom at a defect was greater than that on a normal perfect rocksalt surface, and less than that at a stable gold island; having established an initial density of islands by decoration of defects, further adatoms would be preferentially adsorbed by these islands.

### 4.4. *Charged material in the sputtered beam*

There is a complication in the interpretation of the observed results because the high-energy sputtered beam contains not only neutral gold atoms, but also an amount of charged material. There may be a few per cent of singly-ionized gold atoms of low energy and a much smaller number of multiply-ionized gold atoms of quite high energy, perhaps as high as several kev. Also, a small proportion of the argon ions bombarding the gold target may subsequently strike the substrate, as may the electrons which usually accompany sputtering processes. The incidence of so much charged material makes interpretation more difficult. Assuming (for the moment) that the bombardment does not affect the substrate, we may be observing a dual nucleation process—one of gold atoms, the other of gold ions. Because the latter would have a Coulomb interaction with the ionic rocksalt surface as well as a van der Waals' interaction, both adsorption energy $E_a$ and surface diffusion energy $E_d$ would be increased, consistent with our observations. But how long an ion could migrate across the surface without re-association with an electron to form a neutral atom is the pertinent question in this case. Re-association towards the end of a surface diffusion path would not affect the previous history of the atom, and so would not significantly alter its total diffusion path; late re-association may even be advantageous because otherwise the Coulomb repulsion between like gold positive ions would inhibit nucleation. Similar arguments would apply if the gold atoms became negatively charged.

It may be instead that only the charged incident material is responsible for causing the surface defects discussed above. In this case, the high energy of the incident beam would not be directly affecting the nucleation process, serving only to produce the low condensation coefficients observed.

4.5. *Orientation effects*

The change in orientation may be due to an initial improved ordering of atoms in an island because a decorated defect in the surface produces a good foundation, or to a subsequent re-arrangement of multiply-oriented islands when they are struck by incident energetic particles. Each configuration of an island is quasi-stable because a potential barrier discourages re-arrangement, even into a configuration which is energetically more favourable; the collision of an incident particle may enable potential barriers to be surmounted because of the subsequent energy transfer.

The different effects of pre-bombardment observed by Palmberg *et al.* (1967) and by Stirland have been noted above. The former achieved the single orientation below 80 °C without simultaneous bombardment, which supports the 'defect foundation' model; the latter's results at 150 °C suggest that bombardment during deposition is necessary and hence support the 're-arrangement' model, although Stirland has suggested that the high density observed may have been due to decoration of carbonaceous material which had formed, under electron bombardment, from hydrocarbons in the vacuum system by 'cracking' and subsequent cross-linking at the substrate. Possibly the electron-induced defects had annealed out at this elevated temperature, consistent with the observation of Palmberg *et al.* Jordan and Stirland have produced much better singly-oriented deposits with electron bombardment than in the present work. This would not be surprising on the 're-arrangement' model, since their electron energy input flux to the substrate was several thousand times larger than with the high-energy beam. (The 'high energy' of the sputtered beam is relative only to the energy of a thermal evaporation beam.) On the other hand, Stirland suggests that the threshold for electron bombardment is at much lower energy inputs.

The evidence in favour of either model is not overwhelming, but the 'defect foundation' model seems more likely, although we are unable to suggest a mechanism for the ordering effect.

## 5. Conclusions

It has been shown that poor thermal accommodation of high-energy incident atoms would not lead to the changes in island density behaviour which are observed. But lack of accommodation may be responsible for the low condensation coefficients.

There is evidence to suggest that the increased island densities may be due to the creation of 'special' sites, with higher surface diffusion energy than usual. It has been shown that this could lead to saturation density behaviour. But whether the special sites are created by the impulse of high-energy neutral atoms or by associated charged particles has not been resolved. If the latter, then the high-energy neutral material is having no effect on island densities. The density effects observed in the present work and the effects produced by electron bombardment may both be due to the production of surface sites of higher adsorption energy, but it has not been established that the same type of site is formed in both cases.

The changes in deposit orientation may be due to the ordering effect of a decorated special site, or to the rearranging effect of impinging energetic particles on an already existing island. It is concluded that the former is more likely.

## Acknowledgments

We are grateful to the Atomic Energy Research Establishment Harwell for the use of the high-energy linear ion accelerator (HILDA), in particular to R. S. Nelson and D. F. Holloway of that establishment, and to Professor M. W. Thompson for the use of his unpublished results. We are also indebted to our colleagues D. J. Stirland, B. Lewis, M. R. Jordan and R. Ogden for their extremely useful advice and help.

Thanks are due to The Plessey Company Limited for permission to publish. The work was supported by the Ministry of Technology.

## References

BEAVITT, A. R., TURNELL, R. C., and CAMPBELL, D. S., 1967, *Thin Solid Films*, **1**, 3–11.
CABRERA, N., 1959, *Discuss. Faraday Soc.*, **28**, 16.
LEWIS, B., and CAMPBELL, D. S., 1967, *J. Vacuum Sci. Technol.*, **4**, 209–18.
PALMBERG, P. W., RHODIN, T. N., and TODD, C. J., 1967, *Appl. Phys. Lett.*, **10**, 122–4.
STIRLAND, D. J., 1966, *Appl. Phys. Lett.*, **8**, 326–8.
—— 1968, *Thin Solid Films*, **1**, 447–73.
THOMPSON, M. W., 1968, *Phil. Mag.*, **18**, 361–424.
TOWNSEND, P. D., and KELLY, J. C., 1968, *Phys. Lett.*, **26A**, 138–9.

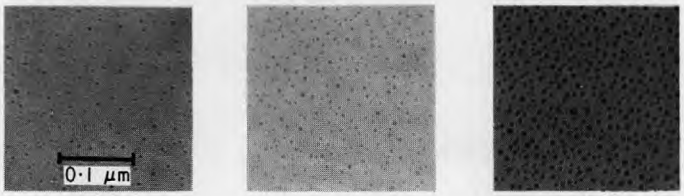


Figure 4. Growth sequence of sputtered gold on rocksalt.

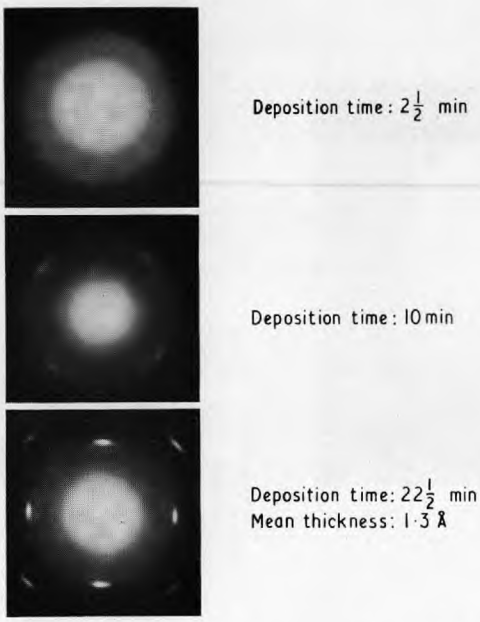


Figure 7. Diffraction patterns of high energy sputtered deposits. Substrate temperature 150 °C, incidence rate 0·5 Å $min^{-1}$.

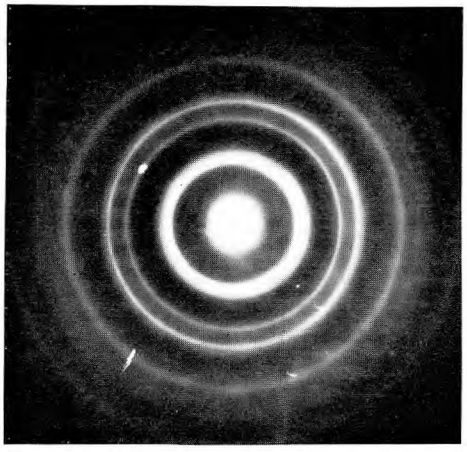

Figure 1. Transmission electron diffraction pattern from an equimolecular mixture of argon and krypton at 7 °K (50 kev electrons).

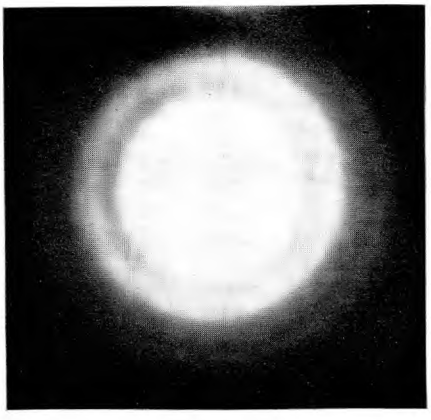

Figure 3(*a*). Transmission electron diffraction pattern from a deposit containing 75% neon and 25% argon at 7 °K (50 kev electrons).

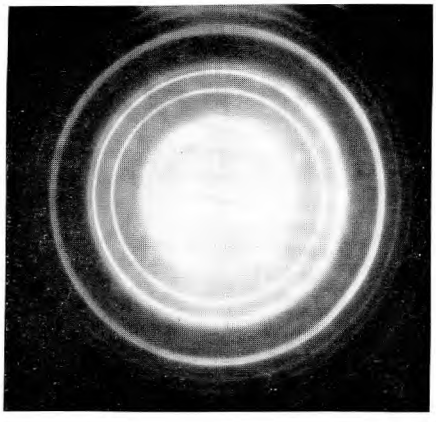

Figure 3(*b*). Transmission electron diffraction pattern from a deposit at approximately 30 °K which originally consisted of an equimolecular A–Ne mixture at 7 °K. The neon has evaporated and the remaining argon has recrystallized (50 kev electrons).